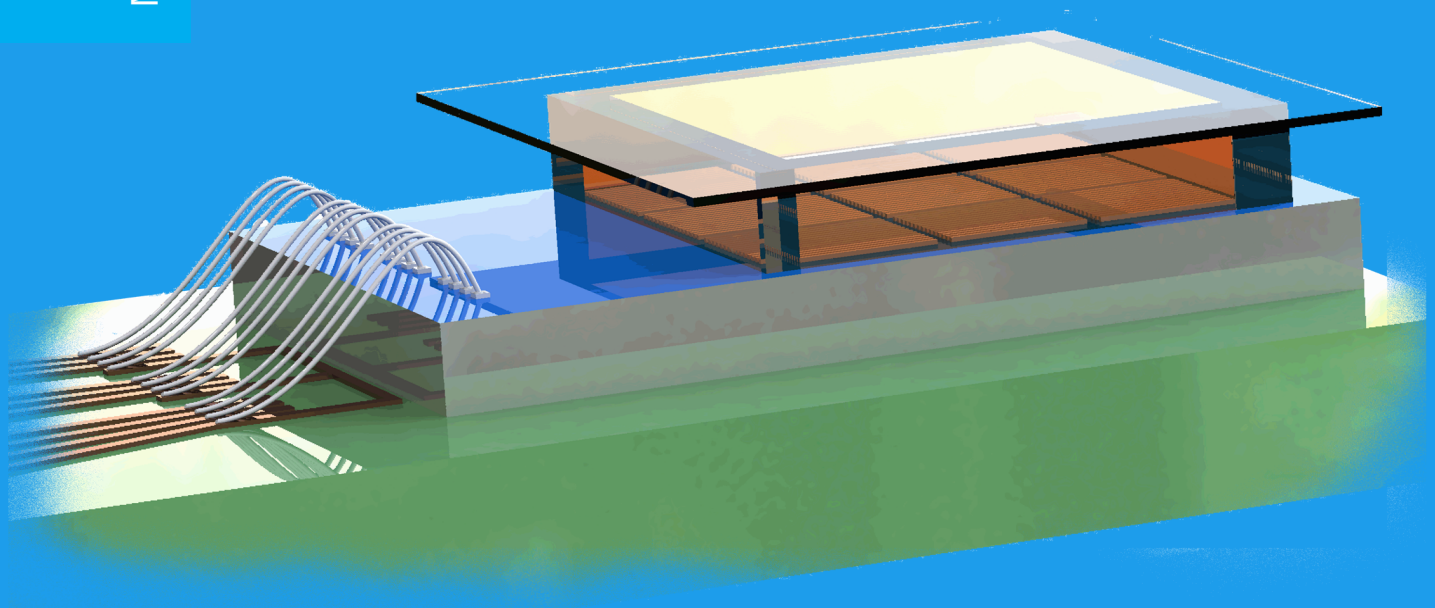


# Concentrating and inactivating the surrogate of SARS CoV-2 using electric fields on micro-chip platforms

Devashish Mantri

Master of Science Thesis





# **Concentrating and inactivating the surrogate of SARS CoV-2 using electric fields on micro-chip platforms**

MASTER OF SCIENCE THESIS

For the degree of Master of Science in Biomedical Engineering: Medical Devices at Delft University of Technology

Devashish Mantri

October 28, 2022

Faculty of Mechanical, Maritime and Materials Engineering (3mE) · Delft University of Technology



DELFT UNIVERSITY OF TECHNOLOGY  
DEPARTMENT OF  
MECHANICAL MARITIME AND MATERIALS ENGINEERING (3ME)

The undersigned hereby certify that they have read and recommend to the Faculty of  
Mechanical, Maritime and Materials Engineering (3mE) for acceptance a thesis  
entitled

CONCENTRATING AND INACTIVATING THE SURROGATE OF SARS CoV-2 USING  
ELECTRIC FIELDS ON MICRO-CHIP PLATFORMS

by

DEVASHISH MANTRI

in partial fulfillment of the requirements for the degree of  
MASTER OF SCIENCE BIOMEDICAL ENGINEERING: MEDICAL DEVICES

Dated: October 28, 2022

Supervisor(s):

\_\_\_\_\_  
prof.dr. GuoQi Zhang

\_\_\_\_\_  
Henk van Zeijl

Reader(s):

\_\_\_\_\_



---

# Abstract

Since the unravelling of the Covid-19 pandemic, studying methods of virus inactivation have become more important than ever. Many studies focus on the chemical and optical methods of inactivation. Very limited work has been carried out in studying the electrical methods of virus inactivation. The work presented in this thesis attempts to pioneer a study that examines the effect of electric fields generated by micro-electrodes on the survival of the surrogate of the SARS CoV-2 virus.

For this purpose, electrodes with 7 different geometries were micro-fabricated and characterized. A liquid suspension of the phi-6 bacteriophage (a surrogate of the SARS virus) was tested on all the different electrodes with different input voltages, frequencies and medium parameters.

The study showed that the treatment on specific electrode designs tailored with specific voltage and medium parameters showed a decrease in the virus titer ranging from half a log to a maximum of 2 logs. These results are promising for the development of products like electric facemasks, micro-filters and m-TAS systems.



---

# Table of Contents

<b>Preface</b>	<b>ix</b>
<b>1 Introduction</b>	<b>1</b>
1-1 Motivation . . . . .	1
1-2 Objective . . . . .	2
1-3 Thesis outline . . . . .	2
<b>2 Background and literature</b>	<b>3</b>
2-1 Dielectrophoresis . . . . .	3
2-1-1 Concentration of the viruses using DEP . . . . .	5
2-1-2 Modelling of the SARS COV-2 under the influence of DEP . . . . .	7
2-2 Inactivation of viruses using electric fields . . . . .	9
2-2-1 Inactivation by Irreversible electroporation . . . . .	10
2-2-2 Inactivation of SARS COV-2 by Spike Deactivation . . . . .	12
<b>3 Electrode design and simulations</b>	<b>15</b>
3-1 Electrode design . . . . .	15
3-2 Electrode design simulations . . . . .	17
3-2-1 Castellated electrodes . . . . .	17
3-2-2 Interdigitated electrodes . . . . .	18
3-2-3 Saw-tooth electrodes . . . . .	21
3-3 Formulation of Hypotheses . . . . .	21
<b>4 Device Fabrication</b>	<b>23</b>
4-1 Process steps for device fabrication . . . . .	23
4-1-1 Design of Photolithographic masks . . . . .	23
4-1-2 Programming the waferstepper . . . . .	26
4-2 Fabrication process . . . . .	27
4-2-1 Challenges in Fabrication and mitigation strategy . . . . .	31

<b>5</b>	<b>Experimental set-up</b>	<b>35</b>
5-1	Virus stock preparation . . . . .	35
5-1-1	Use of surrogate virus phi-6 . . . . .	35
5-1-2	Phage Production . . . . .	35
5-1-3	Stock preparation . . . . .	35
5-2	Experiment table . . . . .	36
5-3	Viral particle titrations . . . . .	38
5-4	Experimental Design . . . . .	38
5-4-1	Experiment 1: Testing hypothesis 1, 2 and 3 . . . . .	38
5-4-2	Experiment 2: To test hypothesis 4 and 5 . . . . .	39
<b>6</b>	<b>Measurements and results</b>	<b>41</b>
6-1	Electric field measurements . . . . .	41
6-1-1	Breakdown and discharge current . . . . .	41
6-1-2	Electric Field calculations . . . . .	42
6-1-3	Influence of different geometries on electrical discharge characteristics . . . . .	43
6-2	Experiment results: Phage titers . . . . .	45
6-2-1	Results of Experiment 1 . . . . .	45
6-2-2	Results of Experiment 2 . . . . .	47
<b>7</b>	<b>Discussion and conclusion</b>	<b>51</b>
7-1	Discussion . . . . .	51
7-2	Conclusions and future recommendations . . . . .	55
<b>A</b>	<b>Process recipe</b>	<b>57</b>
A-1	Process recipe on Glass . . . . .	57
A-2	Process recipe for Silicon . . . . .	63
<b>B</b>	<b>Additional Data</b>	<b>71</b>
B-1	Photos of PFU Assays . . . . .	71
B-2	First run of Experiment 1 . . . . .	71
B-3	Additional Voltage-current graphs . . . . .	71
	<b>Bibliography</b>	<b>77</b>
	<b>Glossary</b>	<b>85</b>
	List of Acronyms . . . . .	85
	List of Symbols . . . . .	85

---

## List of Figures

2-1	The different interactions between the dipolar charges with the local electric fields.	4
2-2	Core shell model of SARs CoV-2 . . . . .	8
2-3	CM factor of coronavirus (Conductivity and the permittivity of the membrane are loosely assumed) . . . . .	9
2-4	The electroporation of a micro particle with a bilipid membrane suspended in a conductive medium . . . . .	10
2-5	Inactivation of the SARS CoV-19 by damaging the spike protein using moderate electric fields [1] . . . . .	12
3-1	Different 2D and 3D electrode geometries (A) parallel or interdigitated, (B) castellated, (C) oblique, (D) curved, (E) quadrupole, (F) microwell, (G) matrix, (H) extruded, (I and J) top-bottom patterned [2] . . . . .	16
3-2	Electric field distribution of in phase castellated electrodes . . . . .	17
3-3	Electric field distribution of out of phase castellated electrodes . . . . .	18
3-4	Electric field distribution of interdigitated electrodes with $1\mu\text{m}$ pitch . . . . .	19
3-5	Comparison of the penetration of the electric field displacement in the medium with increasing pitch distances . . . . .	20
3-6	Electric field generated by different pitch distances of the out of phase castellated electrode . . . . .	21
3-7	Electric field distribution of saw tooth electrodes . . . . .	22
4-1	Definition of Pitch and gap on (a) Electrode geometry Cin4 (b) Electrode geometry Cout4. . . . .	23
4-2	Design of mask for the ASML wafer stepper . . . . .	25
4-3	Design of mask for the contact aligner . . . . .	26
4-4	Quartering of the electrode area in 8 separate arrays . . . . .	27
4-5	Current density in 300nm thick interdigitated electrodes with $2\mu\text{m}$ pitch. . . . .	28
4-6	The fabrication process of the micro-electrodes . . . . .	30
4-7	Backend processing and packaging of a processed wafer . . . . .	30

4-8	Short-circuits under microscope . . . . .	31
4-9	Shortcircuits between the electrodes observed on cascade measurements . . . . .	31
4-10	Optical inspection of a non-adhesive Bondpad . . . . .	32
4-11	Optical inspection of a non-adhesive bondpad after 20 min etch in PES . . . . .	33
4-12	Optical inspection of the bondpad after making changes to the process flow. . . . .	34
5-1	Process for culturing colonies of <i>Pseudomonas</i> sp. . . . .	37
5-2	Experiment set-up . . . . .	37
5-3	5-fold serial dilutions of the original treated sample . . . . .	38
6-1	SEM image of a particle between the gaps of the gratings that may influence the discharge currents by altering the dielectrics within the gaps of the arrays. . . . .	42
6-2	Current-Voltage characteristics of planar electrodes on glass with the largest pitch. . . . .	43
6-3	Comparison of the performance of different pitch distances of the same pattern on the discharge current . . . . .	44
6-4	Comparison of castellated in phase vs castellated out of phase vs interdigitated patterns on silicon substrates . . . . .	44
6-5	Counting plaque forming units on the different samples of the virus . . . . .	45
6-6	Effect of DC treatment . . . . .	46
6-7	Effect of AC treatment with 30kHz frequency . . . . .	47
6-8	Effect of electrode geometries on virus inactivation . . . . .	48
6-9	Effect of frequency and dilution on the treatment . . . . .	49
6-10	Effect of medium conductivity on the treatment . . . . .	50
7-1	Geometric definitions of the electrode in the study[3] . . . . .	52
7-2	Effect of pitch/height ratio on the concentration efficiency [3]. . . . .	52
7-3	CM factor of E-coli under different medium conductivities[4] . . . . .	53
7-4	Effect of dilution on the virus density . . . . .	54
A-1	3D printed micro-dam . . . . .	70
B-1	Pfus assays for experiment 1 . . . . .	72
B-2	Experiment 1 with DC input voltage . . . . .	73
B-3	Thermal images of electrode I2 with 3 short circuits input with 20V DC voltages . . . . .	73
B-4	Breakdown voltage graphs for (a) Pattern Cin4: castellated in-phase gap $1\mu\text{m}$ and (b) Pattern Cin8: Castellated in-phase gap $6\mu\text{m}$ on glass substrates. . . . .	74
B-5	Breakdown voltage graphs for (a) Pattern I2: interdigitated Comb gap $1\mu\text{m}$ , (b) Pattern I5: Interdigitated Comb gap $4\mu\text{m}$ , (c) Pattern I10: interdigitated comb pitch $9\mu\text{m}$ on glass substrates. . . . .	74
B-6	Breakdown voltage graphs for (a) Pattern Cout4: Castellated out of phase gap $500\text{nm}$ , (b) Pattern Cout5: Castellated out of phase gap $1\mu\text{m}$ on glass substrates . . . . .	75

---

## List of Tables

2-1	Type of Viruses and their dielectrophoretic trapping parameters . . . . .	6
4-1	Patterns and their respective pitch distances designed on the photo-lithographic mask . . . . .	24
A-1	Gasses and flow rates needed to etch 300nm of Aluminium . . . . .	59
A-2	Gasses and flow rates needed for the deposition of a TEOS layer . . . . .	62
A-3	Gasses and flow rates needed to etch 300nm of Aluminium . . . . .	65
A-4	Gasses and flow rates needed for the deposition of a TEOS layer . . . . .	68



---

# Preface

This document is a part of my Master of Science graduation thesis. My primal motivation for pursuing my masters was to explore the field of micro-fabrication and micro-machines. My fascination for making tiny devices that have the potential to manipulate and interrogate with the human body and biology started when I read Richard Feynman's essay. It was aptly titled 'There is plenty of room at the bottom'; I found the the world of micro-electronics to be truly amazing and very exciting. Studying at TU Delft and pursuing my thesis at the Micro-electronics department provided me with the opportunity to further this fascination.

I would like to thank my daily supervisor Dr. Henk van Zeijl from whom I learnt so much about micro-fabrication and cleanroom processing. I also want to thank Luutzen Wymenga for all his valuable inputs during the planning, writing and execution phase of this project. I would like to extend my gratitude to Professor Jan van Turnhout for providing me with the right resources and the right material to steer this project in the right direction. I also want to thank Prof. Ron Fouchier and Sander from the Erasmus Medical Center for giving me valuable inputs and taking interest in the conception of this project. I would also like to thank and show my heartfelt gratitude to my supervisor Professor Kouchi Zhang for believing in me and presenting me with this opportunity. Thanks are also due to Ana Rita Costa and Jelger Esser at Stan Brouns lab for conducting the virus titers for me and providing me with the virus stock solution. Finally, a big thanks to all my friends and family who kept me sane and in good spirits throughout my thesis.

I hope you enjoy reading the document as much as I enjoyed writing it.



---

# Chapter 1

---

## Introduction

### 1-1 Motivation

The Severe Acute Respiratory Syndrome Corona Virus -2 (SARS CoV-2), a virus belonging to the coronavirus family and the agent responsible for the Covid-19 pandemic, claimed over 5 million lives over the span of 2 years across the globe. Drastic measures that included social distancing, mandatory facemasks and long periods of isolation and quarantine to curb the spread of the virus were put in place. The research community was put to test as it had to struggle against the tide of time to study and deliver practical solutions that allowed us to test, cure and prevent the respiratory disease. Studying and researching mechanisms of virus inactivation could have huge implications on the betterment of public health by allowing us to develop methods for instant killing of the virus to ward off deadly pandemics.

Current virus inactivation methods rely on optical [5, 6, 7], chemical and physical agents [8, 9]. Electrical methods provide new means of instant inactivation that can be integrated in an all in one platform to trap, concentrate, sample and kill viruses. These methods can be deployed on products like face masks, laboratory equipment, Lab On Chip (LOC) and micro-Total Analysis Systems (mTAS). Non-uniform electric fields have been used before, although only separately, to manipulate and electrically lyse single celled organisms and bacteria. The effect of such fields has been studied on bacteria and single celled organisms in great detail. Viruses, on the other hand, given to their smaller size are more difficult to manipulate and show resistance to inactivation treatments using Pulsed Electric fields (PEF) even as high as 29kV/cm [10]. Micro-fabrication allows us to scale down and create high electric field regions between the electrodes even with moderate voltages. Electric methods of virus inactivation developed with the help of such fabricated micro-electrodes engineered on micro chips may open doors to an all-in-one integrated system to concentrate, sample and in-activate the virus. Scaling down may allow us to inactivate individual virus particulate by creating local focused electric field spots that are difficult to create using PEF in macro-devices. For this, it is important to understand the mechanisms behind the inactivation of viruses as small as the SARS CoV-2 under practical settings.

## 1-2 Objective

There will be two primary objectives of this project. The objectives have direct relevance to the research domain and will help to further the study of developing micro-devices for instant inactivation of viruses:

1. Determine whether electric fields can inactivate the surrogate of SARS CoV-2 and also to reason with the physio-chemical mechanisms that may bring about the inactivation of the virus in the light of experiment.
2. Assess how different electrode geometries with different pitches perform in concentrating and inactivating the virus.

Additionally, there will be two secondary objectives:

1. Find the electrode geometry that optimizes concentration of viral particulate as well as killing.
2. Assess how the change in the permittivities and conductivities of the conducting medium affect the concentration and inactivation of the virus in the sample.

Through this endeavour we wish to explore the techniques that we can exploit to manipulate and inactivate the SARS COV-2 virus using only electric fields. As articulated, the prime focus throughout literature, has been only on bacteria and cells. Very few studies, detail the manipulation and killing of smaller viruses. This study will attempt to provide a base that can be used to further the research in electrical viral inactivation.

## 1-3 Thesis outline

Chapter 1 lays out the motivation and the need of furthering the research in this field. Chapter 2 will give a discourse on the literature that is relevant to the topics of this project. Chapter 3 will elucidate more on the electrode geometries and the design considerations for the fabrication of the device based on the simulation results of different electrode designs and relevant literature. This chapter also lays out hypothesis that we wish to test through the course of this project. Chapter 4 presents the fabrication process in great detail and highlights the manufacturing challenges faced during the fabrication process. Chapter 5 discusses the process and the protocols that were followed to perform the experiments. This chapter covers the techniques to prepare the virus, discusses the experimental set-up of treating the virus samples on the planar micro-electrodes and elucidates on the methods of testing the efficiency of the treatment process on the virus sample. Chapter 6 presents the results of the experiments. Finally, the results are followed up by a discussion and a conclusion in chapter 7.

# Background and literature

The aim of this chapter is to provide a concrete ground for devising an experimental set up and determining electrical parameters for the manipulation and the inactivation of the SARS CoV-2 virus by exploring and understanding the mechanisms of electrical inactivation and manipulation of other viruses and smaller bacteria. For higher inactivation rates of viruses in a sample, the virus needs to be concentrated near the high field regions. A higher electric field divergence warrants a higher concentration efficiency. Higher electric divergences can be achieved by specific electrode geometries. It is hypothesized that a higher electric field penetration within the sample would influence the virus particles that are further away from the electrodes. The viruses under the influence of the electric field are effected by the Di-electrophoretic force and are brought close to the high electric field spots near the electrodes. The electrode geometry also influences the efficiency of high electric field inactivation regions near the electrodes. More number of high electric field hot spots result in higher inactivation rates of the virus. Thus, subjecting the virus to the right non-uniform electric fields can be hypothesised to comprise of simultaneous concentration and inactivation of the virus particulate. The total inactivation rate of the virus in the sample would be dependent on

- Concentration efficiency of the electrodes
- Inactivation efficiency of the electrodes

In this chapter we look at the concepts of dielectrophoresis and how it is used to concentrate viruses and the inactivation mechanisms that are hypothesized to take course when the SARS CoV-2 surrogate is subjected to a non-uniform electric field.

## 2-1 Dielectrophoresis

Dielectrophoresis (DEP) was first discovered by Pohl in 1951 [11]. A polarizable particle suspended in a liquid medium under the influence of a non-uniform electric field experiences a force which is known as the dielectrophoretic force. The direction of the force on the particle

depends on the Clausius Mossotti (CM) factor which depends on the polarizability of the suspending medium and the polarizability of the particle. If the polarization of the particle is greater than that of the suspending medium, the particle moves towards the region of high electric field (positive Dielectrophoresis (pDEP)) while if the particle is less polarizable than the medium the particle moves away from the high electric field region (negative Dielectrophoresis (nDEP)). The polarizability of the particles are a function of the input electric field frequency. The type of force (pDEP or nDEP) on the particle can be controlled by varying either the polarizability and conductivity of the surrounding medium or the electric field frequency. This dependence can be seen in the illustration given in figure 2-1 and in the equations 2-3 and 2-4. In the given figure on the left, there are no net forces on the particle as the electric fields generated are uniform. The middle figure shows that the particle experiences a positive DEP as polarizability of the particle is higher than that of the surrounding medium. The particle then moves to the point of highest electric field. On the right, the particles is shown to be effected by a negative DEP force as the polarizability of the particle is lower than that of the surrounding medium. The particle is repulsed from the electrode and moves to a point that has the lowest electric field.

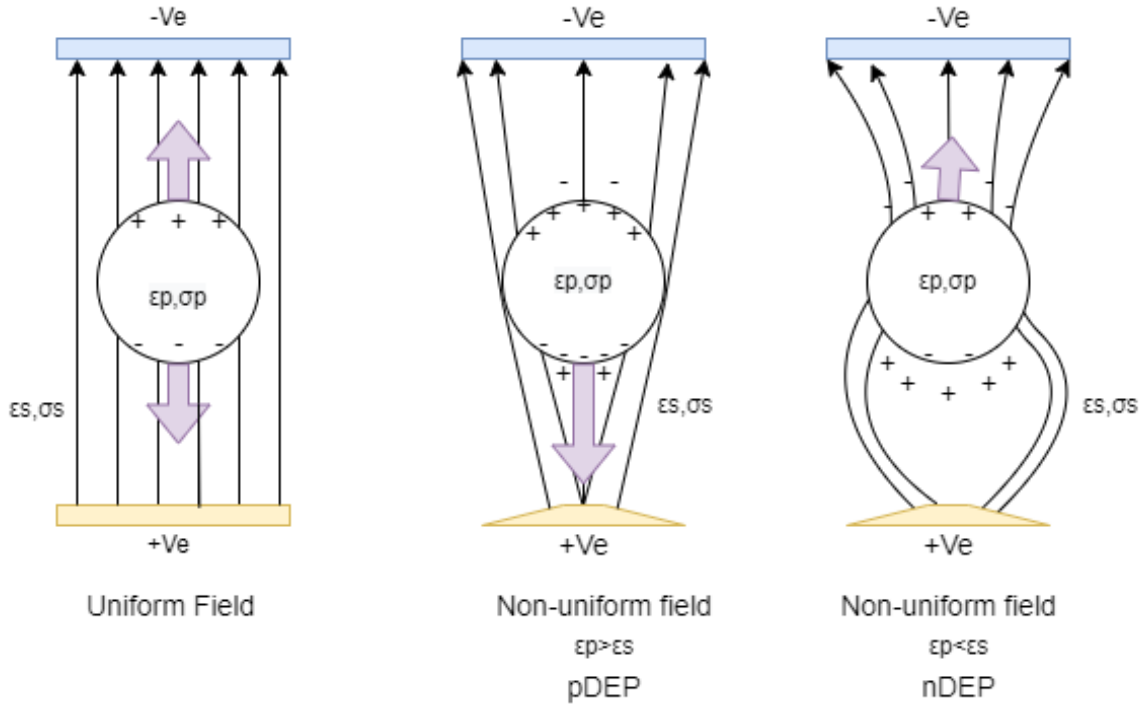


**Figure 2-1:** The different interactions between the dipolar charges with the local electric fields.

$$F = 2\pi\epsilon_s\epsilon_o R^3 \text{Re}[(\epsilon_p^* - \epsilon_s^*)/(\epsilon_p^* + 2\epsilon_s^*)] \nabla E^2 \quad (2-1)$$

$$CM = \text{Re}[(\epsilon_p^* - \epsilon_s^*)/(\epsilon_p^* + 2\epsilon_s^*)] \quad (2-2)$$

The force scales with the third power of the radius of the particle. It also depends on the permittivity of the surrounding solute and the Divergence of the electric field strength.  $\epsilon_p^*$

and  $\varepsilon_s^*$  are complex permittivities of the particle and the medium making up the CM factor. They are derived as follows-

$$\varepsilon_p^* = \varepsilon_p - j \frac{\sigma_p}{\omega} \quad (2-3)$$

$$\varepsilon_s^* = \varepsilon_s - j \frac{\sigma_s}{\omega} \quad (2-4)$$

Dielectrophoretic manipulation has been used to successfully trap and concentrate bacteria and viruses. Concentration of viral particulate facilitates the formation of localized clusters that can be easily quantified and inactivated. As highlighted by the equations, the manipulation of viruses need a higher and a more focused electric field to compensate for their smaller size. Device miniaturization facilitates the generation of higher electric field strengths using low electric powers[12], reduced analysis time and greater control over manipulation of the particles [13]. Pushing the limits of micro-fabrication and scaling down further it may be possible to achieve electric field strengths capable enough to concentrate smaller viruses.

### 2-1-1 Concentration of the viruses using DEP

Viruses can be grouped according to shape, size, chemical composition and structure of genome. All these different attributes dictate the electrical properties of the virus particle. The different classifications based on the structural and chemical compositions of the virus are covered in book by Hans R. Gelderblom [14] and are also compiled in table 2-1. The electric manipulation and concentration of the viruses in the context of this review is studied across two categories defined by the virus size; Large viruses ( $>200\text{nm}$ ) and small viruses ( $<200\text{nm}$ ).

The virus particulate can be concentrated by positive dielectrophoresis. Thereafter, localized clusters of the viral particulate can be formed around areas where the field is the highest which may further facilitate better inactivation. Morgan and Green et al. successfully demonstrated the use of DEP in concentrating viruses. The group concentrated Tobacco Mosaic Virus (TMV) (280nm) using positive pDEP using saw-tooth electrodes with  $2-6\mu\text{m}$  pitch spacing [15]. The virus was found to be highly polarizable and the polarizability was attributed to the absence of the insulating membrane. The group also showed that TMV could also be separated and filtered out from a mixture of TMV and Herpes Simplex Virus (HSV) by exploiting the difference in the CM factor which is entirely dependent on the virus's composition and structure[23]. Finally, the group also explored the prospects of DEP on HSV. A pDEP was observed when the HSV virus was subjected to a non-uniform field with frequencies below 4.5MHz with a 5V peak to peak voltage and a field strength equivalent to  $10^6 \text{ V/m}$  [16]. Manipulation of Vaccinia virus is also well documented in the literature. A study reported the use of Interdigitated Ti/pt electrodes to trap Vaccinia virus using pDEP with a 7V peak to peak Voltage and 1MHz frequency [17]. Recent years have seen the use of nano fibres for trapping viruses [24]. Although, nanofibres are particularly good at trapping the virus from a flowing sample, they cannot concentrate the virus. Similar inferences can be gathered from the studies that suggest the use of electrostatics to trap the corona virus[25, 26]: The virus can only be trapped not concentrated. However, all of the above viruses are moderately large Deoxyribonucleic Acid (DNA) viruses with an inner surface area high enough to amass enough

Name	Size	Type	Capsulation	Trapping Force	Electrodes
Tobacco Mosaic Virus	280nm	RNA virus	Non-enveloped	pDEP	Sawtooth (6um) [15]
Herpes Simplex Virus	240nm	DNA virus	Enveloped	pDEP	Quadrupole (6um) [16]
Vaccinia	360x270 x250 nm	DNA virus	Enveloped	pDEP	Interdigitated (10um) [17]
Influenza	90nm	RNA virus	Enveloped	nDEP	Quadrupole, Interdigitated (6um)(40um) [18]
Hepatitis A virus	27nm	RNA virus	Non-enveloped	nDEP/ pDEP	Quadrupole/ Octupole (2um)[18]
Cowpea Mosaic virus	30nm	RNA virus	Non-enveloped	pDEP	Castellated (2um)[19]
Adeno Virus	90nm	DNA virus	Non-enveloped	iDEP	Castellated/ interdigitated (10um)[20]
Sindb virus	130nm	RNA virus	Enveloped	iDEP	Sawtooth electrodes (gradient gap) [21] (0-700V)
T4 bacteriophage	90nm	DNA virus	Non-enveloped	iDEP	Circular and oval (80um) (~1100V)[22]

**Table 2-1:** Type of Viruses and their dielectrophoretic trapping parameters

charges to facilitate its manipulation. As particle dimensions shrink, controlled manipulation of particles becomes increasingly difficult due to the fact that induced dipole moments scale with the third power of the particle radius.

Nonetheless, smaller viruses were also shown to respond to the dielectrophoretic effect. Influenza (80nm) and Hepatitis virus (32nm) were manipulated and concentrated using negative Dielectrophoresis (nDEP) on planar electrode arrays. Planar platforms and 3D structures that made use of quadrupole and octupole electrode cages established points of confluence where the virus can be trapped effectively [18]. Cowpea Mosaic Virus (CPMV) (30nm) which is a spherical virus was shown to be successfully trapped using castellated electrodes with a pitch size of  $2\mu\text{m}$  [19]. Despite having a small size, CPMV shows a higher polarizability than that of the medium which is because of its non-enveloped nature. Same is true for Adeno Virus and Rota virus which despite having a small size were easily trapped and concentrated using pDEP [20]. pDEP trapping of viruses was observed in mediums with lower solution conductivities than that of bacteria. A challenging problem here is that with the increase in electro-lyte conductivity, the ionic strength increases which may result in more electro-chemical reactions and usually, virus samples require a relatively high ionic strength of media for their storage. Another challenging problem is that smaller viruses ( $<100\text{nm}$ ) show a random brownian motion under the application of a non-uniform electric field. Brownian motion is characterized by random movements which could cause hindrance in the trapping of viruses [20, 27]. These problems can be resolved by attaching the virus to a larger molecule; for eg Hepatitis A virus (27nm) bonded to a streptavidin coated particle [28].

Insulator based DEP (iDEP), a technique that uses insulating structures to concentrate the electric field, seems to be more common place in concentrating smaller viruses as well as larger viruses. For example, influenza virus (90nm) [29], Sindb virus (130nm) [21], bacteriophages like T4 and SPN3UP (90nm) [22] and other larger viruses like TMV [30] have been concentrated by this technique. A study which made use of circular and oval shaped electrodes employed this method to trap 3 different strains of the same bacteriophage demonstrating the high specificity of this technique [22]. However, no study has scientifically established the better efficiency of iDEP over DEP in terms of trapping and concentrating the virus particles. Moreover, iDEP devices are more susceptible to joule heating and electrolysis of the medium [31]

### 2-1-2 Modelling of the SARS COV-2 under the influence of DEP

The SARS CoV-2 Virus is characterized by a lipid insulating membrane and hence the particle may not be easily polarizable. Tuning properties of the medium becomes instrumental if we desire to attract and concentrate the virus particles with pDEP. The Clausius Mossotti factor of the SARS CoV-2 can be modelled by using a core shell model. The inner layer represents the core and the outer layer represents the lipid membrane. We have DEP force on a neutral particle described by the equation:

$$F = 2\pi\epsilon_s\epsilon_o R^3 Re[(\epsilon_p^* - \epsilon_s^*)/(\epsilon_p^* + 2\epsilon_s^*)] \nabla E^2 \quad (2-5)$$

Where  $\epsilon_p$  is the permittivity of the particles  $\epsilon_s$  that of the suspending solute, R the radius of the particle, E the applied field and  $\nabla E$  the divergence. According to eq. 2-1, the force can

be attractive or repulsive depending on the values for  $\varepsilon_p$  and  $\varepsilon_s$ . Note that the permittivities are actually complex quantities, the real and imaginary part of which usually will change with the applied  $\omega$ . Keeping the value of  $\varepsilon_s$  constant, changes in the CM factor contributed only by the conductivity and permittivity of the particle's membrane and core can be observed. For a two shell model, the equation for the real part of  $\varepsilon_p$  is given by:

$$\varepsilon_p^* = \varepsilon_m^* \frac{(R/r)^3 + 2(\varepsilon_c^* - \varepsilon_m^*/(\varepsilon_c^* + 2\varepsilon_m^*))}{(R/r)^3 - (\varepsilon_c^* - \varepsilon_m^*/(\varepsilon_c^* + 2\varepsilon_m^*))} \quad (2-6)$$

We can visualize the virus as core-shell structure, in which the permittivity of the RNA-core  $\varepsilon_c$  and that of the membrane proteins  $\varepsilon_m$  are complex, frequency dependent quantities. The radius of the core is  $r$  and that of the outer layer is  $R$ . See figure 2-2.

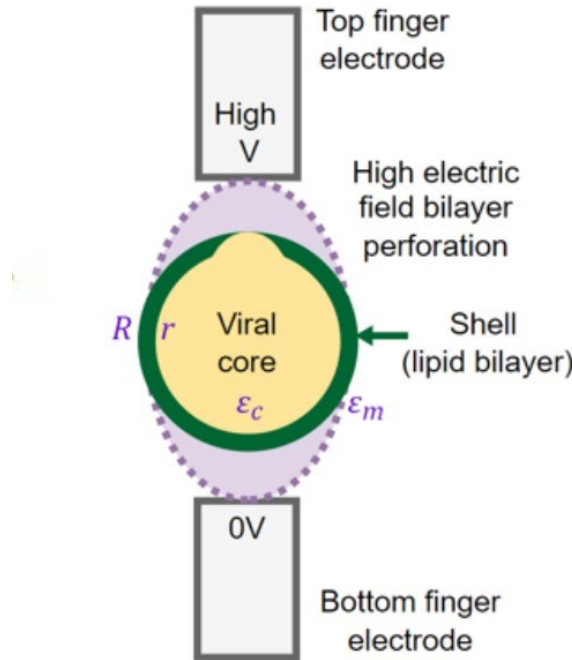


**Figure 2-2:** Core shell model of SARs CoV-2

When we substitute equation 2-6 in the real factor of CM factor we get:

$$\frac{\varepsilon_p^* - \varepsilon_s^*}{\varepsilon_p^* + 2\varepsilon_s^*} = \frac{R^3(\varepsilon_c^* + 2\varepsilon_m^*)(\varepsilon_m^* - \varepsilon_s^*) + r^3(\varepsilon_c^* - \varepsilon_m^*)(2\varepsilon_m^* + \varepsilon_s^*)}{R^3(\varepsilon_c^* + 2\varepsilon_m^*)(\varepsilon_m^* + 2\varepsilon_s^*) + 2r^3(\varepsilon_c^* - \varepsilon_m^*)(\varepsilon_m^* - \varepsilon_s^*)} \quad (2-7)$$

Selecting a medium such that  $\varepsilon_s < \varepsilon_m$ , a pDEP force on the corona virus to effectively concentrate the virus can be produced at lower frequencies. Of course, the force would also depend on the frequency of the electric field as all of the parameters are complex quantities.

Unfortunately, studies have not delineated the electrical parameters of the SARS CoV-2. Thus the simulation presented in figure B-3 assumes values of permittivity and conductivity by looking at the parameters of other viruses like the Vaccinia virus or the Herpes simplexvirus [32]. Nonetheless, for a KCL solution with a lower conductivity ( $<0.05\text{mS/m}$ ) and

as long as  $\varepsilon_m > \varepsilon_s > \varepsilon_c$ , the graph in figure 2-3 shows that the virus would be attracted to the electrodes at achievable electric field frequencies. Of course, the permittivity of the membrane and core of the particle are intrinsic and cannot be controlled. Moreover, we do not suspect the permittivity of the membrane of coronavirus to be higher than 78 (permittivity of water). The attraction by pDEP then depends heavily on the medium conductivity. This is also highlighted by the graph; for lower conductivity of the medium the range of frequencies at which we can attract the virus by pDEP increases regardless of membrane and core permittivity of the virus particle. This calculation does not take into consideration the negative charges that are already present on the RNA molecule inside the core of the virus. This assumption is supported by previous studies that show the dielectrophoretic mobility is not affected by the interior charges in Cowpea Chlorotic Mottle virus [33] as well as the Corona virus [25]. The parameters considered for the given simulation are as follows-  $\varepsilon_s = 78$ ,  $\varepsilon'_c = 70$ ,  $\varepsilon'_m = 12$ ,  $\gamma_c = 0.2 \text{ S/m}$ ,  $\gamma_m = 1 \times 10^{-9} \text{ S/m}$ ,  $R = 60 \text{ nm}$ ,  $r = 54 \text{ nm}$ .

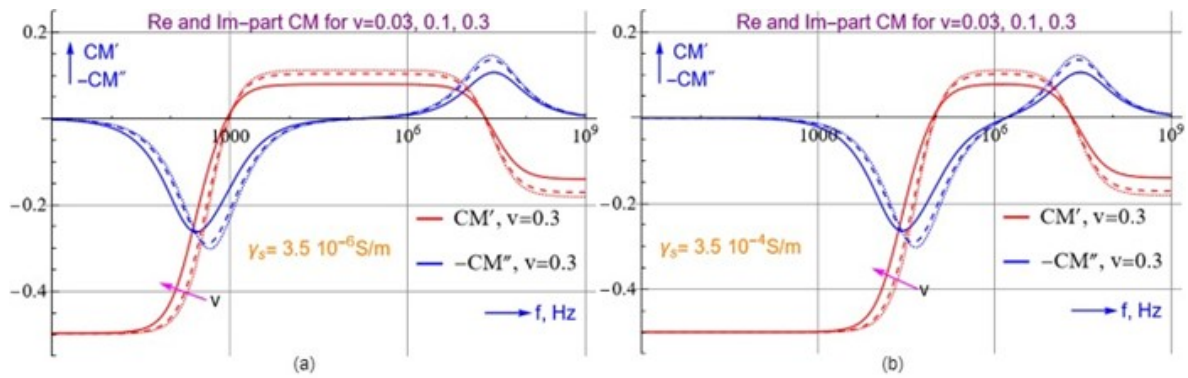


**Figure 2-3:** CM factor of coronavirus (Conductivity and the permittivity of the membrane are loosely assumed)

As long as a medium conductivity of  $<0.05 \text{ mS/m}$  is maintained, there is a high chance that corona virus can be concentrated with moderately high frequencies and electric fields. For the experiments, it is crucial that we suspend the virus in a medium with a very low conductivity.

## 2-2 Inactivation of viruses using electric fields

Electrical inactivation of bacteria or viruses is a technique that refers to a process that uses electric fields to render the organism incapable of replicating or infecting a host. So far very few studies have focused on the inactivation of viruses, let alone the SARS COV-2; many studies focus on the inactivation of bacteria and have successfully demonstrated their inactivation by irreversible electroporation. The mechanism of inactivation of viruses is still unexplored and is uncertain. Nonetheless the probable mechanisms of inactivation (irreversible electroporation and Spike deactivation) of the SARS COV-2 are discussed below.

### 2-2-1 Inactivation by Irreversible electroporation

Irreversible electroporation results in electrical lysis which refers to the breaking down of plasma membrane using electric fields. The lysis results from the creation of a transmembrane potential that is directed from outside to inside of the cell as a result of accumulation of charges. The transmembrane potential causes the dipoles in the phospholipid membrane to reorient themselves which creates pores. When the transmembrane potential exceeds a certain threshold, the pores become larger and electroporation occurs (refer figure 2-4). With further increase in the electric field, the pore formation becomes irreversible which results in lysis. The transmembrane voltage to achieve cell lysis is around 1 V [34]. The transmembrane

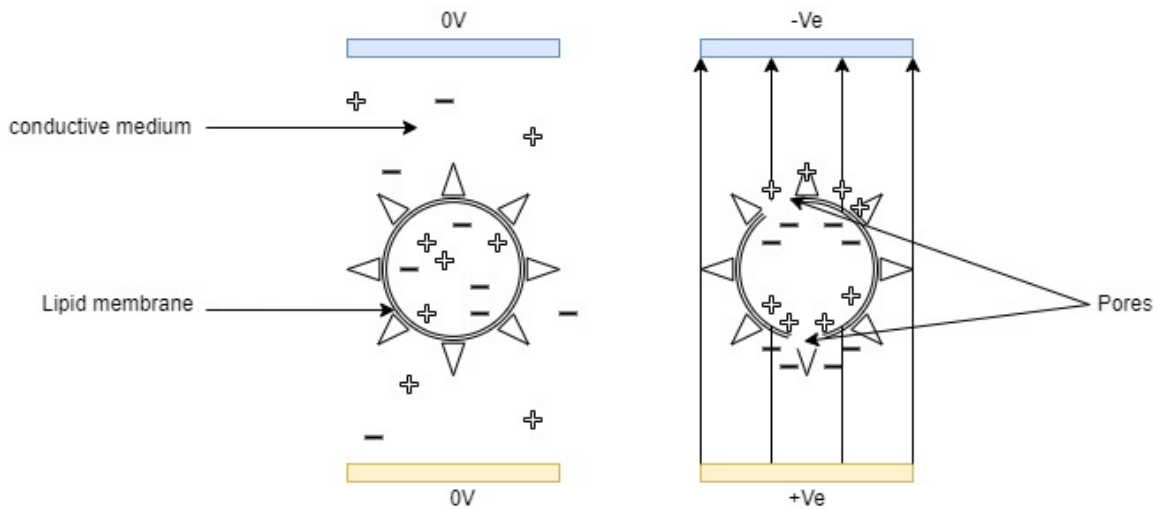


**Figure 2-4:** The electroporation of a micro particle with a bilipid membrane suspended in a conductive medium

potential produced by an AC electric field was first derived by Mernier et al. [35] is given by the following equation:

$$\nabla V_{memb} = \frac{F.a.E.\cos\theta}{(1 + (\omega.\tau)^2)^{1/2}} \quad (2-8)$$

Where  $\omega$  is the frequency of the alternating current; and  $\tau$  is a coefficient determined by the capacitance of the cell membrane, resistance of the cytoplasm, and resistance of the suspended liquid in the cell. The electric field strength depends on the voltage supplied and the distance between the electrodes. To create a transmembrane potential around smaller particulate like viruses with safe voltages smaller pith between the electrodes is needed.

### Inactivation of viruses and bacteria by irreversible electroporation

The only paper that reported the inactivation of a virus by irreversible electroporation used AC field to concentrate and lyse the virus. The study reported the electrical lysis of Vaccinia virus and it is the only virus shown to have been successfully lysed using electric fields [32]. The damaged virus particles and DNA traces tagged by fluorescent agents on chip surfaces were found on the device surface were confirmed with the Scanning Electron Microscope (SEM) images. The use of electric fields has been used extensively to inactivate bacteria by

irreversible electroporation. The parameters used for the electrical excitation are also crucial in achieving higher inactivation rates. Many of the studies used Pulsed excitation to kill the bacteria [36, 37, 38]. With pulsed electric field, the parameters that need to be set are the pulse number, pulse shape, pulse amplitude and the pulse width. The parameters used across lysis experiments seem to have been influenced by the shape and size of the particle being lysed. However in general, in bacteria as well as in cells, it was noted that higher lysis levels were attained with a longer pulse duration. Furthermore, higher pulse amplitudes were needed to lyse particles with smaller diameters[39, 40, 41]. If a medium with a low conductivity is used, a higher pulse amplitude and a larger pulse duration is required to achieve irreversible electroporation[42]. Higher lysis rates were observed with bipolar rectangular pulses than with sinusoidal pulses [43] while another study maintains that monopolar pulses were found to be better than bipolar pulses[40]. Albeit a larger pulse amplitude may facilitate a higher lysis rate, it may well result in the electrolysis of the conducting medium. To avoid electrolysis of the conducting medium an AC excitation may be employed. Cells and bacteria have been effectively lysed using AC excitation [44, 45, 46]. In general, while the large magnitude of  $\nabla E^2$  is useful to induce a strong DEP force in most dielectrophoretic studies, increase in the field strength  $E$  causes electroporation. We can optimize the geometry such that the divergence as well as the field strength are maximized to attract the particles at points of high electric field for an effective lysis.

### Modelling inactivation of the SARs COV-2 by irreversible electroporation

We can assume the virus to be suspended in a buffer solution with a relatively high (ionic) conductivity  $\gamma_e$ . The core of the virus will most likely also have a significant conductivity  $\gamma_c$ . The membrane, which consists of lipids can be expected to have a low conductivity  $\gamma_m$ . These parameters of the virus were hinted at by K. Sholanov in his scientific essay [47]. It is the conductivities that rule the steady state value of the membrane voltage, if a DC step voltage is applied. This value can be derived by solving the Laplace equation for a layered spherical particle. A comprehensive description of the derivation can be found in Kotnik et al [42, 48]. They derived the following expression:

$$V_m = f E_a R \cos \theta \quad (2-9)$$

where  $f$  is the conductivity factor,  $E_a$  the applied field,  $R$  the radius of the virus and  $\theta$  the direction of  $E_a$ . The factor  $f$  equals:

$$f = \frac{2\gamma_e[(\gamma_y - \gamma_c)(r/R)^3 + \gamma_c - 3\gamma_m r/(R + 2\gamma_m)]}{2(\gamma_c - \gamma_m)(\gamma_m - \gamma_e)(r/R)^3 + (\gamma_c + 2\gamma_m)(\gamma_m + 2\gamma_e)} \quad (2-10)$$

Where  $r$  is the radius of the core. Note that we have modified Kotnik's formula to the one given earlier by Neumann in 1989 [34]. Schwan et al. has given an approximation of the formula for the final value of  $V_m$  in response to a step voltage[49].

$$V_m = 3/2 E_a R \cos \theta \quad (2-11)$$

Here, the  $3/2$  coefficient corresponds to  $f$  for when  $\gamma_m = 0$ . To produce a trans-membrane potential of 1V we need a field of  $8.3 \text{ V}/\mu\text{m}$ . Grosse et al extended the model to a spherical cell with 2 layers [50]. The expression for  $f$  then reduces to eq. 2-11, if the thickness of the

2nd layer is insignificantly thin. Under the influence of AC voltages, conductivities in eqs. 2-9 and 2-10 are replaced by complex permittivities. This leads to an  $f$  that depends on the radial frequency  $\omega$ .

### 2-2-2 Inactivation of SARS COV-2 by Spike Deactivation

In 2021, a lot of studies focused on the inactivation of the SARS CoV-2 using agents other than the primary chemical and optical disinfectants. Chief among these studies was the simulation study carried out by Arbeitman et al. [1] that suggested the use of moderate electric fields could be enough to in-activate the corona virus. Through molecular dynamic simulations Arbeitman showed that electric fields as high as  $10^5 - 10^7$  V/m stretch the dipoles found in the Spike proteins of the virus and change the protein structure permanently. Irreversible structural changes especially on the Receptor Binding Domain (RBD) of the spike protein render the virus incapable of docking to the the host cell's receptors (see fig B-3).

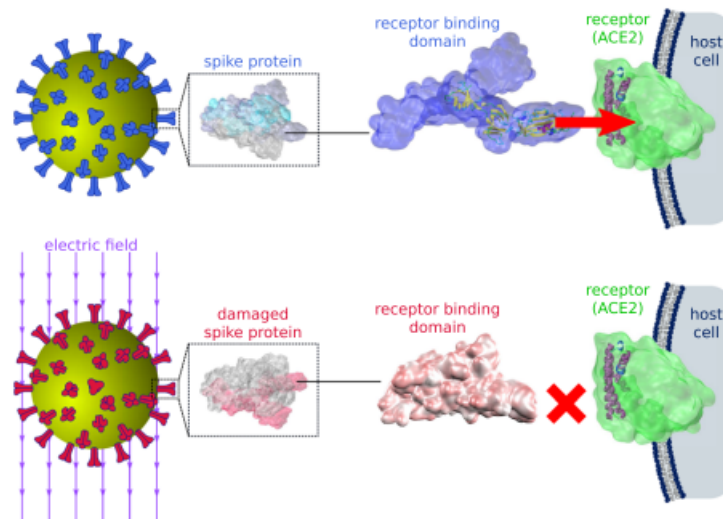


**Figure 2-5:** Inactivation of the SARS CoV-19 by damaging the spike protein using moderate electric fields [1]

Another study elucidated more on the effect of pulse electric fields on the conformational changes of the virus' proteins [51]. It suggested that different amplitudes and intensities of pulses have different effects on the conformational changes at different locations of the RBD on the spike protein. The study further expounded that a stimulus with a higher amplitude and higher intensity is better at reducing the structural stability of the protein. The underlying conclusion from this study was the same as that from the Arbeitman's study: Corona virus can be deactivated using moderate electric fields. The fields used for the simulations in this study however were slightly higher than the fields used in previous study. ( $1.5 - 2.9 \times 10^9$  V/m). Another study showed successful inactivation of the SARS virus using metal nano-particles. The study reported inactivation of the virus by exposing aerosols of the virus sample to face masks embedded with zinc and silver nanoparticles. The two different metal particles created tiny batteries when the droplets containing the virus settled between them. The electric potential generated between the two metal particles decreased the stability of the virus and

resulted in a quite significant inactivation rates [52]. Although the study does not delve into the mechanisms of inactivation, it may be possible that the inactivation reported in Ghatak's study is a result of the inactivation mechanisms suggested by Arbeitman [1].



# Electrode design and simulations

### 3-1 Electrode design

Using electric fields as a tool may allow us to integrate concentration and inactivation on a single microchip platform. In the previous chapter we learnt that the distribution of nonuniform electric field inside the suspending fluid depends on the excitation potential applied, the electrical parameters of the particle and on the fluid itself. Deciding the electrical parameters of the conducting medium are instrumental in facilitating pDEP to trap the virus between the electrodes at points of high electric field for efficient inactivation. However, the electric field also depends on the configuration and geometry of the micro-electrodes. The electrode geometry is an important parameter; Geometries that maximize both concentration and killing should be employed. This chapter explores the efficiency of some of the electrodes through simulations and literature.

Experiments have used a variety of configurations to concentrate and to inactivate bacteria and virus. These configurations are either 3D or 2D in structure. 3D electrode configurations produce a DEP force with a larger divergence and hence have a greater penetrating power within the sample. For concentrating and killing smaller viruses, studies focus on 3D nano-electrode arrays with carbon nanotubes that create extremely high electric field strengths at the tips [53, 24, 54]. A few studies have demonstrated that the use of micro-channels to generate high electric fields by controlling the channel width. These 3D structures are shown to be more effective at concentrating bigger organisms [55, 56]. Furthermore, various studies that have compared the performance of 3D electrodes to that of 2D electrodes maintain the superiority of 3D electrodes in inactivation of various larger organisms like bacteria and yeast cells [57, 58]. Smaller viruses could as well be more susceptible to inactivation fields created by 3D electrodes than by 2D electrodes. However, 3D electrodes are more difficult to fabricate and often need a microchannel to contain the sample. Planar electrodes are very easy to fabricate. 2D Electrode layouts like the quadrupole [59, 18, 60] and micro-well electrodes [61, 62] are good for single cell analysis and do not generate many high electric field points for effective concentration and killing. Whereas, electrode geometries like the matrix geometries [63, 64] create many local electric field points that facilitate concentration but the

local electric fields are not high enough for an efficacious inactivation. In another literature it was found that oval ducts are better at generating non-uniform fields than circular ducts [22]. The different electrode geometries and their performance in concentrating has been tabulated by other studies [2]. These different geometries have been shown in figure 3-1.

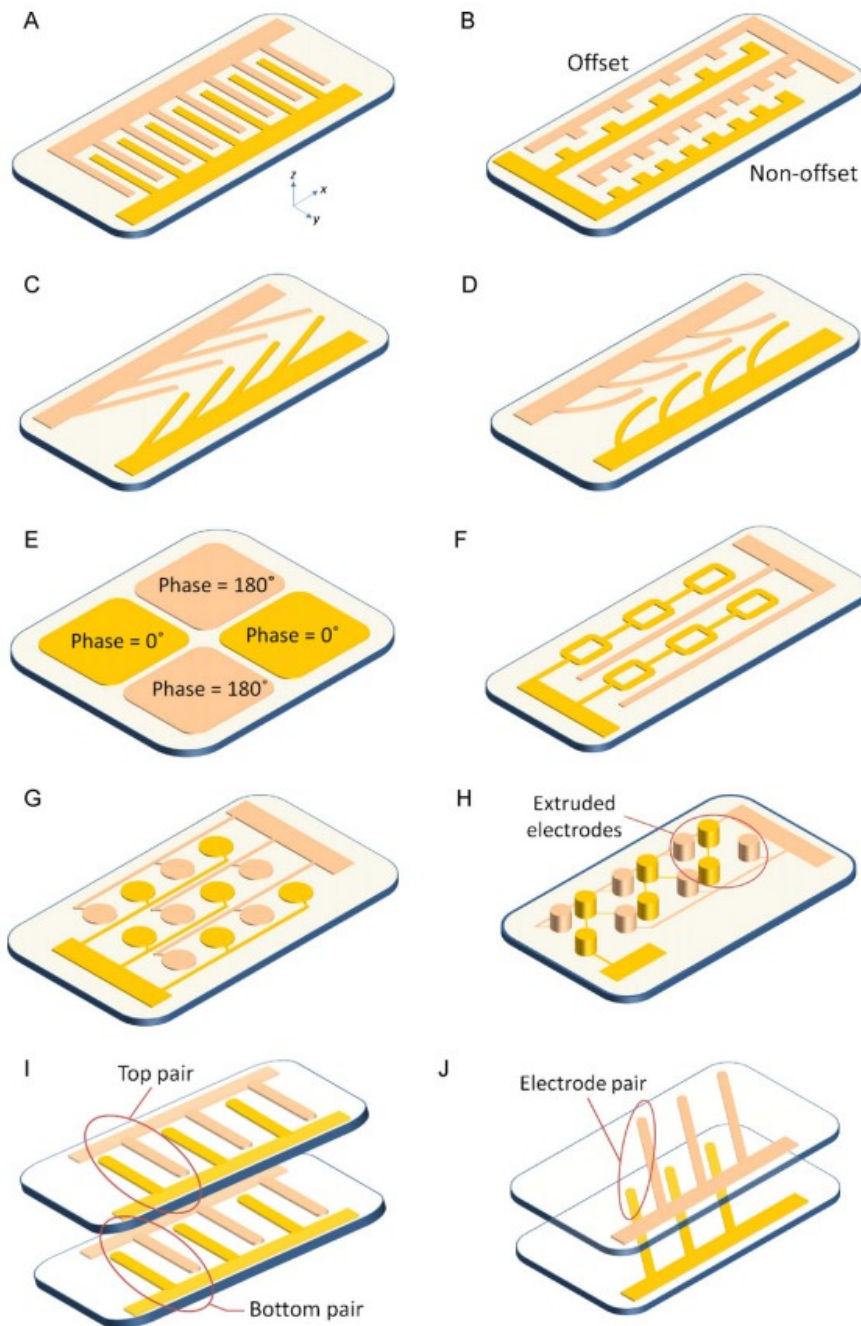


**Figure 3-1:** Different 2D and 3D electrode geometries (A) parallel or interdigitated, (B) castellated, (C) oblique, (D) curved, (E) quadrupole, (F) microwell, (G) matrix, (H) extruded, (I and J) top-bottom patterned [2]

Prominent among the 2D configurations that maximize the high electric field spots and that provide a wider area for virus inactivation are the sawtooth, parallel/interdigitated and the castellated electrodes. These electrode geometries have been simulated on COMSOL Multiphysics and the results of the simulation have been discussed below.

## 3-2 Electrode design simulations

### 3-2-1 Castellated electrodes

Castellated electrodes can be in phase and out of phase. Given in the figure 3-2 and 3-3 bellow are the electric field distributions of in phase and 90 deg out of phase castellated electrodes respectively.

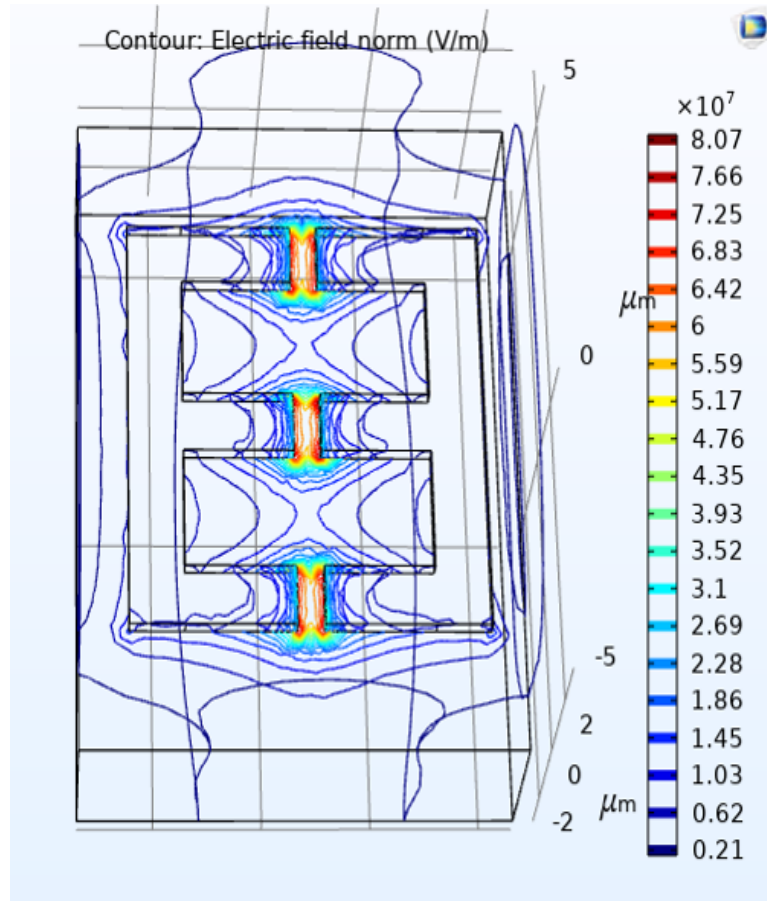


**Figure 3-2:** Electric field distribution of in phase castellated electrodes

With an DC input of 30V the castellated electrodes generate a field of  $10^7$  V/m which according to Arbeitman's study is enough to inactivate the SARS CoV-2 by spike deactivation. The out of phase castellated electrodes generate more local spots of high electric field than the in phase castellated electrodes. Nonetheless, the in-phase castellated electrodes create a larger area of the high electric field which could be better for inactivation. These electrodes

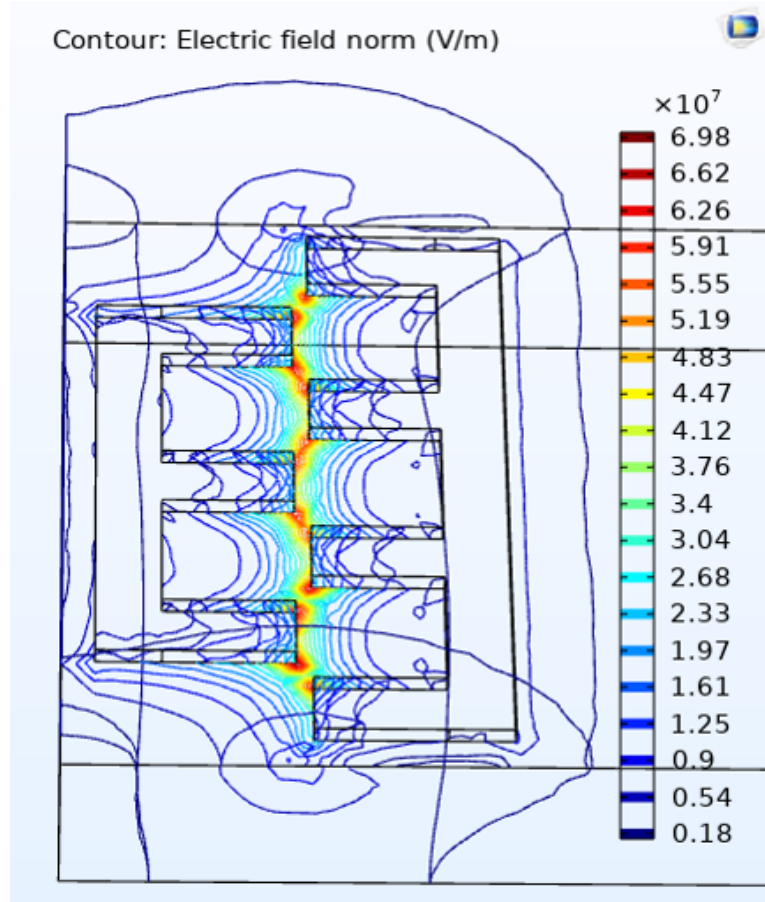


**Figure 3-3:** Electric field distribution of out of phase castellated electrodes

may be better than the parallel/interdigitated electrodes as they have more local spot of high electric field.

### 3-2-2 Interdigitated electrodes

Interdigitated electrode create a less non-uniform electric field with very few high electric field points. Tathireddy et al. have already given the equations for electric field on interdigitated electrodes in x and in y direction[65]. The behaviour of the electric field by interdigitated electrodes can be modeled by these equations.

$$Ex = \sum_{n=1}^{\infty} f_n b_n \sin(b_n \cdot x) \exp(-b_n \cdot y) \quad (3-1)$$

$$Ey = - \sum_{n=1}^{\infty} f_n b_n \cos(b_n \cdot x) \exp(-b_n \cdot y) \quad (3-2)$$

where,  $b_n = n\pi/2d$  where,  $d = (d1 + d2)/2$  where,  $d1$  is the width of the electrode and  $d2$  is the gap distance. and  $f_n$  is the fourier coefficient given by

$$f_n = \frac{2V_{eff}}{b_n^2 d^2} [\cos(b_n \cdot d/2) - \cos(3b_n \cdot d/2 - b_n d/2 \sin(2b_n d))] \quad (3-3)$$

These equations suggest that with increase in  $d_1$  and  $d_2$  the field in  $x$  and  $y$  directions increases. The penetration power of the electrodes into the medium can be hypothesized to increase only slightly with the increase in the pitch and with a higher pitch to gap ratio. A higher penetration power of the electric field and a higher divergence ensure a higher dielectrophoretic force on the particles. Likely so, these configurations are mostly used for dielectrophoresis [20, 66, 17, 67]. Nonetheless, interdigitated electrodes can still be used for the lysis of larger cells and bacteria ( $> 1\mu\text{m}$ )[68]. Interdigitated electrodes usually have a simple fabrication. A DC input of 30V generates a more uniform lower electric field that reaches a maximum value of  $3 \times 10^7$  V/m only at the corners of the electrode. The electrode generates very few regions of high electric field and thus provide very few virus inactivation zones.

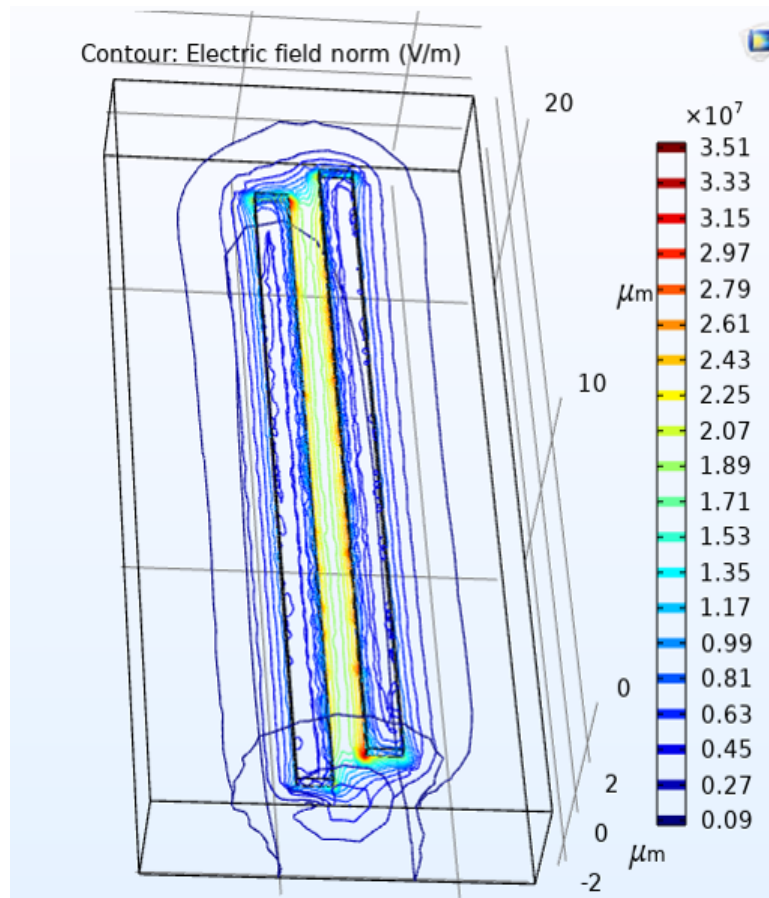


**Figure 3-4:** Electric field distribution of interdigitated electrodes with  $1\mu\text{m}$  pitch

The increase in penetration power of the electric field as suggested by Tathireddy et al. is also supported by the electrode simulations. In fig. 3-5 the electric field displacement is mapped on the points of a vertical cut line that extends from the base of the substrate to  $20\mu\text{m}$  penetrating through the sample medium. The gap between the electrodes is  $500\text{nm}$ ,  $5\mu\text{m}$  and  $10\mu\text{m}$ . The graphs show that there is no electric field within the substrate (glass). The electric field shoots up as soon as the medium begins and is highest for the electrode geometry with the smallest gap and pitch. The high field is very close to the surface of the substrate and reduces quickly in the  $z$  direction along the cut line. Penetration of electric

field through the medium is slightly higher in electrodes with a larger electrode gaps than the smaller electrode gaps (see fig. 3-5) However, for all practical purposes it is important that the virus sample to be treated is deposited as a thin film of around  $20\mu\text{m}$  on the top of the electrode for all the virus particles to be under the influence of the electric field because after the  $35\mu\text{m}$  the electric field almost becomes negligible across all pitch and gap geometries. The virus particles furthest from the surface are expected to be attracted to the the electrode surface to the high electric field spots. The pitch also has an influence on the electric fields

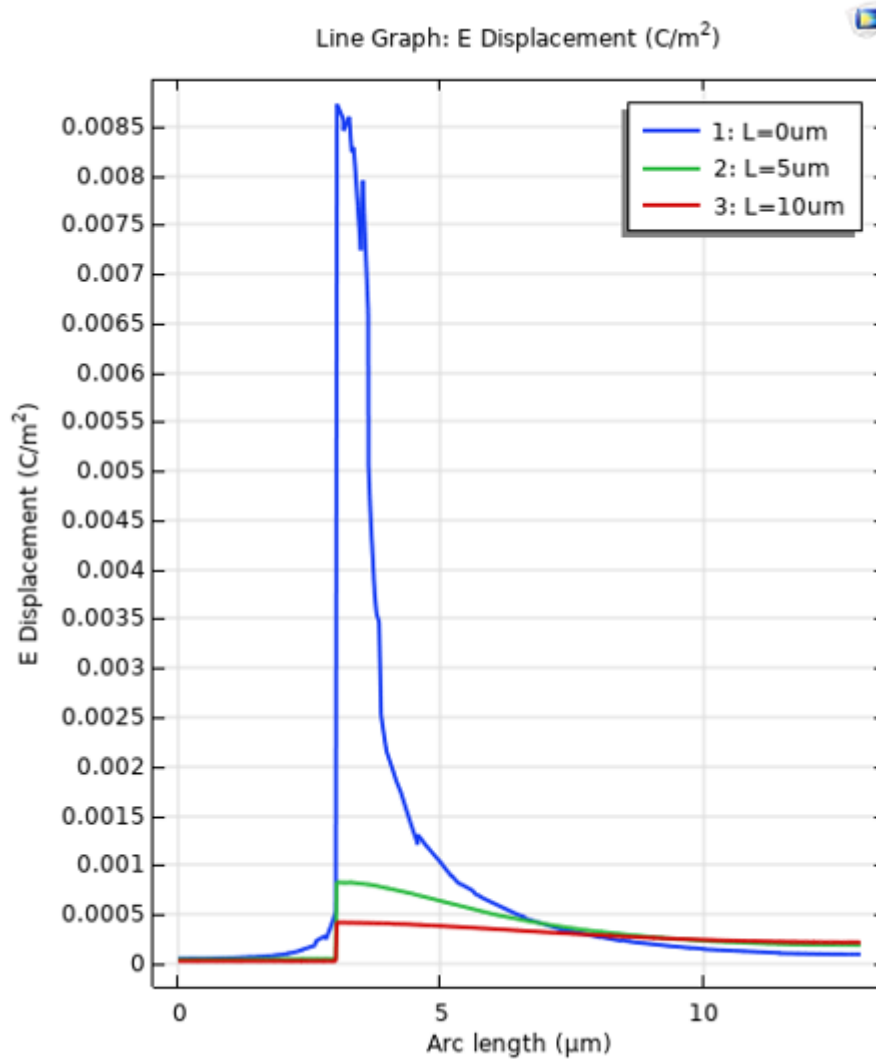


**Figure 3-5:** Comparison of the penetration of the electric field displacement in the medium with increasing pitch distances

created on the X and Y plane. The graph in fig. 3-6 shows that the electrodes with smaller gaps have a higher electric field displacement very close to the substrate than the ones with a larger electrode gap. The electric field falls as the distance between the electrodes increases.

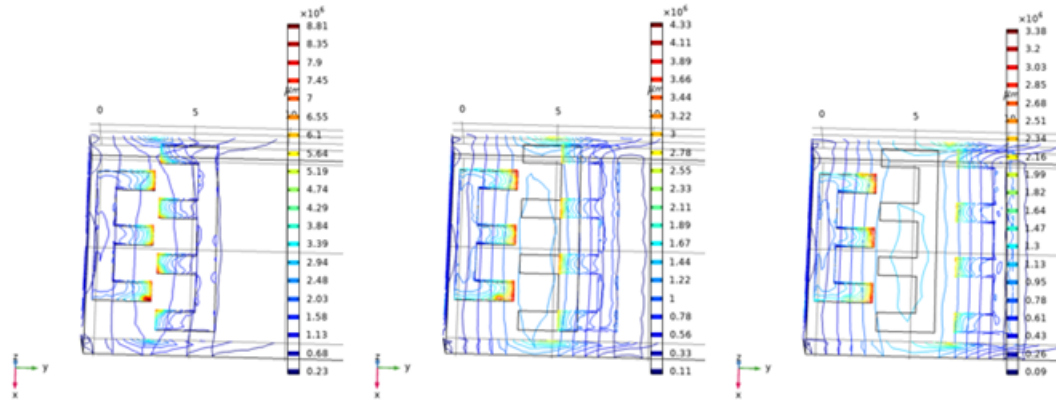


**Figure 3-6:** Electric field generated by different pitch distances of the out of phase castellated electrode

### 3-2-3 Saw-tooth electrodes

Saw tooth electrodes have been extensively used to concentrate [21, 15] as well as inactivate micro-particulate [69]. The pitch distance between the electrodes can be specifically tailored to tune the electric field strengths and the areas of concentration. The figure 3-7 represents model simulation of a saw-tooth electrode with a voltage input magnitude of 30V. Based on the simulations, with a pitch distance of  $1\mu\text{m}$ , the sawtooth configurations create many local high electric field spots. The electric field strength does increase with a decrease in the pitch distance.

## 3-3 Formulation of Hypotheses

Based on the literature study and the simulation results, five hypotheses are formulated. The project thesis aims at testing these five hypotheses. The formulated hypotheses are as follows:

- The SARs CoV-2 virus can be inactivated using electric field generated by planar micro-electrodes.
- Castellated geometries generate more local spots of high electric field and hence are better at inactivating the virus than interdigitated geometries.
- The electrodes with a smaller gap are better at inactivating the virus as they generate higher electric fields than the electrodes with a larger gap.
- For efficient and higher inactivation rates of the sample the virus needs to be attracted to the surface of the electrode where the field is maximum.
- Medium conductivity plays an important role in facilitating DEP attraction to allow efficient inactivation

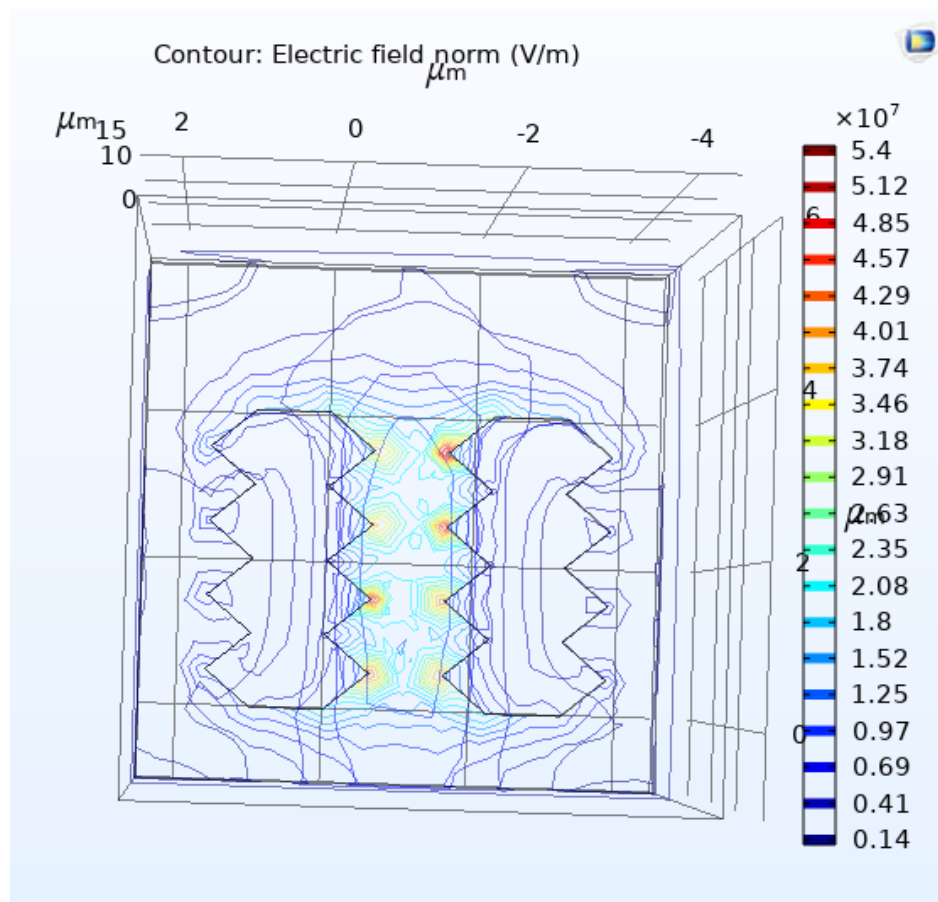


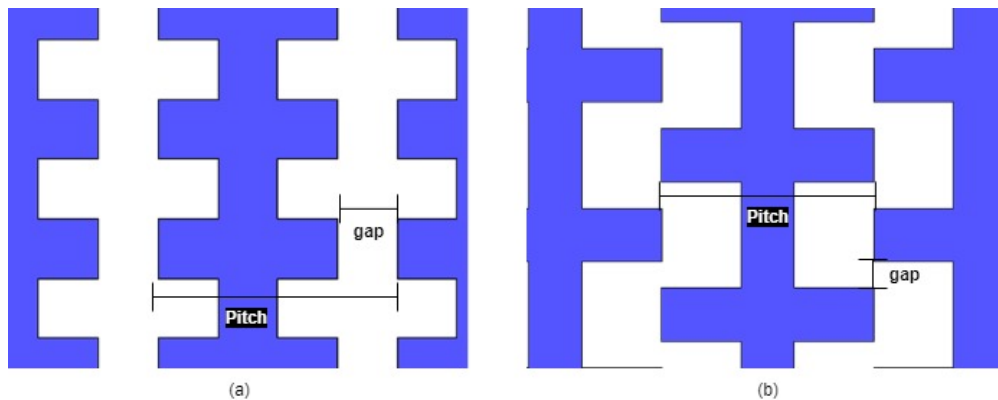
**Figure 3-7:** Electric field distribution of saw tooth electrodes

## Device Fabrication

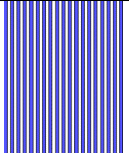
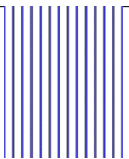
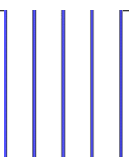
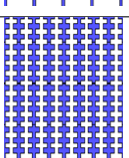
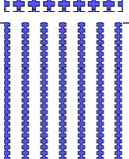
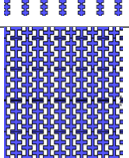
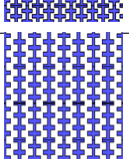
### 4-1 Process steps for device fabrication

#### 4-1-1 Design of Photolithographic masks

The efficiency of the total virus inactivation rate is explored across three different electrode patterns. The three different electrode patterns are shortlisted from the literature and from the simulation results. The electrodes included in this study are the interdigitated and castellated (in phase and  $180^\circ$  out of phase) electrodes. There are different levels of pitch sizes in each electrode pattern (two levels in castellated and three levels in the interdigitated) resulting in 7 different unique electrode geometries. The different geometries designed on the photolithographic mask are covered in table 4-1. The pitch is defined as the sum of the distance between the two digits of the electrodes and the width of the electrode digit. The gap is defined as the shortest distance between the electrodes where the electric field can be produced. These definitions are highlighted in the figure below 4-1.



**Figure 4-1:** Definition of Pitch and gap on (a) Electrode geometry Cin4 (b) Electrode geometry Cout4.

Electrode pattern	Width	Pitch	Gap	Geometry name	Image
Interdigitated	1 $\mu\text{m}$	2 $\mu\text{m}$	1 $\mu\text{m}$	I2	
	1 $\mu\text{m}$	5 $\mu\text{m}$	4 $\mu\text{m}$	I5	
	1 $\mu\text{m}$	10 $\mu\text{m}$	9 $\mu\text{m}$	I10	
Castellated (in phase)	1 $\mu\text{m}$	4 $\mu\text{m}$	1 $\mu\text{m}$	Cin4	
	1 $\mu\text{m}$	8 $\mu\text{m}$	5 $\mu\text{m}$	Cin8	
Castellated (out of phase)	1 $\mu\text{m}$	4 $\mu\text{m}$	500nm	Cout4	
	1 $\mu\text{m}$	5 $\mu\text{m}$	1.5 $\mu\text{m}$	Cout5	

**Table 4-1:** Patterns and their respective pitch distances designed on the photo-lithographic mask

Two photo-lithographic masks were designed using L-Edit v.16.03. The first mask that was designed for the ASML wafer stepper comprised of the different electrode geometries, array cuts, contact openings and other auxillary structures needed to make the electrode arrays (see figure 4-2). The ASML wafer stepper was programmed to arrange all the structures into layers to make the entire electrode pattern. The second mask was a full wafer exposure mask designed for the Contact Aligner. This mask consisted of the wafer level interconnects (see figure 4-3).

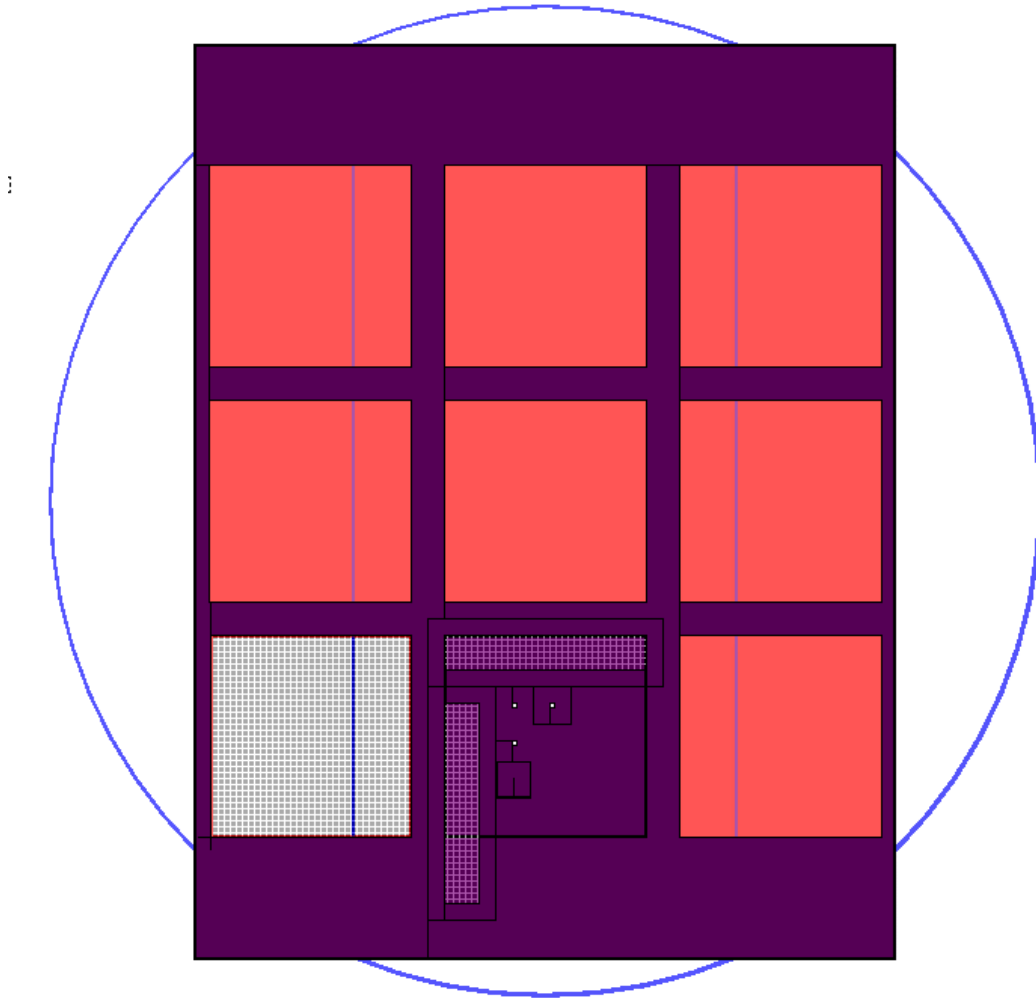


**Figure 4-2:** Design of mask for the ASML wafer stepper

The arrays designed on the wafer stepper mask were  $6mm \times 6mm$ . The wafer stepper was programmed to place these arrays in two columns and four rows to form the entire electrode such that each die pattern is segregated in 8 different square arrays, each housing a separate interconnect to improve the yield of the electrodes 4-4. The entire area of the electrode was  $12mm \times 24mm$ . The arrays were separated by exposing a part of the interconnect by an array-cut which created a divide and two different arrays. To increase the yield of the electrode, each array had its own set of interconnects and contact openings. This way, even

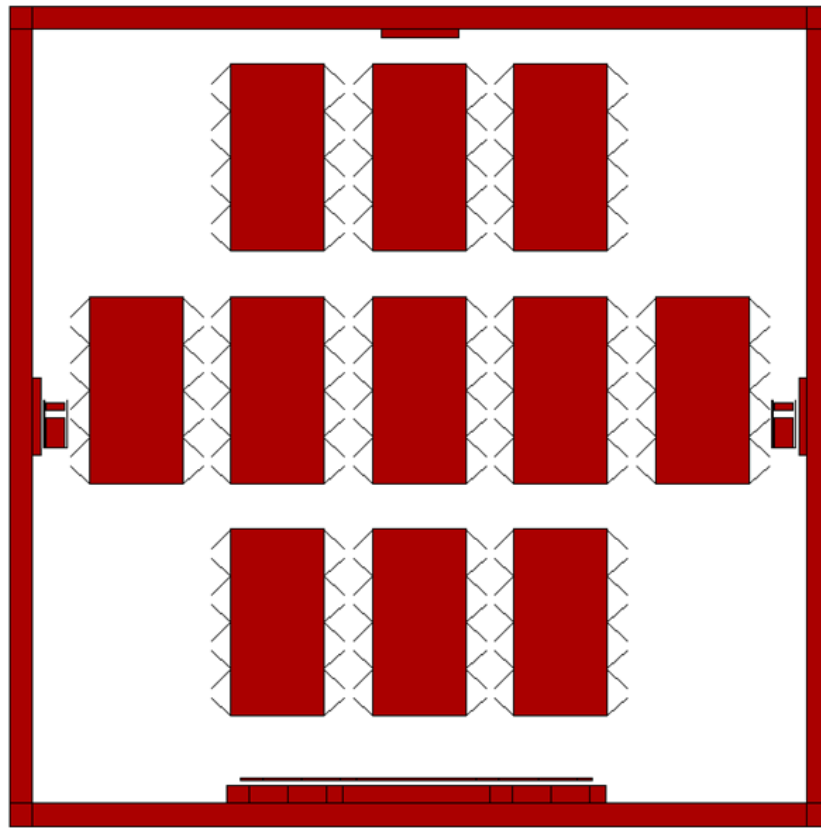


**Figure 4-3:** Design of mask for the contact aligner

if one array short circuits the electrode could still be used for the experiments.

#### 4-1-2 Programming the waferstepper

The structures on the waferstepper were arranged into layers. The first layer consisted of gratings and array cuts. These two structures were programmed in the waferstepper with the coordinates on the wafer where they were to be exposed. This included entering the coordinates of the different patterns on the mask and arranging them into the  $2 \times 4$  array matrix electrode pattern. The arrays were separated by entering the co-ordinates for the cut line that separated the arrays. The second layer had the contact openings. The contact opening were positioned over the the ends of the global interconnect such that they exposed the aluminium underneath. The third layer consisted of the vertical and horizontal bars for the Micro-dams. These structures created reservoirs of photoresist around the electrodes to contain the liquid virus sample. The horizontal and vertical bars were 1mm broad and were arranged around the active electrode area.

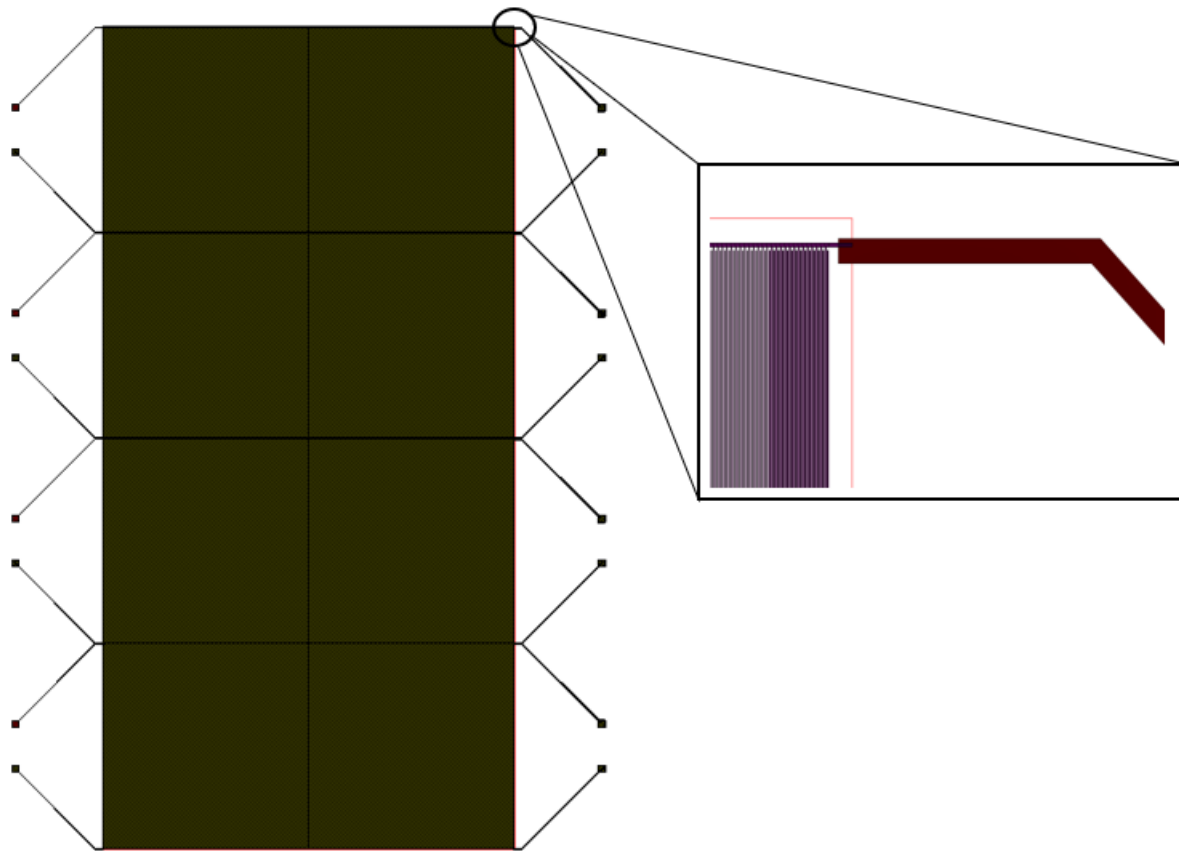


**Figure 4-4:** Quartering of the electrode area in 8 separate arrays

## 4-2 Fabrication process

The fabrication of the chip was done at the Else Kooi Lab at TU Delft. The fabrication process is discussed in detail under appendix A. A short summary of the fabrication process is presented in this section. It is as follows:

- Starting Material: glass wafer (Quartz)
- Aluminium Sputtering: front and back
- Alignment and exposure: electrode designs and interconnects
- Silicon oxide deposition: Plasma Enhanced Chemical Vapour Deposition (PECVD) deposition
- Alignment and exposure: Micro-dam sample container
- Wire bonding

## A. Starting Material

Glass was initially selected as the starting material as electric fields generated by metal-on-insulator are superior to silicon or silicon oxide wafers. However, Glass is a challenging substrate to process on as all the equipment in the cleanroom is designed to handle silicon wafers. Handling and detection in most of the equipment was done with the help of lasers. Hence, The wafers were sputtered with aluminium on both sides to make them opaque and detectable by the equipment's wafer handling system.

## B. Aluminium Sputtering

The wafers are loaded into the carrier on a carrier wafer. A 300nm thick aluminum layer is deposited by using the Trikon Sigma both on the front and back. 300nm thick layer of aluminium generates current densities in the order of  $1 \times 10^{10} \text{ A/m}^2$ . In case of short circuits, the joule heating resulting from this is 0.0159W for a simple interdigitated electrode that this 300nm thick. This is an acceptable value for joule heating and hence 300nm of aluminium was decided to be sputtered on the glass substrate. The current densities generated in the aluminium for a peak to peak sine wave of 20V are plotted in the figure 4-5

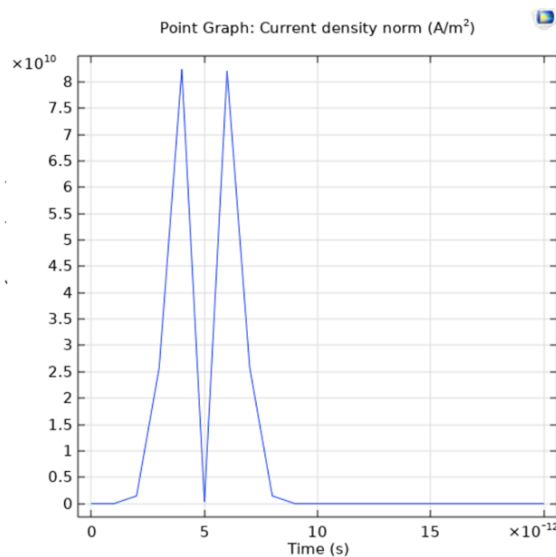


**Figure 4-5:** Current density in 300nm thick interdigitated electrodes with  $2\mu\text{m}$  pitch.

## C. Alignment and exposure

The Wafer stepper mask exposed the alignment markers for the wafer stepper as well as for the contact aligner on the first aluminium layer deposited in last step. The zero layer was exposed and developed without a hard bake. The same layer was then exposed with the contact aligner mask. The layer was then developed and etched which resulted in the alignment markers and interconnects on the glass wafer. The electrode geometries were then separately exposed using the wafer stepper mask, developed and etched on the same aluminium layer. Exposure energy

was tailored to control the width of the electrode. Exposure energies more than  $150\text{kJ}/\text{cm}^2$  resulted in electrode widths of around  $0.8\mu\text{m}$ .

#### **D. Silicon oxide deposition**

150nm of silicon oxide Tetraethyl Orthosilicate (TEOS) was deposited using PECVD to make the surface hydrophilic so that the virus sample spreads evenly on the planar electrode. The Silicon oxide also prevents electrolysis of the medium containing the virus. The thickness of the Silicon oxide is instrumental as an over deposition can reduce the electric field strength or the divergence of the electric field strength. The deposited layer time was calculated by measuring the deposition height on a dummy wafer.

#### **E. Thick photo-resist deposition**

As discussed in Chapter 3, the penetration of electric field reduces after the first  $20\mu\text{m}$ . Hence the the micro-dams that were created by manually depositing a photoresist layer that was  $25\mu\text{m}$  thick. An active electrode area of  $12\text{mm} \times 24\text{mm}$  and a sample height of  $20\mu\text{m}$  allowed for a sample deposition of  $6\mu\text{L}$ . SU-8 was used for the thick photo resist deposition. SU-8 is a negative photoresist and was selected to build the micro-dams for its ability to form strong covalent bonds under light exposure.  $25\mu\text{m}$  of photoresist was deposited with a spin speed of 1450 rpm/min. The process involved prebaking steps- a soft bake lasting for 10 minutes at  $65^\circ\text{C}$  and a hard bake for 25 minutes at  $95^\circ\text{C}$ . The exposure was followed by two post baking steps- soft bake and hard bake and a 5 minute manual development under Propylene glycol methyl ether acetate (PGMEA).

#### **F. Dicing, gluing and wirebonding**

The wafers were diced along the dicing markers. Glass blade with a thickness of  $200\mu\text{m}$  was used to dice the wafers. The separate dies were glued to the PCB using a nonconducting glue. Further, the dies were wedgebonded with a gold wirebond with the connecting pads on the PCB. The parameters on the wirebonder were fine tuned so that the wire bond sticks to the small aluminium pad. These bonds were then encapsulated with a nonconducting glue which was cured under UV light for 20 minutes (refer 4-7)

#### **Electric die measurements**

The electric die measurements were done with a four point probe Cascade 31. The measurements consisted of a voltage current sweep that were taken across all the test square areas to check if all the zones were electrically isolated and that there is no conducting current. The measurements were taken once before the deposition of the silicon oxide layer and again for a second time after silicon oxide and microdam deposition. The first measurements were used to identify dead zones on the electrode. These dead zones that failed to give credible levels of electric field were deposited with photo-resist during the thick photoresist deposition step and blocked off. The blocking of dead zones was done to increase the accuracy of the experiments with the virus. More accurate data about the total inactivation efficiency of the total sample by a particular electrode pattern can then be gathered.

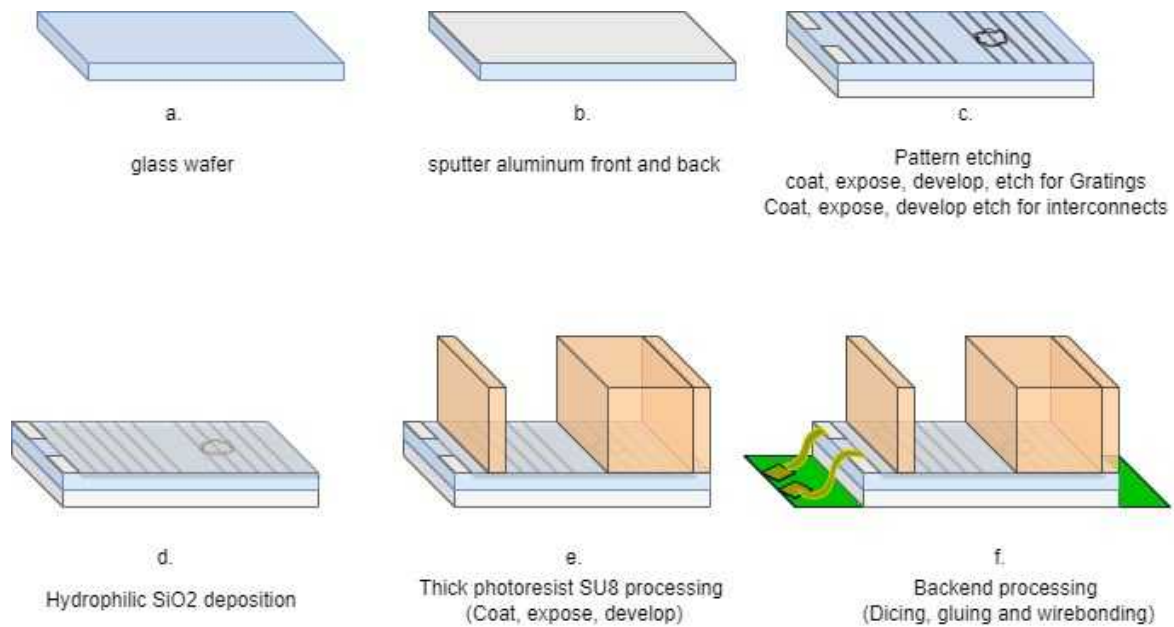


**Figure 4-6:** The fabrication process of the micro-electrodes

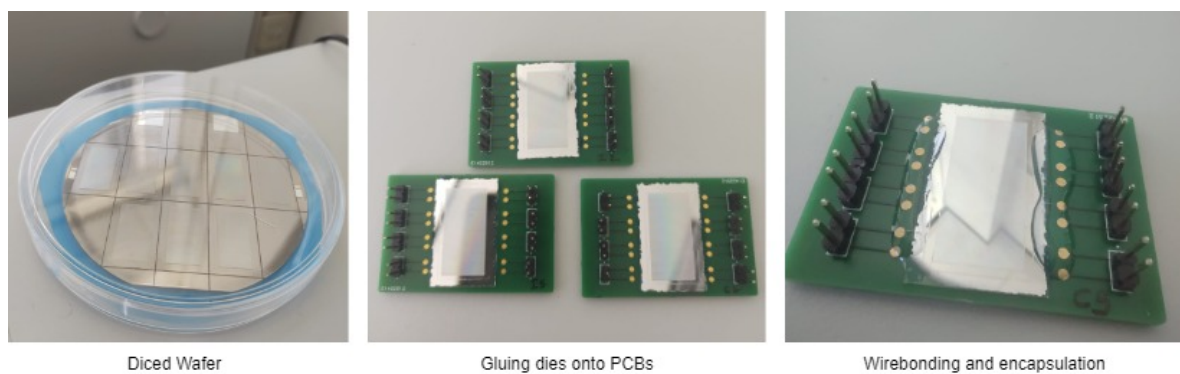


**Figure 4-7:** Backend processing and packaging of a processed wafer

### 4-2-1 Challenges in Fabrication and mitigation strategy

#### Short circuits

Particles that settled on the active areas during the coating, exposure and the development steps of the gratings resulted in short circuiting of the electrodes. Shortcircuits could also be a result of irregularities in the substrate and residues of aluminium after dry etching. Some of the shortcircuits can be easily detected with the help of a microscope (see fig 4-8), whereas some shortcircuits caused by particles that were in the order of nanometers could only be detected by probe point measurements (see fig 4-9) where the voltage current graph shows an ohmic behaviour: The current is in the order of mA and scales linearly with the voltage. Short circuits reduced the yield of the active electrode area.

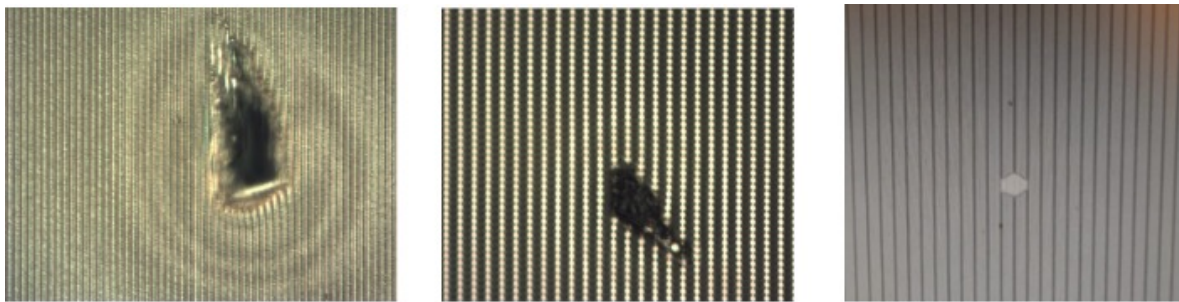


**Figure 4-8:** Short-circuits under microscope

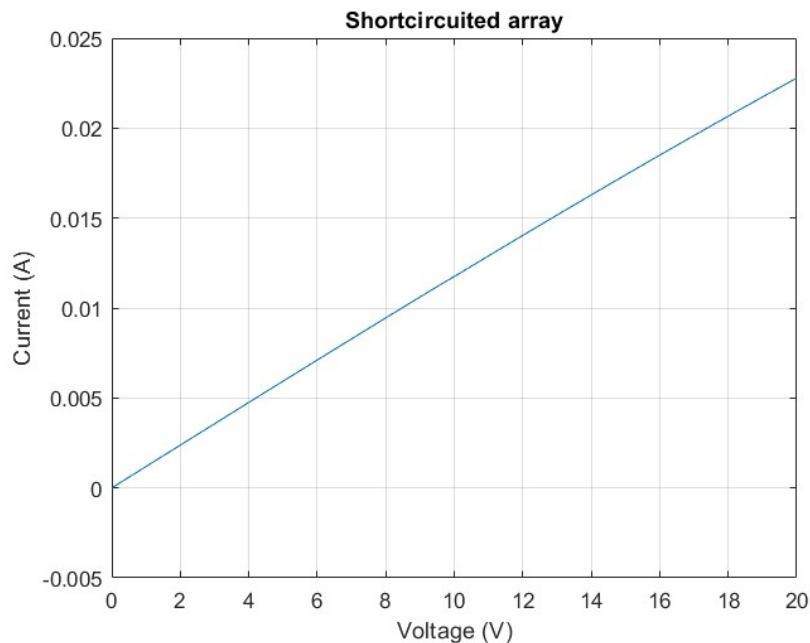


**Figure 4-9:** Shortcircuits between the electrodes observed on cascade measurements

To calculate the size of the particle causing the short-circuit we can take the values from the graph to find the resistance. From the slope of the graph ( $V/I = R$ ) we get  $R=800\Omega$ .

The resistivity of aluminium is  $2.65 \times 10^{-8} \rho$ . From the device fabrication we know that the thickness of the deposited aluminium is 300nm ( $l=300\text{nm}$ ). The gap between the electrodes is 500nm ( $x=A/500\text{nm}$ ). Where A is the area of the shortcircuiting particle. the resistivity of a metal in terms of resistance is given as-

$$\rho = R \times A/L$$

Substituting the values from our device. We get the value  $x= 12.42 \times 10^{-11}$ . A particle of that size magnitude is enough to cause a short circuit.

To mitigate the short-circuits caused by organic contaminants the gratings were exposed and etched twice with the same exposure job. The first etch recipe used an endpoint detection whereas the second etch used an over etch time of 3 seconds. This mitigation strategy cleared most of the visible short-circuit causing contaminants. The yield improved from 65% to 85%. However, some of the electrodes with a smaller gap of  $< 4\mu\text{m}$  (electrodes I2, Cout4, Cin4 and Cout5) still recorded around 25% bad arrays on the probe measurements (average of 6 active electrode arrays among a total of 8 electrode arrays). Another mitigation strategy made use of the Cascade probe stations. A large current with a higher compliance was sent through the short circuited electrode gratings with the registered short-circuit over a long period of time to melt away the the aluminium causing the short circuits. This strategy did not resolve all the short circuits.

### Wire-bonding surface adhesion problems

A gold wire of  $0.25\mu\text{m}$  was used to wedge wire bond the aluminium pads on the substrate to the gold pads on the PCB. The aluminium bonds failed to stick on the aluminium pad despite an optimal ultrasound energy, bonding time and bonding force. The failed samples were taken back to the cleanroom for a closer inspection. Optical inspection of the substrates under a microscope revealed a rough, porous discolored bondpad layer (see fig. 4-10)

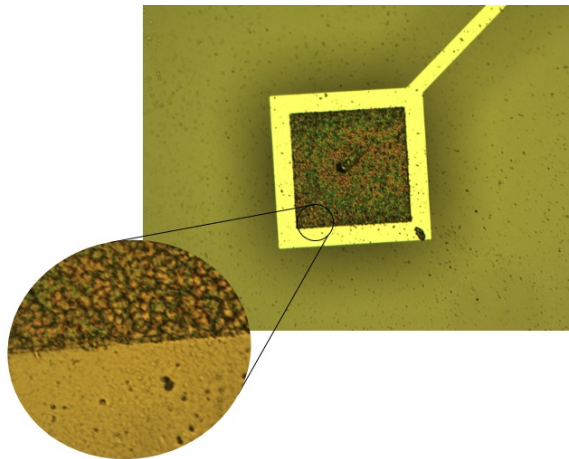


**Figure 4-10:** Optical inspection of a non-adhesive Bondpad

Through these optical inspections it was concluded that aluminium had reacted with some compound and had resulted in the formation of an unknown layer in the region of the bond

pad opening. To test the chemical properties of this layer the substrate was treated with Phosphoric acid etching mixture (PES 77-19-4). The mixture was allowed to etch the substrate for 20 minutes. After 20 minutes the substrate was observed under a microscope and it was noted that the PES etch resulted in isotropic non-uniform craters across the aluminium pad (see figure 4-11). This confirmed the presence of a compound other than aluminium on the surface of the bondpad. This chemical compound is Aluminium hydroxide and the

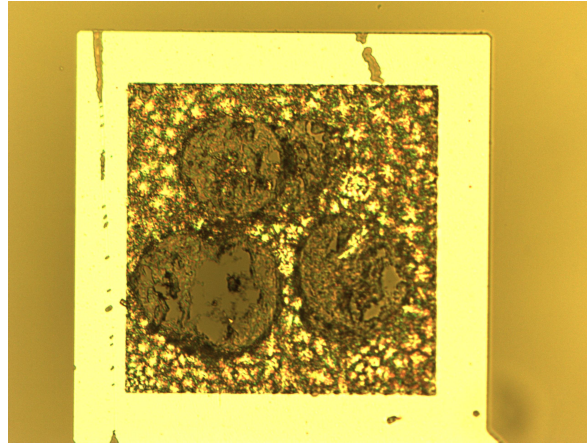


**Figure 4-11:** Optical inspection of a non-adhesive bondpad after 20 min etch in PES

formation of Aluminium Hydroxide could be a result of galvanic corrosion introduced during the wafer dicing process due to exposure of the dies to moisture or DI water for long periods of time [79,80]. This corrosion can be reduced by using higher sawing speeds in the dicing tool to minimize the contact of the substrate with water. It was also noticed during optical inspections right after wet etching in a BHF bath resulted in rough and scaly contact openings. However, no study explicitly states the effects of BHF etching on aluminium bond pads. Nonetheless, as a mitigation strategy the wet etching was substituted by dry etching. Dry etching was performed on the triode drytek plasma etcher. The Triode drytek plasma is unable to process glass wafers as it uses mechanical clamping to handle wafers. Mechanical clamping is not suitable for glass wafers and hence, silicon substrates were used instead of glass. For silicon substrates,  $5\mu\text{m}$  thick TEOS oxide was deposited on the bare substrate to provide insulation between the electrically conductive aluminium and the electrically semi-conductive silicon. The aluminium layer was then deposited over this silicon oxide layer which was etched to form all the structures of the electrode arrays. the process recipe for electrodes on Silicon is covered in Appending A-2. The cascade measurements for silicon wafers recorded a higher leakage current than glass wafers. The leakage current was in the order of  $10^{-6}\text{A}$ , which was one order higher than what was observed for glass  $10^{-7}\text{A}$ . These increased leakage currents are a result of the higher conductive properties of the silicon substrate. Moreover, silicon wafers can be diced faster (10mm/sec as opposed to 2mm/sec on glass wafers) limiting the contact of aluminium pads with water. All these mitigation strategies resulted in a bond pad that allowed good adhesion of the gold wire. The optical inspection of the bond-pad after all these mitigation strategies is shown in figure 4-12. The inspection shows a much smoother bond pad layer without any discoloration. The bond-pad also provided good surface adhesion to the bond wires.

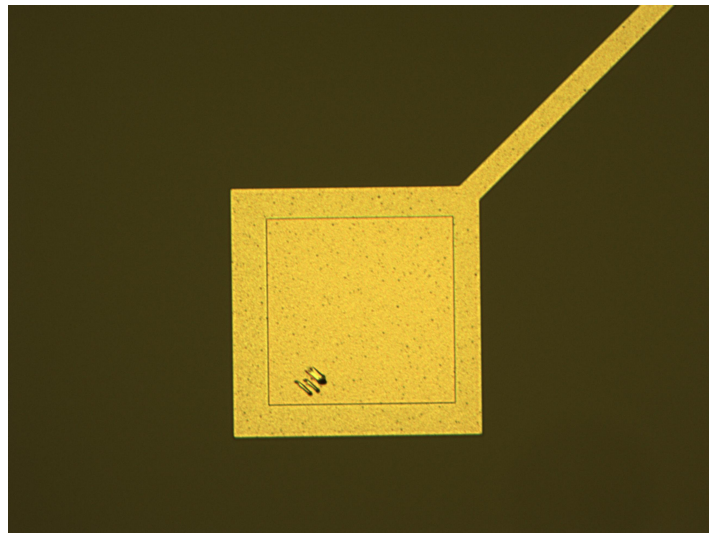


**Figure 4-12:** Optical inspection of the bondpad after making changes to the process flow.

# Experimental set-up

## 5-1 Virus stock preparation

### 5-1-1 Use of surrogate virus phi-6

Given the safety challenges of working with bio safety level - 3 (BSL-3) viruses like the corona viruses, the use of the bacteriophage phi-6, a surrogate to the SARs CoV-2, can be useful in assessing the effect of electric field generated by the device on the viability of the virus. Bacterial viruses of bio safety level - 1 (BSL-1) like the phi-6 virus pose no risk to humans and their study does not require specialized bio-containment tools. The phi-6 bacteriophage is a double stranded RNA virus of the Cystoviridae family which infects the bacterium *Pseudomonas Syringae*. Bacteriophage 6 is also an enveloped virus with a lipid membrane having a spike complex(p3, p6) which is structurally and morphologically similar to the coronavirus spike proteins[70, 71]. It has been used before as a surrogate to corona virus for various other experiments [72, 70, 71]. It has also been used as surrogates to study the inactivation mechanisms of coronaviruses (CoVs) using light, corona discharge and electrostatics [7, 73, 74, 75].

### 5-1-2 Phage Production

The host strain, *Pseudomonas syringae* pv, was grown to early exponential phase and infected with phage. Phage stocks were obtained by harvesting the supernatant containing the phage, filter-sterilized with a polyethersulfone membrane (0.2  $\mu$ m, PES), and stored as phage at 4°C. The supernatant was the mixed with the buffer solution.

### 5-1-3 Stock preparation

The supernatant was mixed with a buffer to make the virus stock. The buffer selected for the stock initially was the Lysogeny broth. The phages are usually prepared in a culture broth known as the lysogeny broth. The formulation of 1 litre of Lysogeny broth requires

- 10 g Peptone
- 5 g Yeast Extract
- 5 g sodium chloride

The stock prepared in lysogeny broth had a higher conductivity due to the presence of salts. Higher conductivity of the medium is unwanted as it might not facilitate pDEP attraction. Hence distilled water was selected as a medium buffer. The use of distilled water as a buffer however reduced the viability of the virus stock. The virus stability in distilled water is less than in other saline solutions. The virus in distilled water was viable for a period of 1 week after which it started to decay. To increase the stability and prevent environmental decay of the virus in the sample solution the phage was produced with an initial concentration of  $10^{11}$  pfu/ml. Larger input amounts of bacteriophage Phi6 are shown to delay and protect the phage from environmental decay [76]. A higher concentration was achieved by producing a bigger batch of the phage (100ml) and then concentrating it to a volume of  $500\mu\text{L}$ . The Phage samples were 8-fold serially diluted in LB and the dilutions were spotted onto double layer agar (DLA) plates of the host strain following the small plaque drop assay [77]. The plates were incubated overnight at  $30^\circ\text{C}$  and the phage plaques were counted to determine phage concentration 5-1. The same process was used to determine the plaque forming units (pfu) of the treated samples after the treatment on the electrodes.

### Conductivity of suspending medium/buffer solution

10 ml of LB stock also contained 0.05 g of NaCl which contributed to the conductivity of the medium. From the previous chapters we learnt that conductivity of the medium is an important parameter and helps to decide the frequency at which the virus could be attracted using pDEP. Using the following equation we can find the conductivity of the medium.

$$\text{Conc.}[g/dm^3] = \frac{\rho_m[S/m] \cdot M[g/mol]}{\lambda[S/m \text{ per } mol/dm^3]}. \quad (5-1)$$

Where  $\rho_m$  is the conductivity of the medium.  $M$  is the molar mass of the salt and is the Molar ionic conductivity of the individual ions in the medium. The molar mass of NaCl is 58 g/mol. The molar ionic conductivity of the sodium ion is  $5.01 \text{ S/m per } mol/dm^3$  and that for chlorine is  $7.23 \text{ S/m per } mol/dm^3$ . Together they add up to give us the molar ionic conductivity of NaCl which is  $12.24 \text{ S/m per } mol/dm^3$ . 0.05g of NaCl in 10ml of water gives us  $5g/dm^3$  of salt concentration. Substituting all of these values in the given formula. We get the medium conductivity as  $1.02 \text{ S/m}$ . According to the CM simulations this conductivity is too high for pDEP. Saliva is noted to have a baseline conductivity of  $4.2 \times 10^{-4} \text{ S/m}$  [78]. And hence distilled water was selected to make the stock solution. The conductivity of the medium with distilled water as the buffer is  $5 \times 10^{-6} \text{ S/m}$  which may allow us to attract the virus at 1000Hz till 10MHz.

## 5-2 Experiment table

The signals were generated on Rigol DG1062Z - Function/Arbitrary Waveform Generator. The output from the function generated was distributed across all the pins of the electrode

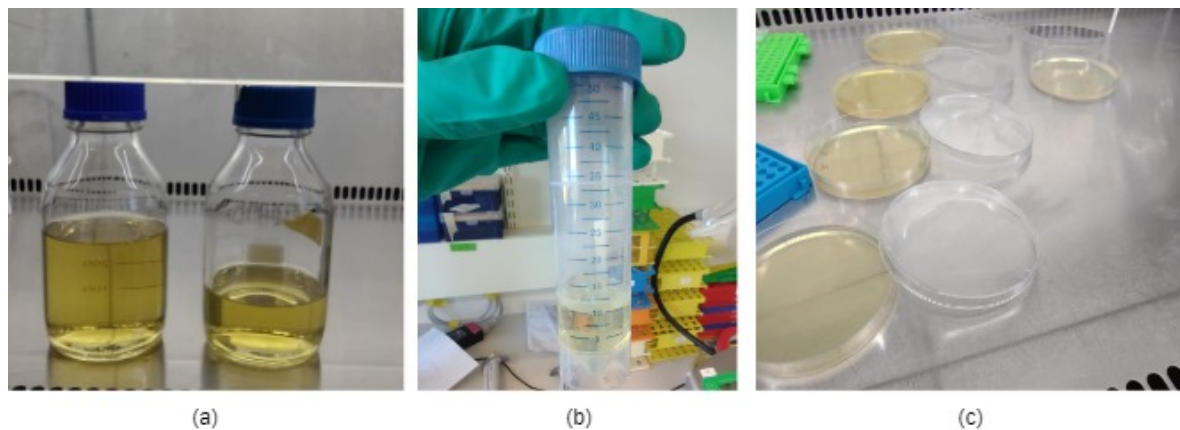


**Figure 5-1:** Process for culturing colonies of *Pseudomonas* sp.

using a breadboard and jumper cables. A transformer was used to amplify voltage values from 10Vpp to 60Vpp (30Vmax) for AC stimulation whenever it was needed. A DC input was given with the help of a EL302RD power supply. A micro-pipette with a significant figure of  $0.1\mu\text{L}$  was used to sample out  $10\mu\text{L}$  of the virus from the stock solution and load it on the electrodes. The electrodes were then covered with glass slips. The glass slips prevented evaporation of the sample. The glass slip was made by dicing an unprocessed glass wafer with a glass blade in the dimensions of 12.4mm x 24.5 mm. This glass slips directly lodged onto the micro-dams created during the processing. The treated samples were pipetted out and were loaded into PCR tubes that were then labeled and stored in the fridge at  $4^{\circ}\text{C}$ . The experimental set up is highlighted in the figure 5-2

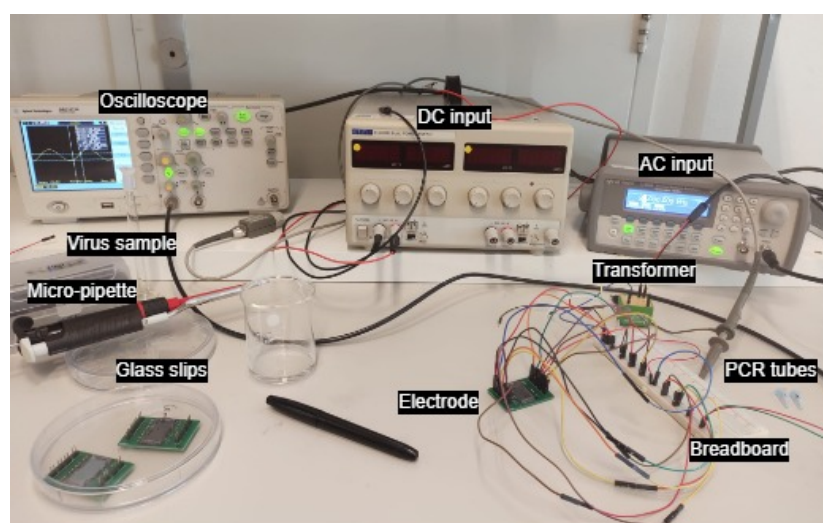


**Figure 5-2:** Experiment set-up

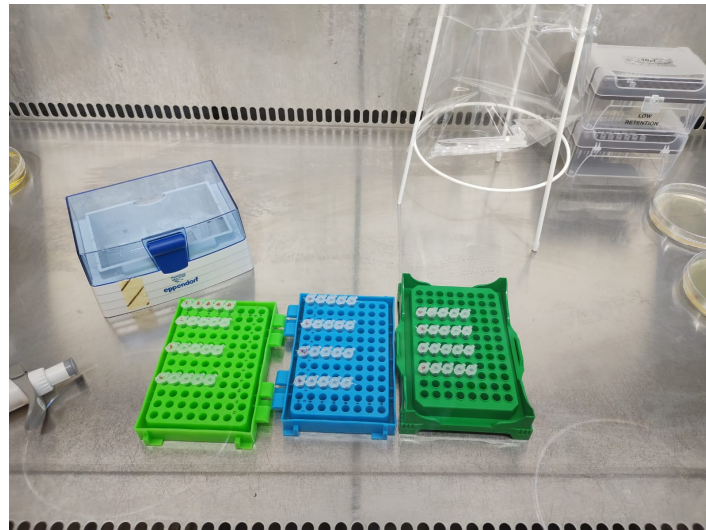


**Figure 5-3:** 5-fold serial dilutions of the original treated sample

## 5-3 Viral particle titrations

The treated virus samples were then titrated against the prepared bacterial colonies. For the titration the samples were diluted by adding distilled water and brought up to the level of  $10\mu\text{L}$ . The main diluted sample was diluted once again with increasing levels of five-fold sequential dilutions according to the Appelman method. Serial dilutions are made by making the same dilution step over and over, using the previous dilution as the input to the next dilution in each step. The dilution factor taken was  $1/10\mu\text{L}$  such that the next dilution is one log higher. These dilution levels of each sample are then loaded onto the petri-dish along with the bacteria and the culture medium. The petri dishes are then incubated at  $28\text{-}30^\circ\text{C}$  for approximately 30 h. Once colonies appear on the plate, the concentration of the virus can be measured by counting the plaques formed on it. These colonies can be stored at  $4^\circ\text{C}$  for up to 10 days.

## 5-4 Experimental Design

### 5-4-1 Experiment 1: Testing hypothesis 1, 2 and 3

Hypothesis 1: *The SARs CoV-2 virus can be inactivated using electric field generated by planar micro-electrodes.*

All the electrodes that were fabricated generate electric fields upto  $10^5\text{V/m}$  with a 30V DC and a 60Vpp AC voltage with varying frequencies. For this experiment the virus samples were treated for 12 minutes across all electrode design with 30V DC and separately with 60-70Vpp AC, 30kHz frequency. The effectiveness of the test was measured against two control samples; one of which was directly sampled out from the stock into the PCR tube and the other one was loaded onto the electrode without the electrical output and then into the PCR tube.

Hypothesis 2: *Castellated geometries generate more local spots of high electric field and hence are better at inactivating the virus than interdigitated geometries.*

To test the second hypothesis, the treated samples were measured and statistically tested across the three different pattern (Cin4, Cout5, I2) each having the same gap distances ( $1\mu\text{m}$ ).

Hypothesis 3: *The electrodes with a smaller gap are better at inactivating the virus as they generate higher electric fields than the electrodes with a larger gap.*

The performance of electrodes with the same pattern were statistically tested across their pitch sizes (I10 vs I5 vs I2, Cin8 vs Cin4, Cout4 vs Cout5).

### 5-4-2 Experiment 2: To test hypothesis 4 and 5

Hypothesis 4: *For efficient and higher inactivation rates of the sample the virus needs to be attracted to the surface of the electrode where the field is maximum.*

The inactivation rates are hypothesized to be dependent on the attractive pDEP forces exerted by the electric field on the virus particle. The virus particle needs to be close to the electrode surface to be subjected to electric fields for its inactivation. To test this, samples with two different levels of dilution were treated on the same electrode pattern. The base sample (no dilution) consisted  $10\mu\text{L}$  of virus stock and the second sample consisted of  $10\mu\text{L}$  of virus stock solution +  $10\mu\text{L}$  of distilled water. Both treated samples would be measured and tested for significant difference. If the difference in the pfu is significant, the inactivation rates do not depend on the pDEP forces.

Hypothesis 5: *Medium conductivity plays an important role in facilitating DEP attraction to allow efficient inactivation*

A higher medium conductivity is hypothesised to need a higher frequency to attract the particles suspended within it. To test this hypothesis, virus samples suspended in LB are treated across all electrodes with 60Vpp and 30,000kHz frequency. The results are compared with treated virus samples suspended in distilled water. If the inactivation is higher within the samples suspended in distilled water, then we can conclude that medium conductivity does play an important role in allowing efficient inactivation.



# Measurements and results

## 6-1 Electric field measurements

### 6-1-1 Breakdown and discharge current

Studies show that the microelectrode configuration has a crucial influence on the breakdown voltage and discharge current response to varying electrode gaps and patterns [81]. The DC voltage across the electrode on the Cascade was serially increased by a step size of 5 volts to find the breakdown voltage without damaging the electrodes. However, because of safety reasons and the limitations of the probe point measuring equipment, the voltages were limited to 100V and the maximum compliance current was set to 50mA. None of the electrodes showed any destructive breakdown under 100V.

There are two physical processes that can initiate an electrical breakdown: avalanche ionization and electric field emissions. Under normal pressure, the breakdown will typically be brought about by an avalanche ionization. In avalanche ionization, the gap between the electrodes, which acts as a dielectric material, generates free electrons and starts conducting when it is subjected to high voltages. However, as the electrode gap shrinks, breakdown initiated by the electric field emissions become the more dominating mechanism of breakdown. This breakdown occurs when the gap between the electrodes is small enough to conduct electrons generated by the electric field. The voltage at which the electrodes start recording a cascading current is called the breakdown voltage. Nonetheless, a point where the onset of current discharge before the electrode breaks down is usually reported. As suggested by J.S Townsend, this discharge is due the conduction by free electrons generated by the electric field in the gap environment [82]. At these low voltage levels recombination of the ions and the electrons dominates and hence the current is very low. As we approach breakdown voltages the ions and electrons move quickly through the gap and recombination is very low. At breakdown voltage the velocity of the ions is high enough to result in drifting and collisions that eventually result into a cascade of electrons and ions across the gap that increase exponentially with an increase in the electric field. The onset of these discharge currents can be seen in all the electrode patterns. The voltage-current characteristics for the electrodes with the

largest pitch is shown in figure 6-2. These values are similar to the ones obtained by Takahito et al. [83]. Townsands discharge current is seen around 25V in electrode Cin8 and 40V in electrode I10. Deviations in the magnitude of discharge currents do exist. The differences in the current leakage values among various electrodes of the same pattern and pitch may be a result of the presence of aluminium residues and metallic contaminants present between the electrodes that alter the dielectrics values for that array. As a result, sometimes the same type of electrode pattern may record a higher or lower discharge current. These tiny particles affecting the cascade measurements could only be detected by SEM images as seen in figure 6-1. Nonetheless, all the electrode patterns on glass record a discharge current less than  $1\mu A$  till 100V in glass and  $20\mu A$  in silicon before breakdown which suggests their electric isolation.

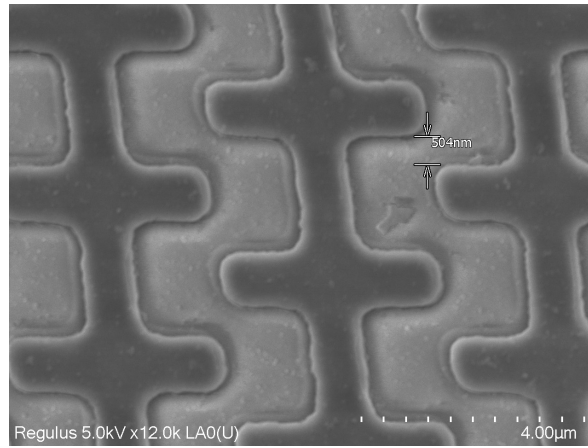


**Figure 6-1:** SEM image of a particle between the gaps of the gratings that may influence the discharge currents by altering the dielectrics within the gaps of the arrays.

### 6-1-2 Electric Field calculations

The maximum electric field of each electrode can be calculated as follows-

$$\text{maximum electric field} = \frac{\text{breakdown voltage}}{\text{gap distance of the electrode pattern}} \quad (6-1)$$

Since none of the electrodes recorded a cascading breakdown within the sweepable voltage range we may use the voltage at which we notice the onset of Townsend's discharge current as the breakdown voltage for calculating the max electric field that can be generated across that specific electrode pattern. For all the electrodes this point was between 25-40V. For Cin4 electrodes the supposed breakdown is observed around 40V. The max electric field generated by this electrode is  $4 \times 10^7$  V/m. For Cin8 electrodes the breakdown was observed at 25V and the electric field generated  $5 \times 10^6$  V/m. Similarly, the maximum electric fields generated by the electrodes I2, I5, I10 are  $4.5 \times 10^7$  V/m,  $4 \times 10^6$  V/m and  $1.5 \times 10^5$  V/m respectively. For electrode Cout5 and Cout4 the fields generated are equal to  $2 \times 10^7$  V/m and  $6.0 \times 10^7$  V/m. These values are also in accord with the simulations of different patterns of electrodes we had in chapter 3.

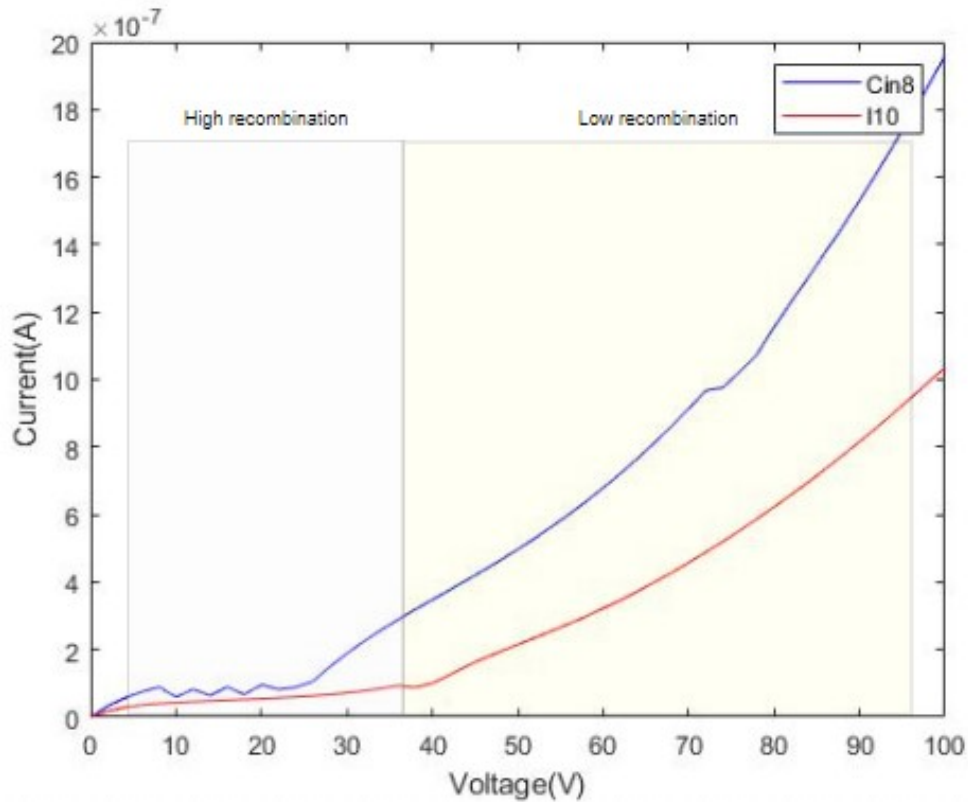


**Figure 6-2:** Current-Voltage characteristics of planar electrodes on glass with the largest pitch.

### 6-1-3 Influence of different geometries on electrical discharge characteristics

The influence of geometric patterns (interdigitated and castellated) on the breakdown characteristics and current discharge response were studied. Current breakdown characteristics of 3 arrays of electrode patterns Cin4, Cout5 and I2 each having a gap of  $1\mu\text{m}$  reveal that castellated electrodes showed a softer current discharge response with lower values of leakage current than the interdigitated electrodes (refer figure 6-4). The higher discharge current recorded in the interdigitated electrodes may be a result of the continuous close proximity of the two electrode digits. In castellated electrodes the gap between the edges of the two electrode digits varies and less electrode area is in close proximity resulting in more recombination of discharged ions and a smaller discharge current. Different pitches of the same electrode geometry were also studied. Data from 3 different arrays each of castellated out-of-phase electrodes with pitch  $2\mu\text{m}$  and  $5\mu\text{m}$  located on separate wafers were plotted against the electric fields. It can be noted that electrodes with a smaller pitch generate higher electric fields at the same voltage. Electrodes with a higher pitch have higher discharge currents for the same electric fields generated by the electrodes of a smaller pitch.

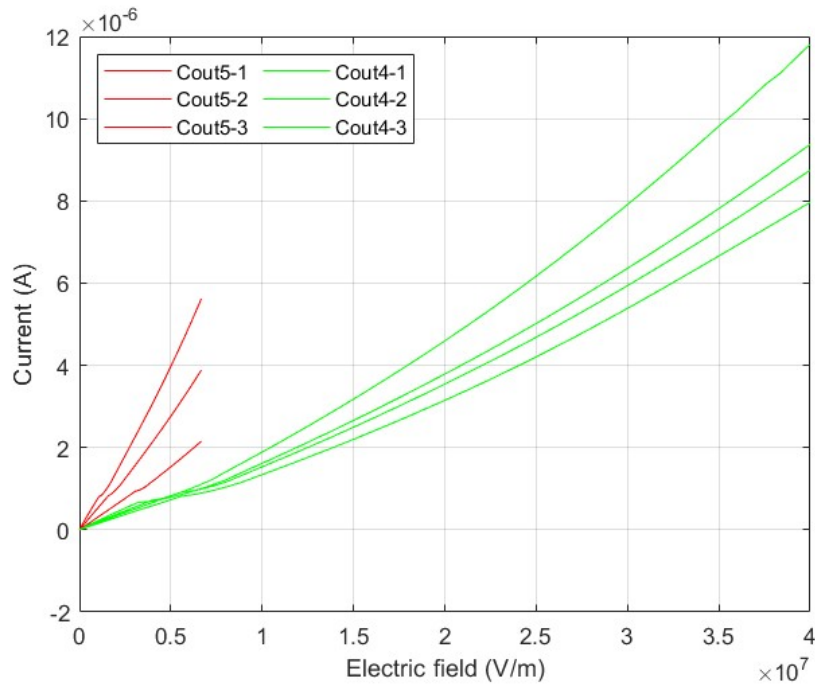


**Figure 6-3:** Comparison of the performance of different pitch distances of the same pattern on the discharge current

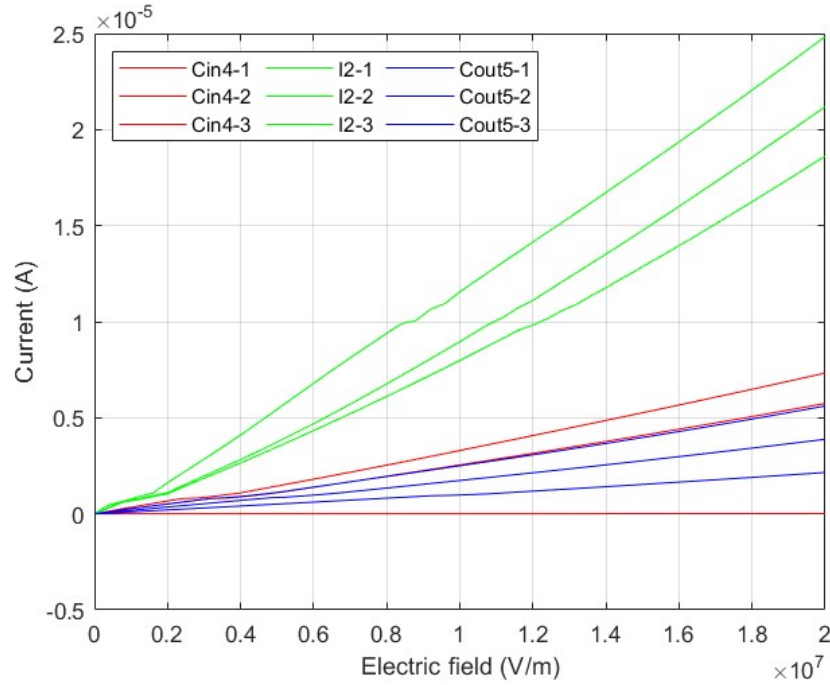


**Figure 6-4:** Comparison of castellated in phase vs castellated out of phase vs interdigitated patterns on silicon substrates

## 6-2 Experiment results: Phage titers

The plaques produced by the virus samples that were treated by the electrodes were counted and the concentration of the virus in the sample was calculated and compared with the concentration of the control sample. The difference in plaques formed by different samples can be seen in the figure given below (ref figure 6-5). The figure shows that there are more plaques formed by the (b) control samples that were not treated by the electrodes than the plaques produced by virus samples that were treated by the electrodes. From the countable

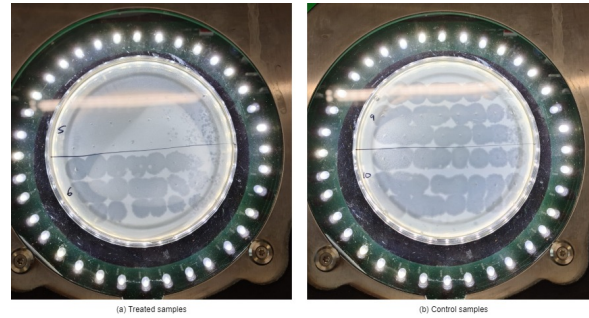


**Figure 6-5:** Counting plaque forming units on the different samples of the virus

plaques the total concentration of the virus in pfu/ml was calculated as follows-

$$PFU/mL = \frac{Np \times D}{V \times R} \quad (6-2)$$

Where

- $Np$  is the number of plaques counted
- $D$  is the level of dilution at which the plaques were counted
- $V$  is volume of the sample from the serial dilutions that was plated
- $R$  is the dilution ratio of the sample that was treated

### 6-2-1 Results of Experiment 1

The samples were treated across all electrode for 12 minutes with a 30V DC as well as AC voltages (40-45Vmax) and 30KHz frequency. The values of calculated phage concentrations ( $\log_{10}$  pfus/ml) are plotted for every sample in DC (refer fig. 6-6) as well as AC (refer fig. 6-7). The concentration of the virus in the stock solution recorded before the experiment was  $10^{12}$ pfu/ml for the sample used for the DC experiments and  $10^{11}$ pfu/ml for the sample used for the AC experiments. The control samples record around the same infectivity that was recorded by the plaque assays before the experiment indicating that there was little to no decay of the virus stock solution. Control sample 1 was sampled by loading a volume of  $10\mu\text{L}$  on to an electrode without the voltage input. Whereas, control sample 2 was directly sampled out of the stock solution. Any difference between the two control samples would have revealed any inactivation of the virus caused by the loading process.

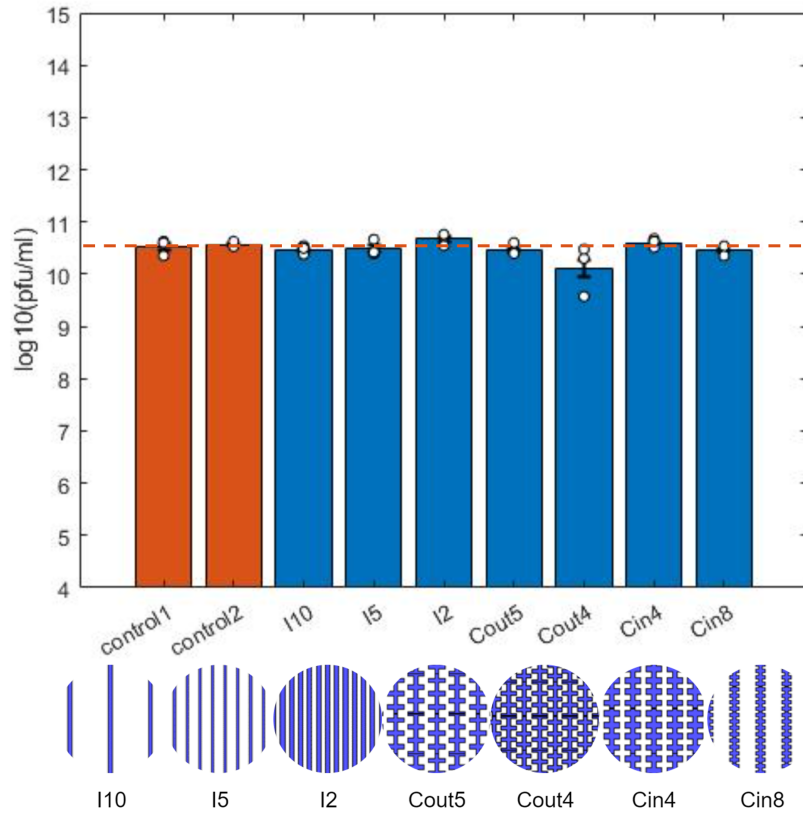


**Figure 6-6:** Effect of DC treatment

The results show that DC excitation does not result in any statistically significant inactivation on any electrode. AC excitation however results in some significant inactivation on the I10 ( $p(0.02) < 0.05$ ), Cout5 ( $p(0.02) < 0.05$ ), Cout4 ( $p(0.004) < 0.01$ ), Cin4 ( $p(0.01) < 0.05$ ) and Cin8 ( $p(0.04) < 0.05$ ).

The increase in pitch distance has a weak positive correlation with the decrease in the phage titers which contradicts the results obtained from the simulations; electrodes with a larger pitch that create a lower electric field were found to be better at inactivating the virus. This could be a result of a smaller active areas on electrodes with a smaller gap distance due to the presence of more number of dead zones.

The effect of geometry on the inactivation can be clearly seen on the inactivation rates of the electrode. Figure 6-8 compares three different electrode patterns at two different excitation frequencies. All the three geometries have a gap distance of  $1\mu\text{m}$ . It can be noted that Castellated patterns perform much better than Interdigitated patterns. The virus titer decreases quite significantly by 1 and 2 log when treated with excitation frequencies of 1000Hz and 30KHz respectively on the castellated out-of-phase pattern. Whereas, the interdigitated pattern observes a lower inactivation rate of less than half a log when excited with 1000Hz and no inactivation with 30KHz. These findings coincide with the results obtained from the simulations where castellated geometries were found to create more focused electric field spots than interdigitated geometries.

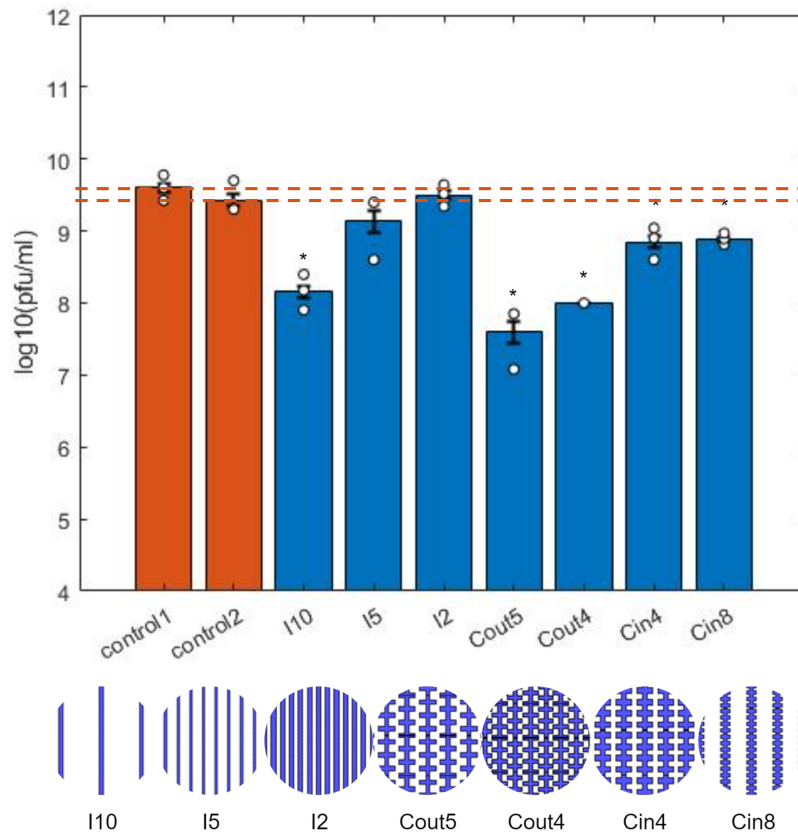


**Figure 6-7:** Effect of AC treatment with 30kHz frequency

### 6-2-2 Results of Experiment 2

Experiment 2 was designed to study the effect of dielectrophoresis on the inactivation rates of the samples. The inactivation rates are hypothesized to be dependent on the attractive pDEP forces exerted by the electric field on the virus particle. The experiment studies the effect of different frequencies, dilutions and medium concentrations that influence the forces on the virus particle and thus its inactivation.

In figure 6-9, the inactivation rates of concentrated virus samples and their dilutions are presented. Because of drying of the bacterial plate, the data for the diluted sample treated on I5 could not be obtained. The other samples were diluted to a factor of 0.5 ( $R=0.5$ , refer eq 6-2) by adding distilled water ( $10\mu\text{L}$  of virus sample +  $10\mu\text{L}$  of distilled water). The diluted samples were then loaded on the electrode. In the diluted samples, less number of virus particles are close to the electrode surface. To have significant inactivation rates that are comparable to that of concentrated samples treated on electrodes, there needs to be a significant pDEP attraction of virus particles. The results show a significant difference between the concentrated and the diluted samples treated with 30kHz frequency indicating that there was no significant pDEP attraction of the virus. Nonetheless, the diluted samples do show a decrease in the phage titer on electrode geometries Cin8 Cout5 and Cout4 when compared to the  $20\mu\text{L}$  control. Although it is not as high as the concentrated samples,

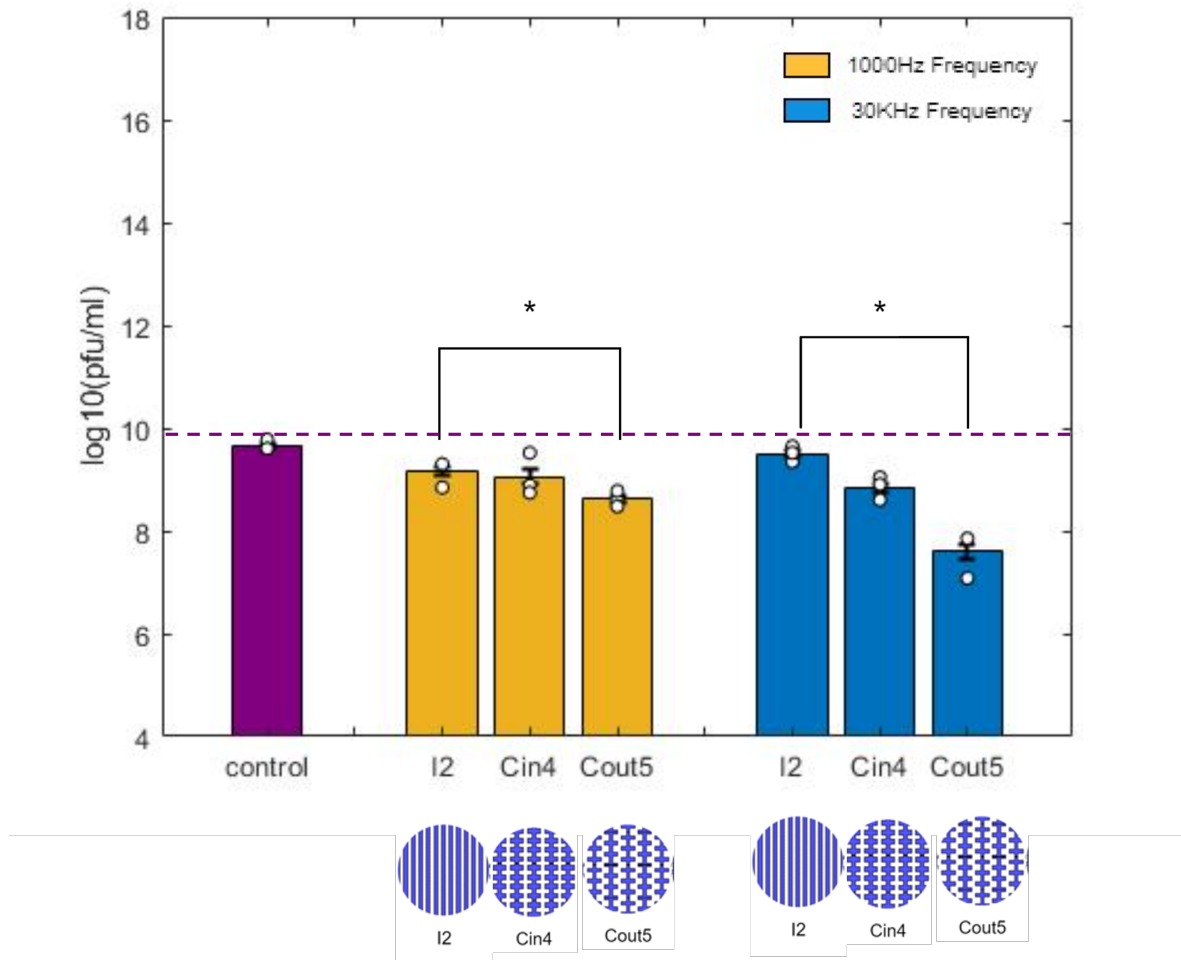


**Figure 6-8:** Effect of electrode geometries on virus inactivation

the decrease in the log titer may suggest a very weak attractive force. There are three control samples to provide a reference to compare the decrease in log titers of the treated samples; 2 controls for the  $10\mu\text{L}$  samples and one control for  $20\mu\text{L}$  diluted samples. The graph also suggests the correlation of input voltage frequency on the inactivation rates. The electrodes that facilitate inactivation show a higher inactivation rate when supplied with a higher frequency.

The ability to attract virus particles is heavily dependent on the medium conductivity. In figure 6-10, the effect of medium conductivity on the inactivation rate of the virus can be compared. LB ( $1.02\text{ S/m}$ ) shows a lower decrease in the log titer as compared to distilled water ( $5 \times 10^{-6}\text{ S/m}$ ). This is supported by the CM simulations where increasing the medium conductivity requires very high stimulation frequencies to make the virus particle more polarizable than the surrounding medium. As a result, the virus particle in LB was more difficult to attract to the areas of high electric field with the 30KHz frequencies that were able to better attract virus particles suspended in DI water.

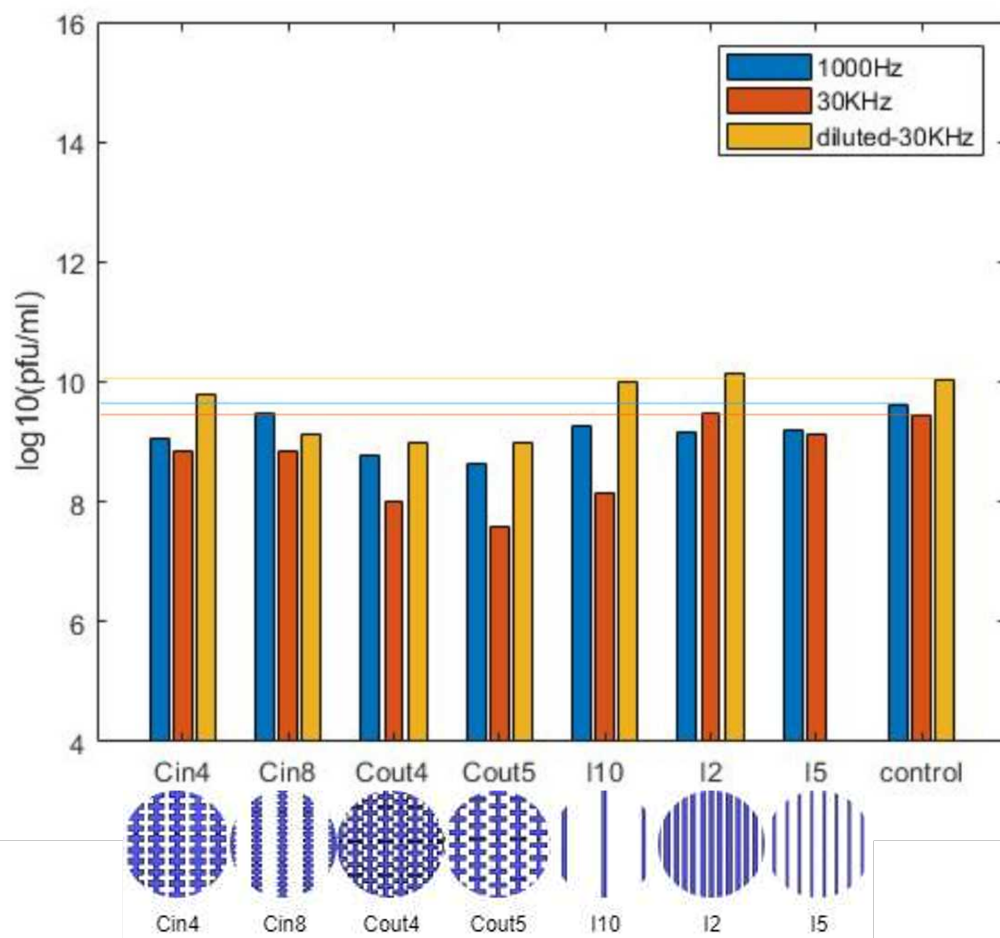


**Figure 6-9:** Effect of frequency and dilution on the treatment

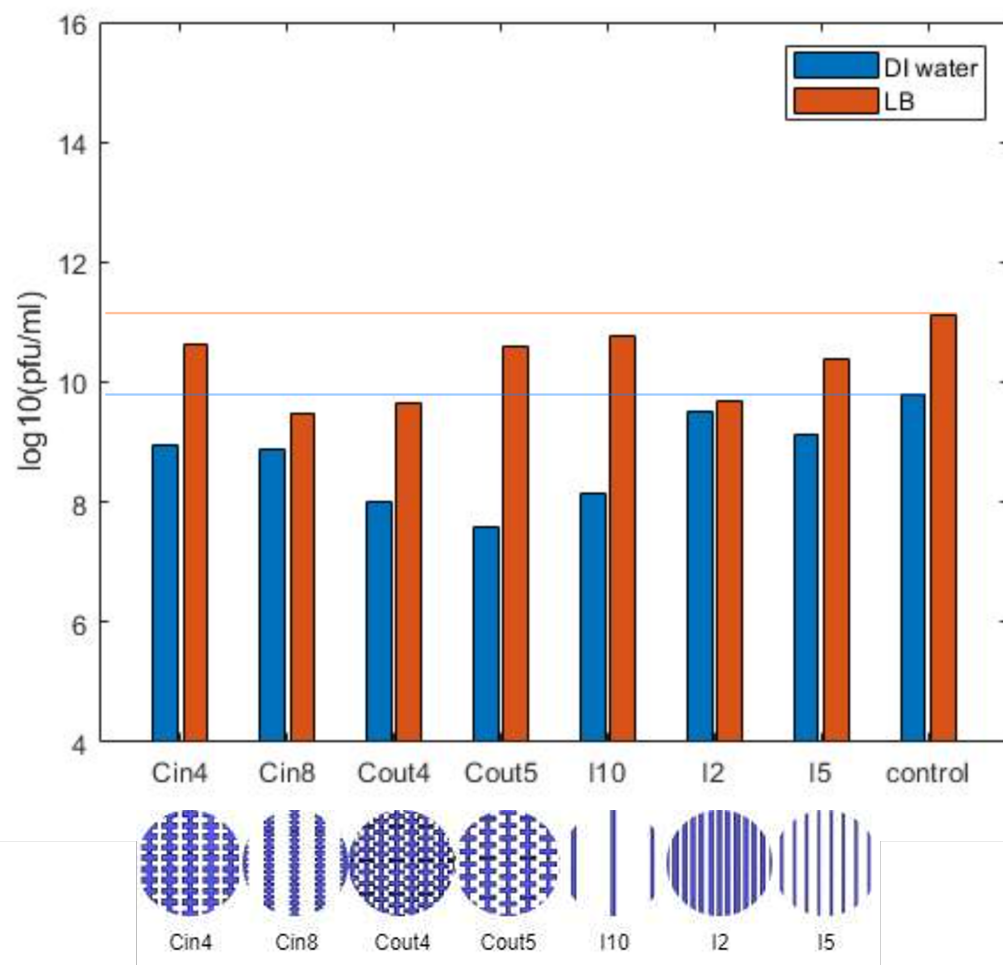


**Figure 6-10:** Effect of medium conductivity on the treatment

# Discussion and conclusion

## 7-1 Discussion

In this section, all the experiment results are discussed.

The results show that there is a decrease in the titers of around 0.5-2 logs on specific electrodes only when they are stimulated with AC voltages. With AC Voltages, the cells undergo dielectric force in addition to the inactivation which could also be responsible stretching of the cells between electrodes that contribute to the inactivation. This is consistent with the reasoning given by lee et al[69]. Moreover AC voltages attract the virus to areas of high electric field which may also be a reason why we see a significant decrease in the survival of the viruses treated with AC. Continuous DC voltages have only been used previously to lyse larger organisms like red blood cells, hamster ovaries and human leukemia cells and plant protoplasts [84,85,86]. Higher DC voltages are needed to inactivate smaller organisms [87]. To inactivate virus particles using continuous DC we might need very high electric fields which are difficult to attain without sustaining an electrical breakdown on the electrodes.

Nonetheless, in the light of the DC experiment we may be able to hint at the inactivation mechanism of the virus. According to Arbeitman, a minimum electric field of  $10^5$  V/m should have been enough to in-activate the surface proteins of the phi-6 virus[1], assuming that the phi-6 virus has exactly the same RBD protein structure as that of SARS CoV-2. Scientific reviews do maintain that the spike protein found in the corona virus is structurally similar to the surface proteins found phi-6 [71]. However, no studies were found that detail the structure of the RBD within the protein complex of the phi-6.

Inactivation observed in AC was the most prominent in the out-of-phase castellated electrodes. As iterated in chapter 2, Castellated electrode geometries or geometries with pointed tips are the preferred structures for bacteria and virus inactivation [55, 32]. This is also supported by simulations where focused spots of high electric field were observed among the castellated geometries. Whereas, in interdigitated geometries the electric field created was

relatively more uniform and less focused.

Contrary to our expectations, the electrodes with a smaller pitch have a lower inactivation rate as compared to electrodes with a larger pitch. There are a couple of possible reasons for this. The first reason is the electrodes with a smaller pitch were more susceptible to be short circuited and thus recorded more dead arrays than the electrodes with a larger pitch. Electrodes I10, Cin8 and Cin4 had no short circuited arrays. I5 and Cout5 had 1 short circuited array, whereas, Cout4 and I2 had 3 shortcircuited arrays that needed to be blocked off or disconnected. The higher inactivation efficiencies of electrodes with a smaller gap may have been offset by the lesser available active areas on the electrode. Another contributing reason could be the higher efficiency of the electrodes with a larger pitch in concentrating the virus. This is consistent with the findings of Sadeghian et al, where the effect of electrode pitch on the concentration efficiency of the electrode was studied [3]. The concentration efficiency of the electrode was found to decrease initially with an increase in the electrode pitch/height but with further increase in the electrode pitch/height ratio the efficiency of electrode to concentrate particulate increases significantly. In our experiment, the sample height above

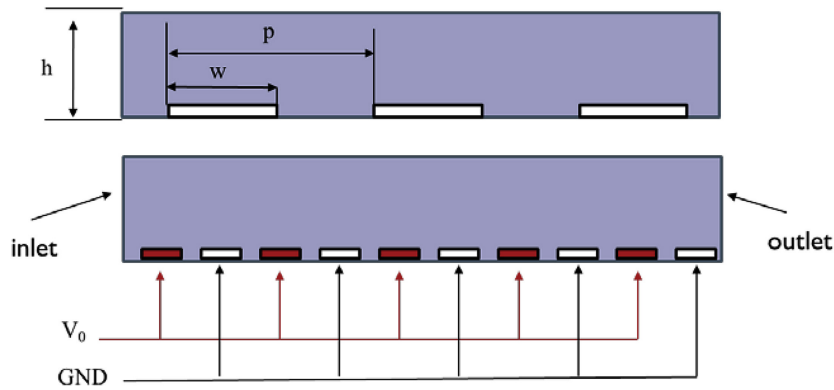


**Figure 7-1:** Geometric definitions of the electrode in the study[3]

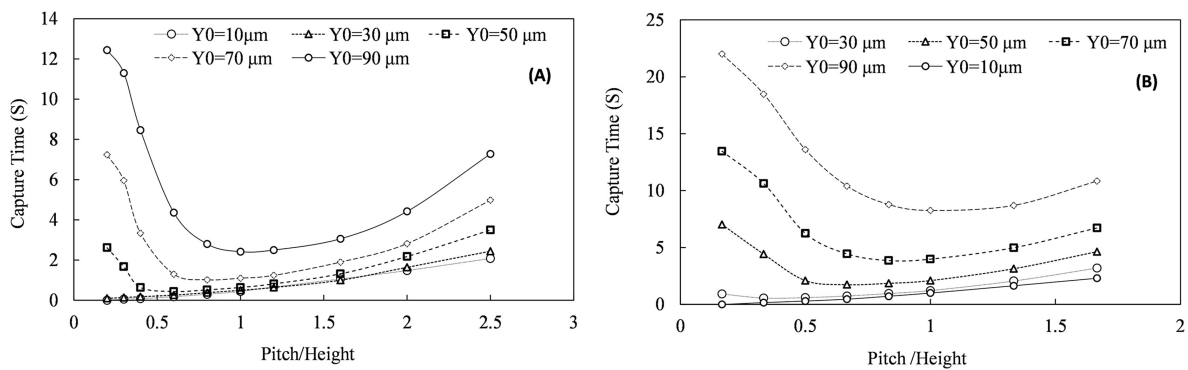


**Figure 7-2:** Effect of pitch/height ratio on the concentration efficiency [3].

the electrodes was designed to be around  $20\mu\text{m}$  assuming ideal wettability of the  $\text{SiO}_2$  layer. In reality, this was not the case. The sample height above the electrode surface was more than  $30\text{--}50\mu\text{m}$ . In this case, the electrode with the highest pitch (I10) would be the most efficient in concentrating the virus. This may explain the high rate of in-activation observed

in I10. This is also in accordance to the numerical simulations presented by Tathireddy et al. that were discussed in Chapter 3 [65]. In equation 3-3 the dual dependence of the electric field on the electrode pitch can be seen.

The results in figure 6-9 show the effect of using different frequencies on the inactivation of the virus sample. Lower frequencies result in less concentration of the virus and hence lower inactivation rates. This observation is supported by our dielectrophoresis model simulations (ref. figure 2-3) in chapter 2. Considering a medium with very low conductivity, pDEP begins at 1000Hz (crossover frequency). At 30kHz, the CM factor is +0.1 resulting in a very weak pDEP force on the particle. A maximum CM factor of +0.1 is very low when compared to other more polarizable bacteria and cells. For example, E-coli shows a maximum CM factor of +1 even with a higher medium conductivity, which leads to a significant pDEP force[4]. The small size of the Corona virus/Phi-6 and the lower polarizability of their membranes results in a very weak attraction force. This weak attraction is very evident in the figure 6-9 where the diluted samples do show some inactivation but not as much as seen in concentrated samples despite being attracted towards the electrode by pDEP.

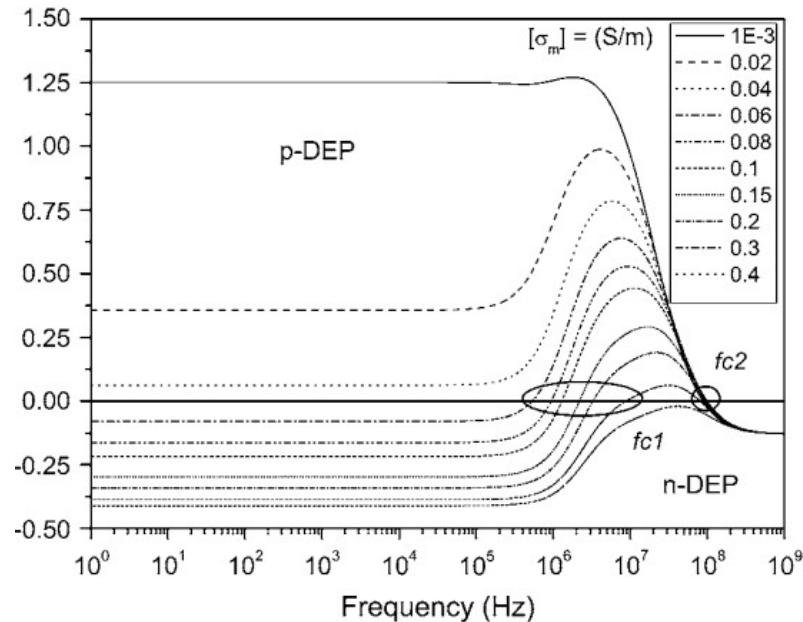


**Figure 7-3:** CM factor of E-coli under different medium conductivities[4]

The presence of a weak DEP attractive force can also be proven with the help of the following calculations:

The electric field simulations show that the electric field was highest at the surface (see fig. 3-5). It decreases as we move away from the surface of the electrodes into the virus sample. For this purpose we can assume the inactivation region in the sample to be up to  $10\mu\text{m}$ . The virus particles beyond this region need to be attracted to the electrodes in order to be inactivated. In diluted samples, less number of virus are present in the inactivation region. This is shown in the figure 7-4. Only some part of virus present within the inactivation height would be deactivated if no DEP force was present. If we assume that the electrodes inactivate 100% of viruses within that region we would expect that that fraction part of the volume is

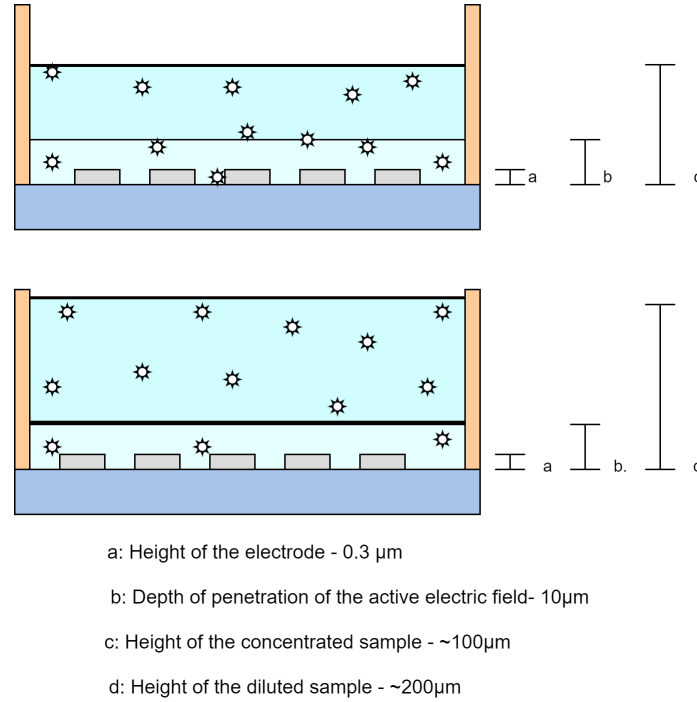


**Figure 7-4:** Effect of dilution on the virus density

equal to the inactivation fraction of total viruses in the sample. Consider the equations given below:

$$\frac{\text{Height of the inactivation area}}{\text{Height of the sample}} = \frac{\text{Total no. of viable viruses after the exp}}{\text{total number of viable viruses before exp}}$$

This would mean there are no attractive forces

$$\frac{\text{Height of the inactivation area}}{\text{Height of the sample}} < \frac{\text{Total no. of viable viruses after the exp}}{\text{total number of viable viruses before exp}}$$

This would mean that there are attractive forces at play.

For example, in Cin8, the left hand side for concentrated sample is 0.1 ( $10\mu\text{m}/100\mu\text{m}$ ). The number of virus particles recorded on the control is  $5.50 \times 10^9$  pfu/ml. After in activation on the Cin8 electrode the recorded concentration is  $7.15 \times 10^8$ . This gives a ratio of 0.13. As LHS is only slightly less than RHS we can conclude that the particles may have been attracted by a very weak DEP force. In diluted samples the left hand side is 0.05( $10\mu\text{m}/200\mu\text{m}$ ). The pfus recorded before and after treatment are  $5.50 \times 10^9$  and  $5.0 \times 10^8$  pfu/ml respectively, which gives a ratio of 0.09 which is slightly higher than the LHS. Thus we may conclude that in diluted sample the attractive force is either very weak assuming the phage titers are very accurate.

Finally, the effect of medium conductivity can be seen in figure 6-10. As expected, virus suspended in a medium with a high conductivity show a lower inactivation rate. This attests

to the fact that lower medium conductivity facilitates attraction at lower frequencies given to the CM plot of the corona virus.

## 7-2 Conclusions and future recommendations

In this study, the effect of electric fields on the surrogate of SARS CoV-2 virus was explored. PEF treatments performed on a macro-scale to inactivate smaller micro-organisms like viruses are often ineffective and hence this study focused on electric fields generated by micro-electrodes on micro chip platforms. For this reason, 7 different geometries of micro-electrodes were fabricated, characterized and tested with the virus sample. The conclusions of the study that answer the research questions are as follows:

- *Can the SARs CoV-2 virus be inactivated using electric field generated by planar micro-electrodes?*

The test results clearly show a decrease in the virus titers treated on some of the electrodes patterns compared to the control samples. This does suggest that the virus can be inactivated by the electric fields generated by micro-electrodes.

- *Are castellated geometries better at inactivating the virus than interdigitated geometries?*

Castellated geometries are indeed better at inactivating the virus than the interdigitated geometries as they generate more focused spots of high electric field.

- *Are electrodes with a smaller gap better at inactivating the virus than the electrodes with a larger gap?*

Due to short circuits on the electrodes, the active area of the electrodes decreased. Electrodes with a shorter pitch were more susceptible to short circuits than larger pitch electrodes. The effectiveness of the electrodes with a smaller pitch may have been offset by the lesser available electrode area.

Although, by decreasing electrode gap, electric field intensity increases but the field line of penetration through the sample decreases and as a result, less number of virus particles are concentrated and less virus is inactivated. This could also be a reason why we see less inactivation in electrodes with a shorter pitch. In any case, a redesign is necessary to test this hypothesis.

- *Is it necessary to attract the virus to the electrodes using pDEP for efficient and higher inactivation?*

Diluted samples show lesser inactivation than concentrated samples. Higher frequencies are better at inactivation than lower frequencies. This is all good evidence that the virus indeed needs to be attracted to the surface of the electrode where electric field is higher.

- *Does medium conductivity play an important role in facilitating pDEP attraction?*

Medium conductivity plays an important role in the concentration of the virus.

The work in this study is not sufficient to deduce the mechanism of inactivation of the virus, but it shows a potential for developing electric methods for inactivating viruses. Further work needs to be done:

- First, the experiments need to be repeated with a better electrode design. The redesign should include a smaller electrode area to reduce the probability of short-circuits. The lithography can be done on a single layer with a single wafer stepper mask. Alternatives to run the process on glass electrodes must be researched. A micro-channel should be built around the electrode to minimize evaporation and contamination of the sample. The surface of the electrode should be made more hydrophilic. The experiment runs need to be randomized and more data needs to be gathered with the new design of micro electrodes.
- Second, the experiments need to be repeated on the SARS CoV-2 or structural proteins of both the viruses(Phi6 and SARS) need to be explicitly compared and parallels need to be established; it may be that there are structural dissimilarities in the two viruses and that repeating the experiments on corona virus reveal different conclusions.
- The movement of the virus particle on the electrode needs to be visualized with the help of fluorescent microscopy. Tagging the virus with fluorescent dyes may shed some more light on the dielectrophoretic behaviour of corona virus and the inactivation mechanisms to support the claims made by this study.
- The molecular interactions of the virus proteins and membrane lipids with electric fields and voltage potentials needs to be studied. The effect of electric potentials and electric fields on virus assembly and virus stability needs to be explored.

In short, there is still much work to be done, but gleaned from relevant literature and the results procured from this study, all the signs point in the same direction and reach a unified conclusion: Exposure to the moderate electric fields created by micro-electrodes cause damaging structural alterations to the surface structures of the SARS CoV-2 and also possibly many other harmful viruses.

---

# Appendix A

---

## Process recipe

### A-1 Process recipe on Glass

1. Starting material-

Type: Glass (Quartz)

Resistivity: NA

Thickness:  $525 \pm 15 \mu\text{m}$

Diameter: 100mm

2. Cleaning-

Clean 10 minutes in fuming nitric acid at ambient temperature. This will dissolve organic materials. Use wet bench "HNO<sub>3</sub> 99% (metal)" and the carrier with a red and yellow dot. Rinse Rinse in the Quick Dump Rinser with the standard program until the resistivity is  $5M\omega$ . Dry Use the Avenger Ultra pure-6 "rinser/dryer" with the standard program, and the white carrier with a black dot.

Note- **Do not perform a "HNO<sub>3</sub> 69,5% 110C (Si)" cleaning step!**

3. Metallization: Aluminium Sputtering (back side)

Use the TRIKON SIGMA 204 sputter coater for the deposition of aluminum on the wafers. The target must exist of 99% Al and 1%Si, and deposition must be done at 25°C with an Ar flow of 100 sccm. Use a cleaned carrier wafer to load the glass wafer on the chuck. The carrier wafers can be found in a box next to the machine. Use recipe AlSi-300nm-25C to obtain a 300 nm thick layer. Note: Use dummy wafer in between process wafers to clean the target. Use the same temperature in this in between recipe as the process recipe.

4. Metallization: Aluminium sputtering (front side)

Load the wafers again on the same carrier wafer with glass side facing up. Use the TRIKON SIGMA 204 sputter coater for the deposition of aluminum on the wafers. Use recipe AlSi-300nm-25C to obtain a 300 nm thick layer on the front. Throw the carrier

wafer away. Note: from now on use only the mechanical forceps given to you. Note2: Make sure you identify and keep a track of the front side.

5. Manual Coating HMDS:

Coat manually with HDMS for 10 minutes the HMDS station. Check pressure before starting. Photo resist may strip off after development despite using HMDS. If this is the case heat the wafers in the polymer lab oven at 100 for 1 minute before manually coating the HDMS.

6. Coating

Use the coater station of the EVG120 system to coat the wafers with photoresist. The process consists of:

- spin coating of Shipley SPR3012 positive resist, dispensed by a pump. The approximate spin speed is 3450 rpm.
- a Soft Bake (SB) at 95 for 90 seconds Always check the relative humidity ( $48 \pm 2\%$ ) in the room before coating, and follow the instructions for this equipment. Use program "SpeCo - 3012 - 1.4 $\mu$ m-noEBR-noHMDS".

7. Alignment and exposure: Zero layer

Processing will be performed on the ASML PAS5500/80 automatic wafer stepper. Follow the operating instructions from the manual when using this machine. Does not need the alignment marker mask as the alignment markers are already there on the custom mask Expose COMURK, with job "Custom" and with 150mJ/cm<sup>2</sup> Exposure energy This will print the alignment markers on the wafer

8. Developing

Use the developer station of the EVG120 system to develop the wafers. The process consists of:

- A post exposure bake
- developing with Shipley MF322 with a single puddle process Do not perform a hard bake Always follow the instructions for this equipment. Use program "Dev-Sp- no HB".

9. Alignment and exposure: Wafer level Interconnects

Use the contact aligner to expose the interconnects. Expose mask Contact aligner Interconnects and position the wafers on the contact aligner Select the correct exposure energy. attention: time needs to be changed according to lamp intensity! Set 150mJ/cm<sup>2</sup> as exposure energy and 9.8 seconds as time. Use Soft contact

10. Developing

Use the developer station of the EVG120 system to develop the wafers. Always follow the instructions for this equipment. Use program "Dev - SP".

11. Inspection

Visually inspect the wafers through a microscope and check the line width and overlay. No resist residues are allowed. Check if the local interconnects are in line with the electrodes. Check if the interconnects are overlapping the local interconnects.

12. Dry etching: Aluminium Etch for electrodes and interconnects

Use the Trikon omega 201 plasma etcher. Follow the operating instructions from the manual when using this machine. It is not allowed to change the process conditions and times from the etch recipe! Use sequence AL03-25 (with a platen temperature of 25 °C) to etch the aluminium layer. Switch on the end point detection and note the endpoint when the recipe runs. Process conditions from chamber recipe AL03-350: (use for 0.3 $\mu$ m Al sputtered at 25)

Gasses & flows	Pressure	Platen RF	ICP RF	Platen temp.	Etch time
HBr/Cl <sub>2</sub> = 40/30 sccm	5 mTorr	50 W	500 W	25 °C	endpoint
HBr/Cl <sub>2</sub> = 40/30 sccm	5 mTorr	40 W	500 W	25 °C	endpoint
HBr/Cl <sub>2</sub> = 30/15 sccm	5 mTorr	40 W	500 W	25 °C	60% of bulk

**Table A-1:** Gasses and flow rates needed to etch 300nm of Aluminium

INSPECTION: No aluminium residues or undercut are allowed.

### 13. Plasma strip

Use the Tepla plasma system to remove the photoresist in an oxygen plasma. Follow the instructions specified for the Tepla stripper and use the quartz carrier. Use program 6: 1000 watts power and automatic endpoint detection + 2 min over etching.

### 14. Cleaning

10 minutes in fuming nitric acid at ambient temperature. This will dissolve organic materials. Use wet bench "HNO<sub>3</sub> 99% (metal)" and the carrier with a red and yellow dot.

Rinse in the Quick Dump Rinser with the standard program until the resistivity is 5M $\omega$ .

Use the Avenger Ultra pure-6 "rinser/dryer" with the standard program, and the white carrier with a black dot.

### 15. Manual HMDS

Coat manually with HMDS for 10 minutes the HMDS station. Check pressure before starting. Photo resist may strip off after development despite using HMDS. If this is the case heat the wafers in the polymer lab oven at 100 for 1 minute before manually coating the HMDS.

### 16. Coating

Use the coater station of the EVG120 system to coat the wafers with photoresist. The process consists of:

- spin coating of Shipley SPR3012 positive resist, dispensed by a pump. The approximate spin speed is 3450 rpm.
- a Soft Bake (SB) at 95 °C for 90 seconds

Always check the relative humidity ( $48 \pm 2$  %) in the room before coating, and follow the instructions for this equipment. Use program "SpeCo - 3012 – 1.4 $\mu$ m-noEBR-noHMDS".

### 17. Alignment and exposure: Gratings and cut arrays

Expose mask '**Electrodes**' in box 495. Select job **VIKI-01**. Select layer electrodes. Switch off the exposure for local interconnects top and local interconnects bottom. Select exposure energy 150mJ/cm<sup>2</sup>. This will print the gratings on the wafer.

#### 18. Development

Use the developer station of the EVG120 system to develop the wafers. Always follow the instructions for this equipment. Use program "Dev - SP".

#### 19. Etching

Use the Trikon omega 201 plasma etcher. Follow the operating instructions from the manual when using this machine. Select the recipe AL-res-02. This recipe does not have an endpoint. Change the time in this recipe by entering the time for the endpoint of the previous etching recipe (AL03-25). Add 5 seconds of over etch time. Set the platen temperature to 16 degrees. AL-res-02 is the exact same recipe as AL03-25 without the endpoint.

#### 20. Aluminium Fence removal and photoresist removal

Plasma strip: Use the Tepla plasma system to remove the photoresist in an oxygen plasma. Follow the instructions specified for the Tepla stripper and use the quartz carrier. Use program 6: 1000 watts power and automatic endpoint detection + 2 min over etching.

Moisten: Rinse for 1 minute in wet bench "H<sub>2</sub>O/Triton X-100 tbv Al. Ets". Use the carrier with the yellow dot. The bath contains 1 ml Triton X-100 per 5000 ml deionized water.

Etching: Use wet bench "Al. ets 35°C", and the carrier with the yellow dot. 1 liter buffered aluminium etch fluid contains: 770 ml concentrated phosphorus acid (H<sub>3</sub>PO<sub>4</sub> 85%), 19 ml concentrated nitric acid (HNO<sub>3</sub> 65/140 ml concentrated acetic acid (CH<sub>3</sub>COOH 100%) and 71 ml deionized water

Etch time: The etch rate at 35 °C is  $\pm 150$  nm/min. Etch time can be set to 30 secs to remove 75nm of aluminium

QDR: Rinse in the Quick Dump Rinser with the standard program until the resistivity is 5M $\Omega$ .

Drying Use the Semi tool "rinser/dryer" with the standard program, and the orange carrier with a black dot.

#### 21. Cleaning HNO<sub>3</sub> 99% metal

Clean- 10 minutes in fuming nitric acid at ambient temperature. This will dissolve organic materials. Use wet bench "HNO<sub>3</sub> 99% (metal)" and the carrier with a red and yellow dot.

Rinse- Rinse in the Quick Dump Rinser with the standard program until the resistivity is 5M $\Omega$ .

Dry- Use the Avenger Ultra pure-6 "rinser/dryer" with the standard program, and the white carrier with a black dot. Note Do not perform a "HNO<sub>3</sub> 69,5% 110C (Si)" cleaning step!

#### 22. Manual HMDS

Coat manually with HMDS for 10 minutes the HMDS station. Check pressure before starting. Photo resist may strip off after development despite using HMDS. If this is the case heat the wafers in the polymer lab oven at 100 for 1 minute before manually coating the HMDS.

## 23. Coating

Use the coater station of the EVG120 system to coat the wafers with photoresist. The process consists of: • spin coating of Shipley SPR3012 positive resist, dispensed by a pump. The approximate spin speed is 3450 rpm. • a Soft Bake (SB) at 95 for 90 seconds

Always check the relative humidity ( $48 \pm 2\%$ ) in the room before coating, and follow the instructions for this equipment. Use program "SpeCo - 3012 – 1.4 $\mu$ m-noEBR-noHMDS".

## 24. Alignment and exposure: Double exposure for improving yield.

Expose mask 'Electrodes' in box 495. Select job **VIKI-01**. Select layer electrodes. Switch off the exposure for local interconnects top and local interconnects bottom. Select exposure energy  $130\text{mJ}/\text{cm}^2$ . This will print the gratings on the wafer.

## 25. Development

Use the developer station of the EVG120 system to develop the wafers. Always follow the instructions for this equipment. Use program "Dev - SP".

## 26. Etching

Use the Trikon omega 201 plasma etcher. Follow the operating instructions from the manual when using this machine. Select the recipe **AL-res-02**. This recipe does not have an endpoint. Change the time in this recipe by entering the time for the endpoint of the previous etching recipe

## 27. Plasma strip

Use the Tepla plasma system to remove the photoresist in an oxygen plasma. Follow the instructions specified for the Tepla stripper and use the quartz carrier. Use program 6: 1000 watts power and automatic endpoint detection + 2 min over etching.

## 28. Electric measurements-

Use Cascade probe station with the nickel chuck (Cascade 31 or 33) to check the electrodes on the die. Record the measurements of each die and each section Write the job on the wafer stepper accordingly.

29. Cleaning HNO<sub>3</sub> 99% metal plus line

Clean- 10 minutes in fuming nitric acid at ambient temperature. This will dissolve organic materials. Use wet bench "HNO<sub>3</sub> 99% (metal plus)" and the carrier with a red and yellow dot.

Rinse- Rinse in the Quick Dump Rinser with the standard program until the resistivity is  $5\text{M}\Omega$ .

Dry- Use the Avenger Ultra pure-6 "rinser/dryer" with the standard program, and the white carrier with a black dot. Note **Do not perform a "HNO<sub>3</sub> 69,5% 110C (Si)" cleaning step!**

## 29. PECVD deposition- 150 nm TEOS on aluminium

Use the Novellus Concept One PECVD reactor. Follow the operating instructions from the manual when using this machine. It is not allowed to change the process conditions except the station deposition time from the deposition recipe!

Use recipe **".xxx-siostd"** to deposit a 150 nm thick SiO<sub>2</sub> layer. Check the book next to the machine to calculate the time needed. Usually the time is around 3.2 seconds.

Process conditions from recipe 100nmTEOS:

Gasses & flows	Pressure	HF power	LF power	Temperature	Station Deposition Time
N <sub>2</sub> /SiH <sub>4</sub> /N <sub>2</sub> O = 3150/205/6000 sccm	2.2 Torr	1000 W	0	400	3.2sec

**Table A-2:** Gasses and flow rates needed for the deposition of a TEOS layer

Note: The deposition time is subject to minor changes, in order to obtain the correct film thickness, check the book next to the machine to calculate the time needed. The layer thickness depends on the station deposition time (SDT), which can be calculated from the average deposition rate during recent recipe usage. An extra test wafer can be deposited for measurements and etch tests.

30. Cleaning HNO<sub>3</sub> (99%) metal-

Clean- 10 minutes in fuming nitric acid at ambient temperature. This will dissolve organic materials. Use wet bench "HNO<sub>3</sub> 99% (metal)" and the carrier with a red and yellow dot. Rinse- Rinse in the Quick Dump Rinser with the standard program until the resistivity is 5 Mohm. Dry- Use the "Avenger Ultra-Pure 6" rinser/dryer with the standard program, and the white carrier with a black dot.

Note: Do not perform a "HNO<sub>3</sub> 69,5% 110C (Si)" cleaning step!

31. Coating-

Use the coater station of the EVG120 system to coat the wafers with photoresist. Always check the relative humidity ( $48 \pm 2$  %) in the room before coating, and follow the instructions for this equipment. Use program "1-Co - 3012 - 1.4 $\mu$ m-noEBR"

32. Pad openings- Alignment and exposure

Processing will be performed on the ASML PAS5500/80 automatic wafer stepper. Follow the operating instructions from the manual when using this machine. Expose mask electrodes, Box(495), with job "VIKI1.0" with exposure energy 150mJ/cm<sup>2</sup>. Use the layer bond pad openings. It may be needed to change the alignment strategy at this point. Try using the VIKI35pp55pp instead of VIKI if the waferstepper gives an error. This will print the contact openings on the wafer.

33. Wet etching- Contact openings (100nm of SiO<sub>2</sub>)

Use the wet BHF bath for etching SiO<sub>2</sub> Keep the wafers inside the bath for 2 minutes this will etch 150nm of siO<sub>2</sub> with a half a minute of over etch.

34. Layer stripping: Photoresist

Strip resist Use the Tepla Plasma 300 system to remove the photoresist in an oxygen plasma. Follow the instructions specified for the Tepla stripper, and use the quartz carrier. Use program 1: 1000 watts power and automatic endpoint detection + 2 min. overetching.

35. Cleaning HNO<sub>3</sub> (99%) metal-

Clean- 10 minutes in fuming nitric acid at ambient temperature. This will dissolve organic materials. Use wet bench "HNO<sub>3</sub> 99% (metal)" and the carrier with a red and

yellow dot. Rinse- Rinse in the Quick Dump Rinser with the standard program until the resistivity is 5 Mohm. Dry- Use the "Avenger Ultra-Pure 6" rinser/dryer with the standard program, and the white carrier with a black dot.

Note: Do not perform a "HNO<sub>3</sub> 69,5% 110C (Si)" cleaning step!

36. Manual HMDS

Coat manually with HDMS for 10 minutes the HMDS station. Check pressure before starting. Photo resist may strip off after development despite using HMDS. If this is the case heat the wafers in the polymer lab oven at 100 for 1 minute before manually coating the HMDS.

37. Manual Coating

Use the big chuck for the coating. Assemble the dispenser and attach the SU8 vial on top. Keep the hot plate ready. Set one of the hot plate at 65 degrees and the other hotplate at 95 degrees. Use the pre made recipe Henk-Dave-25um-SU8 on the manual coater. The spin speed of the chuck should be set at **1450rpm** Perform EBR before moving to the preexposure Soft bake

38. Pre-exposure Soft bake-

Use the manual hotplate to bake the wafer for 10 minutes at 65 degrees.

39. Pre-exposure Hard Bake-

Use the hotplate to bake the wafers for 25 minutes at 95 degrees. Use program "Henk-95deg-25-prox-dave"

40. Alignment and exposure: Micro dam

Load the wafers on the ASML PAS5500/80 automatic wafer stepper. Expose mask Electrodes, Box(495) with job "**VIKI-microdams**". Select the layer Microdams. Expose with an exposure energy of  $400\text{mJ}/\text{cm}^2$  This will result in the microdam and the blocks being imprinted on the chip.

41. Post exposure soft bake

Use manual hotplate to bake the wafer at 60deg for 10 minutes.

42. Post Exposure hard bake

Use hotplate for manual baking. Use program "Henk-95deg-25-dave"

43. Development- with PGMEA

Develop on the wet bench with one bath of PGMEA for 5 mins. Shake the container manually. Shake until the sample is free of any SU8 residues. Rinse in DI water.

## A-2 Process recipe for Silicon

1. Starting material-

Type: n type Silicon

Resistivity: 1 – 5m

Thickness:  $525 \pm 15 \mu\text{m}$

Diameter: 100mm

## 2. Cleaning-

C10 minutes in fuming nitric acid at ambient temperature. This will dissolve organic materials. Use wet bench "HNO3 99% (Si)" and the carrier with the red dot. Rinse in the Quick Dump Rinser with the standard program until the resistivity is 5  $M$ . Clean 10 minutes in concentrated nitric acid at 110 °C. This will dissolve metal particles. Use wet bench "HNO3 69,5% 110C (Si)" and the carrier with the red dot. Rinse in the Quick Dump Rinser with the standard program until the resistivity is 5 $M$ . Dry Use the "Avenger Ultra-Pure 6" rinser/dryer with the standard program, and the white carrier with a red dot.

## 3. Metallization: Aluminium Sputtering (front side)

Use the TRIKON SIGMA 204 sputter coater for the deposition of aluminum on the wafers. The target must exist of 99% Al and 1%Si, and deposition must be done at 25°C with an Ar flow of 100 sccm. Use a cleaned carrier wafer to load the glass wafer on the chuck. The carrier wafers can be found in a box next to the machine. Use recipe AlSi-300nm-25C to obtain a 300 nm thick layer. Note: Use dummy wafer in between process wafers to clean the target. Use the same temperature in this in between recipe as the process recipe.

## 4. Manual Coating HMDS:

Coat manually with HDMS for 10 minutes the HMDS station. Check pressure before starting. Photo resist may strip off after development despite using HMDS. If this is the case heat the wafers in the polymer lab oven at 100for 1 minute before manually coating the HDMS.

## 5. Coating

Use the coater station of the EVG120 system to coat the wafers with photoresist. The process consists of:

- spin coating of Shipley SPR3012 positive resist, dispensed by a pump. The approximate spin speed is 3450 rpm.
- a Soft Bake (SB) at 95 for 90 seconds Always check the relative humidity ( $48 \pm 2 \%$ ) in the room before coating, and follow the instructions for this equipment. Use program "SpeCo - 3012 - 1.4 $\mu$ m-noEBR-noHMDS".

## 6. Alignment and exposure: Zero layer

Processing will be performed on the ASML PAS5500/80 automatic wafer stepper. Follow the operating instructions from the manual when using this machine. Does not need the alignment marker mask as the alignment markers are already there on the custom mask Expose COMURK, with job "Custom" and with 150mJ/cm2 Exposure energy This will print the alignment markers on the wafer

## 7. Developing

Use the developer station of the EVG120 system to develop the wafers. The process consists of:

- A post exposure bake
- developing with Shipley MF322 with a single puddle process Do not perform a hard bake Always follow the instructions for this equipment. Use program "Dev-Sp- no HB".

## 8. Alignment and exposure: Wafer level Interconnects

Use the contact aligner to expose the interconnects. Expose mask Contact aligner Interconnects and position the wafers on the contact aligner Select the correct exposure energy. attention: time needs to be changed according to lamp intensity! Set  $150\text{mJ}/\text{cm}^2$  as exposure energy and 9.8 seconds as time. Use Soft contact

## 9. Developing

Use the developer station of the EVG120 system to develop the wafers. Always follow the instructions for this equipment. Use program "Dev - SP".

## 10. Inspection

Visually inspect the wafers through a microscope and check the line width and overlay. No resist residues are allowed. Check if the local interconnects are in line with the electrodes. Check if the interconnects are overlapping the local interconnects.

## 11. Dry etching: Aluminium Etch for electrodes and interconnects

Use the Trikon omega 201 plasma etcher. Follow the operating instructions from the manual when using this machine. It is not allowed to change the process conditions and times from the etch recipe! Use sequence AL03-25 (with a platen temperature of 25 °C) to etch the aluminium layer. Switch on the end point detection and note the endpoint when the recipe runs. Process conditions from chamber recipe AL03-350: (use for 0.3 $\mu\text{m}$  Al sputtered at 25)

Gasses & flows	Pressure	Platen RF	ICP RF	Platen temp.	Etch time
HBr/Cl <sub>2</sub> = 40/30 sccm	5 mTorr	50 W	500 W	25 °C	endpoint
HBr/Cl <sub>2</sub> = 40/30 sccm	5 mTorr	40 W	500 W	25 °C	endpoint
HBr/Cl <sub>2</sub> = 30/15 sccm	5 mTorr	40 W	500 W	25 °C	60% of bulk

**Table A-3:** Gasses and flow rates needed to etch 300nm of Aluminium

INSPECTION: No aluminium residues or undercut are allowed.

## 12. Plasma strip

Use the Tepla plasma system to remove the photoresist in an oxygen plasma. Follow the instructions specified for the Tepla stripper and use the quartz carrier. Use program 6: 1000 watts power and automatic endpoint detection + 2 min over etching.

## 13. Cleaning

10 minutes in fuming nitric acid at ambient temperature. This will dissolve organic materials. Use wet bench "HNO<sub>3</sub> 99% (metal)" and the carrier with a red and yellow dot.

Rinse in the Quick Dump Rinser with the standard program until the resistivity is  $5M\omega$ . Use the Avenger Ultra pure-6 "rinser/dryer" with the standard program, and the white carrier with a black dot.

## 14. Manual HMDS

Coat manually with HMDS for 10 minutes the HMDS station. Check pressure before

starting. Photo resist may strip off after development despite using HMDS. If this is the case heat the wafers in the polymer lab oven at 100 for 1 minute before manually coating the HMDS.

#### 15. Coating

Use the coater station of the EVG120 system to coat the wafers with photoresist. The process consists of:

- spin coating of Shipley SPR3012 positive resist, dispensed by a pump. The approximate spin speed is 3450 rpm.
- a Soft Bake (SB) at 95 C for 90 seconds

Always check the relative humidity ( $48 \pm 2\%$ ) in the room before coating, and follow the instructions for this equipment. Use program "SpeCo - 3012 - 1.4 $\mu$ m-noEBR-noHMDS".

#### 16. Alignment and exposure: Gratings and cut arrays

Expose mask '**Electrodes**' in box 495. Select job **VIKI-01**. Select layer electrodes. Switch off the exposure for local interconnects top and local interconnects bottom. Select exposure energy  $150\text{mJ}/\text{cm}^2$ . This will print the gratings on the wafer.

#### 17. Development

Use the developer station of the EVG120 system to develop the wafers. Always follow the instructions for this equipment. Use program "Dev - SP".

#### 18. Etching

Use the Trikon omega 201 plasma etcher. Follow the operating instructions from the manual when using this machine. Select the recipe AL-res-02. This recipe does not have an endpoint. Change the time in this recipe by entering the time for the endpoint of the previous etching recipe (AL03-25). Add 5 seconds of over etch time. Set the platen temperature to 16 degrees. AL-res-02 is the exact same recipe as Al03-25 without the endpoint.

#### 19. Aluminium Fence removal and photoresist removal

Plasma strip: Use the Tepla plasma system to remove the photoresist in an oxygen plasma. Follow the instructions specified for the Tepla stripper and use the quartz carrier. Use program 6: 1000 watts power and automatic endpoint detection + 2 min over etching.

Moisten: Rinse for 1 minute in wet bench "H<sub>2</sub>O/Triton X-100 tbv Al. Ets". Use the carrier with the yellow dot. The bath contains 1 ml Triton X-100 per 5000 ml deionized water.

Etching: Use wet bench "Al. ets 35°C", and the carrier with the yellow dot. 1 liter buffered aluminium etch fluid contains: 770 ml concentrated phosphorus acid (H<sub>3</sub>PO<sub>4</sub> 85%), 19 ml concentrated nitric acid (HNO<sub>3</sub> 65), 140 ml concentrated acetic acid (CH<sub>3</sub>COOH 100%) and 71 ml deionized water

Etch time: The etch rate at 35 °C is  $\pm 150\text{ nm}/\text{min}$ . Etch time can be set to 30 secs to remove 75nm of aluminium

QDR: Rinse in the Quick Dump Rinser with the standard program until the resistivity is  $5\text{M}\Omega$ .

Drying Use the Semi tool "rinser/dryer" with the standard program, and the orange carrier with a black dot.

20. Cleaning HNO<sub>3</sub> 99% metal

Clean- 10 minutes in fuming nitric acid at ambient temperature. This will dissolve organic materials. Use wet bench "HNO<sub>3</sub> 99% (metal)" and the carrier with a red and yellow dot.

Rinse- Rinse in the Quick Dump Rinser with the standard program until the resistivity is  $5M\Omega$ .

Dry- Use the Avenger Ultra pure-6 "rinser/dryer" with the standard program, and the white carrier with a black dot. Note Do not perform a "HNO<sub>3</sub> 69,5% 110C (Si)" cleaning step!

21. Manual HMDS

Coat manually with HDMS for 10 minutes the HMDS station. Check pressure before starting. Photo resist may strip off after development despite using HMDS. If this is the case heat the wafers in the polymer lab oven at 100 for 1 minute before manually coating the HMDS.

22. Coating

Use the coater station of the EVG120 system to coat the wafers with photoresist. The process consists of: • spin coating of Shipley SPR3012 positive resist, dispensed by a pump. The approximate spin speed is 3450 rpm. • a Soft Bake (SB) at 95 for 90 seconds

Always check the relative humidity ( $48 \pm 2\%$ ) in the room before coating, and follow the instructions for this equipment. Use program "SpeCo - 3012 – 1.4 $\mu$ m-noEBR-noHMDS".

23. Alignment and exposure: Double exposure for improving yield.

Expose mask 'Electrodes' in box 495. Select job **VIKI-01**. Select layer electrodes. Switch off the exposure for local interconnects top and local interconnects bottom. Select exposure energy  $130mJ/cm^2$ . This will print the gratings on the wafer.

24. Development

Use the developer station of the EVG120 system to develop the wafers. Always follow the instructions for this equipment. Use program "Dev - SP".

25. Etching

Use the Trikon omega 201 plasma etcher. Follow the operating instructions from the manual when using this machine. Select the recipe **AL-res-02**. This recipe does not have an endpoint. Change the time in this recipe by entering the time for the endpoint of the previous etching recipe

26. Plasma strip

Use the Tepla plasma system to remove the photoresist in an oxygen plasma. Follow the instructions specified for the Tepla stripper and use the quartz carrier. Use program 6: 1000 watts power and automatic endpoint detection + 2 min over etching.

## 27. Electric measurements-

Use Cascade probe station with the nickel chuck (Cascade 31 or 33) to check the electrodes on the die. Record the measurements of each die and each section Write the job on the wafer stepper accordingly.

29. Cleaning HNO<sub>3</sub> 99% metal plus line

Clean- 10 minutes in fuming nitric acid at ambient temperature. This will dissolve organic materials. Use wet bench "HNO<sub>3</sub> 99% (metal plus)" and the carrier with a red and yellow dot.

Rinse- Rinse in the Quick Dump Rinser with the standard program until the resistivity is 5M $\Omega$ .

Dry- Use the Avenger Ultra pure-6 "rinser/dryer" with the standard program, and the white carrier with a black dot. Note **Do not perform a "HNO<sub>3</sub> 69,5% 110C (Si)" cleaning step!**

## 28. PECVD deposition- 150 nm TEOS on aluminium

Use the Novellus Concept One PECVD reactor. Follow the operating instructions from the manual when using this machine. It is not allowed to change the process conditions except the station deposition time from the deposition recipe!

Use recipe ".xxx-siostd" to deposit a 150 nm thick SiO<sub>2</sub> layer. Check the book next to the machine to calculate the time needed. Usually the time is around 3.2 seconds.

Process conditions from recipe 100nmTEOS:

Gasses & flows	Pressure	HF power	LF power	Temperature	Station Deposition Time
N <sub>2</sub> /SiH <sub>4</sub> /N <sub>2</sub> O = 3150/205/6000 sccm	2.2 Torr	1000 W	0	400	3.2sec

**Table A-4:** Gasses and flow rates needed for the deposition of a TEOS layer

Note: The deposition time is subject to minor changes, in order to obtain the correct film thickness, check the book next to the machine to calculate the time needed. The layer thickness depends on the station deposition time (SDT), which can be calculated from the average deposition rate during recent recipe usage. An extra test wafer can be deposited for measurements and etch tests.

29. Cleaning HNO<sub>3</sub> (99%) metal-

Clean- 10 minutes in fuming nitric acid at ambient temperature. This will dissolve organic materials. Use wet bench "HNO<sub>3</sub> 99% (metal)" and the carrier with a red and yellow dot. Rinse- Rinse in the Quick Dump Rinser with the standard program until the resistivity is 5 Mohm. Dry- Use the "Avenger Ultra-Pure 6" rinser/dryer with the standard program, and the white carrier with a black dot.

Note: Do not perform a "HNO<sub>3</sub> 69,5% 110C (Si)" cleaning step!

## 30. Coating-

Use the coater station of the EVG120 system to coat the wafers with photoresist. Always check the relative humidity ( $48 \pm 2$  %) in the room before coating, and follow the instructions for this equipment. Use program "1-Co - 3012 - 1.4 $\mu$ m-noEBR"

31. Pad openings- Alignment and exposure

Processing will be performed on the ASML PAS5500/80 automatic wafer stepper. Follow the operating instructions from the manual when using this machine. Expose mask electrodes, Box(495), with job "**VIKI1.0**" with exposure energy  $150mJ/cm^2$ . Use the layer bond pad openings. It may be needed to change the alignment strategy at this point. Try using the VIKI35pp55pp instead of VIKI if the waferstepper gives an error. This will print the contact openings on the wafer.

32. Dry etching- Contact openings (100nm of SiO<sub>2</sub>)

Use the Drytek Triode 384T plasma etcher. Follow the operating instructions from the manual when using this machine. It is not allowed to change the process conditions from the etch recipe, except for the etch time. Use the recipe SToxide with a soft landing to etch the Silicon oxide. Edit the time step in the first part of the process according to the thickness of the Siliconoxide.

33. Layer stripping: Photoresist

Strip resist Use the Tepla Plasma 300 system to remove the photoresist in an oxygen plasma. Follow the instructions specified for the Tepla stripper, and use the quartz carrier. Use program 1: 1000 watts power and automatic endpoint detection + 2 min. overetching.

34. 3D printing of Micro-dams- The thick photoresist deposition was substituted by 3D printing a dam and gluing it around the electrode using the same resist and curing it with UV light. This substitution was made to make the processing faster. It was also noticed that SU8 left traces on the silicon oxide which made the surface hydrophobic. Hence the thick photoresist step was substituted with 3D printed dams. The dam was made 0.25mm thick and out of photo-curable resist.

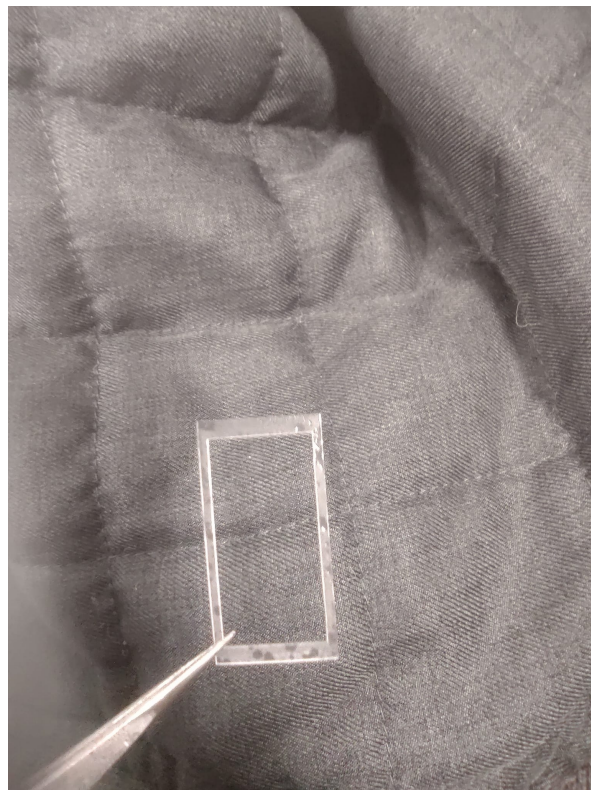


**Figure A-1:** 3D printed micro-dam

---

## Appendix B

---

# Additional Data

### **B-1 Photos of PFU Assays**

### **B-2 First run of Experiment 1**

The first run with DC input resulted in positive results that showed substantial inactivation. This was later debunked to be because of a temperature rise due to joule heating. The electrodes with a smaller pitch had more short circuited arrays than the electrodes with a larger pitch. When the short circuited electrodes were connected with an input, the current flowing through the short circuit resulted in joule heating. The joule heating on the substrate was measured with the help a thermal camera. This is shown in figure where the thermal images of the I2 electrode(3 shorted arrays) were captured every 2 minutes input with 20V source.

### **B-3 Additional Voltage-current graphs**



**Figure B-1:** Pfu assays for experiment 1

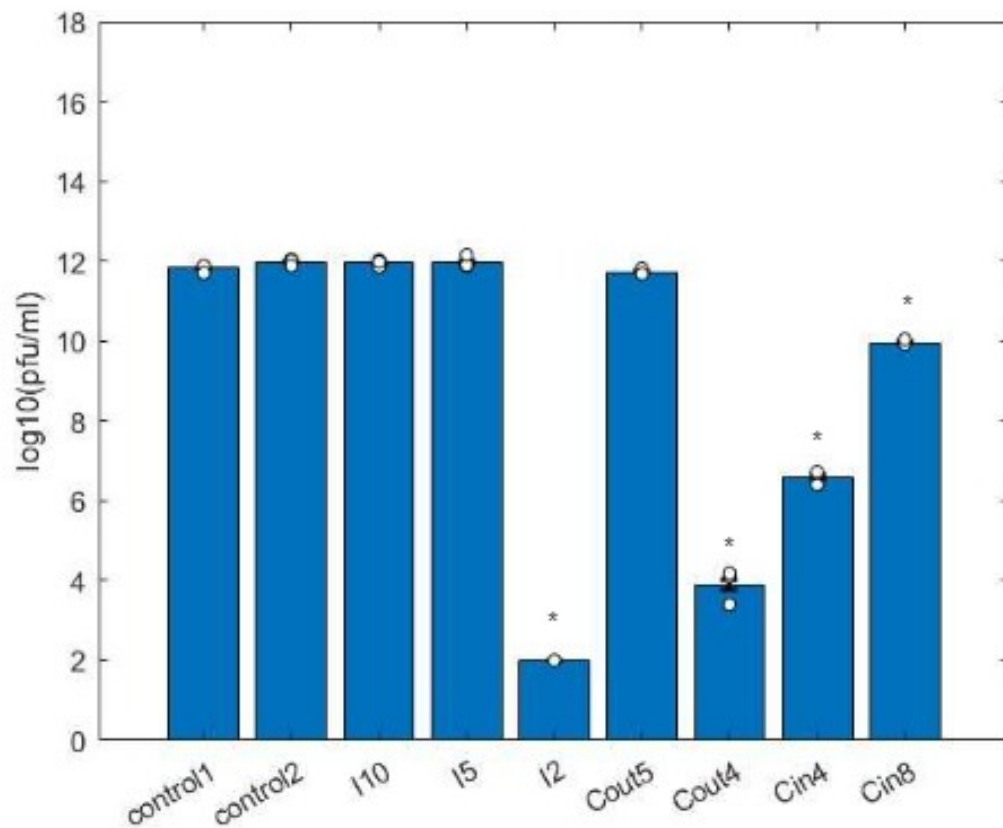


**Figure B-2:** Experiment 1 with DC input voltage

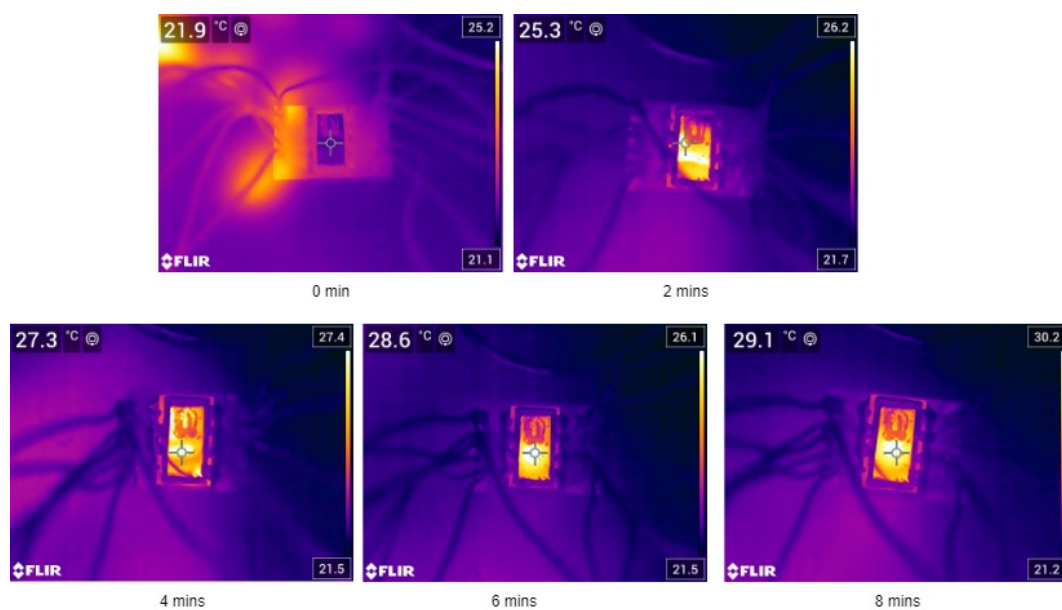


**Figure B-3:** Thermal images of electrode I2 with 3 short circuits input with 20V DC voltages

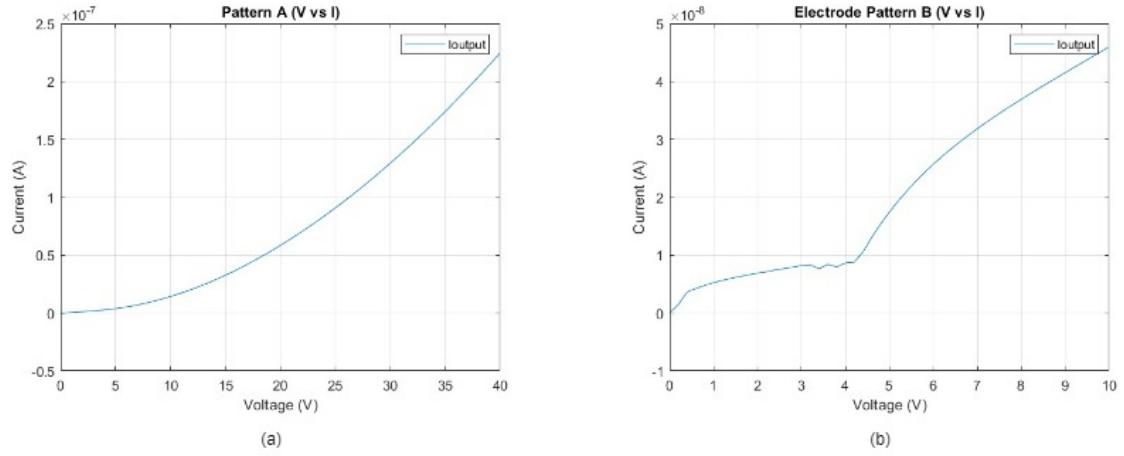


**Figure B-4:** Breakdown voltage graphs for (a) Pattern Cin4: castellated in-phase gap  $1\mu\text{m}$  and (b) Pattern Cin8: Castellated in-phase gap  $6\mu\text{m}$  on glass substrates.

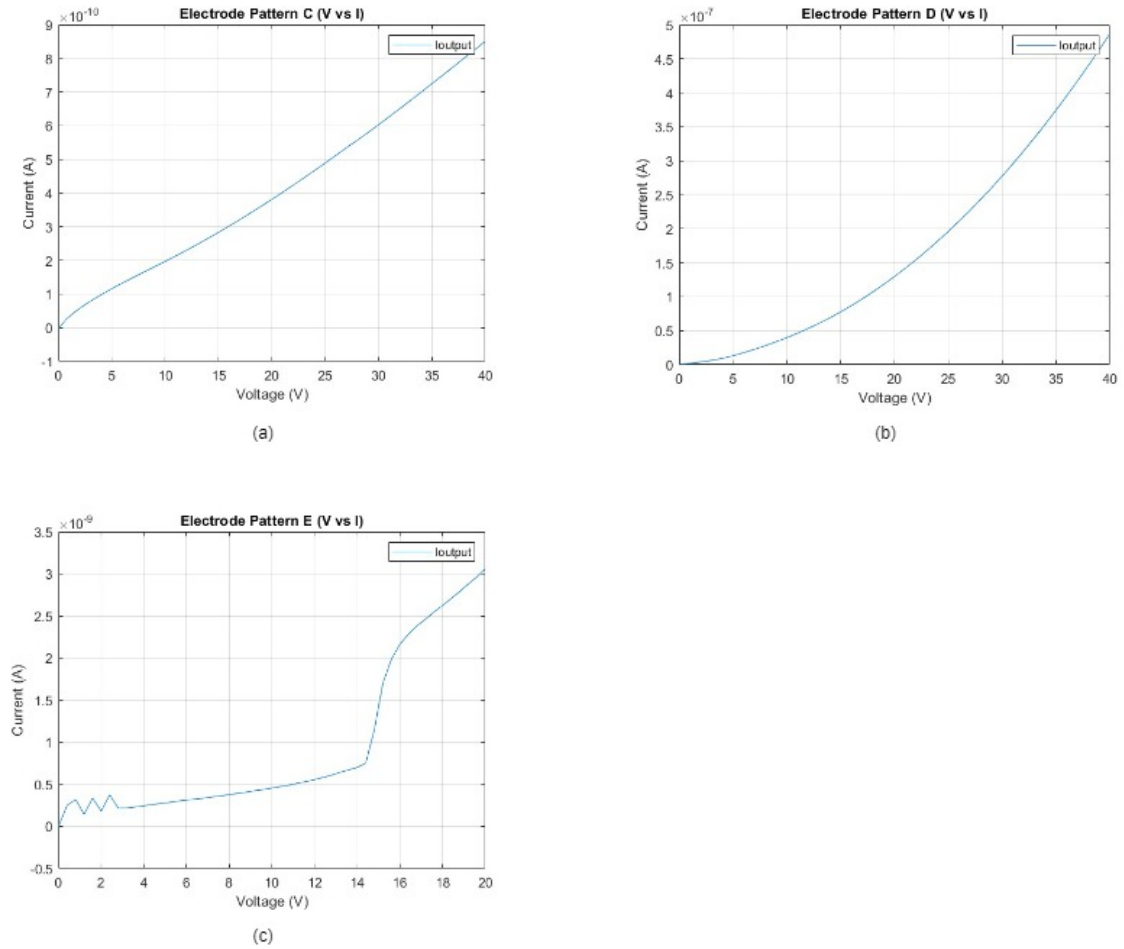


**Figure B-5:** Breakdown voltage graphs for (a) Pattern I2: interdigitated Comb gap  $1\mu\text{m}$ , (b) Pattern I5: Interdigitated Comb gap  $4\mu\text{m}$ , (c) Pattern I10: interdigitated comb pitch  $9\mu\text{m}$  on glass substrates.

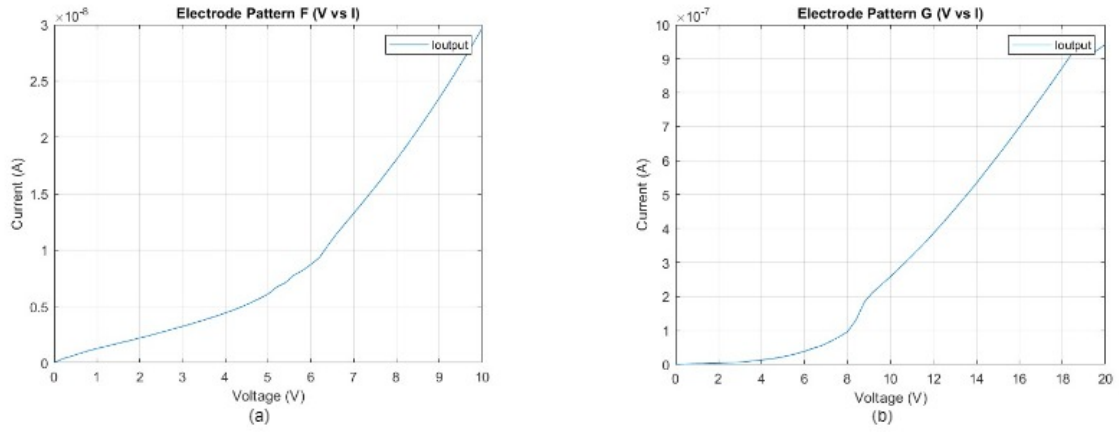


**Figure B-6:** Breakdown voltage graphs for (a) Pattern Cout4: Castellated out of phase gap 500nm, (b) Pattern Cout5: Castellated out of phase gap  $1\mu\text{m}$  on glass substrates



---

## Bibliography

- [1] C. R. Arbeitman, P. Rojas, P. Ojeda-May, and M. E. Garcia, “The SARS-CoV-2 spike protein is vulnerable to moderate electric fields,” *Nature Communications*, vol. 12, no. 1, 12 2021.
- [2] K. Khoshmanesh, S. Nahavandi, S. Baratchi, A. Mitchell, and K. Kalantar-zadeh, “Dielectrophoretic platforms for bio-microfluidic systems,” pp. 1800–1814, 1 2011.
- [3] H. Sadeghian, Y. Hojjat, and M. Soleimani, “Interdigitated electrode design and optimization for dielectrophoresis cell separation actuators,” *Journal of Electrostatics*, vol. 86, pp. 41–49, 4 2017.
- [4] M. Castellarnau, A. Errachid, C. Madrid, A. Juárez, and J. Samitier, “Dielectrophoresis as a tool to characterize and differentiate isogenic mutants of *Escherichia coli*,” *Biophysical journal*, vol. 91, no. 10, pp. 3937–3945, 2006. [Online]. Available: <https://pubmed.ncbi.nlm.nih.gov/16950844/>
- [5] Y. Gerchman, H. Mamane, N. Friedman, and M. Mandelboim, “UV-LED disinfection of Coronavirus: Wavelength effect,” *Journal of Photochemistry and Photobiology B: Biology*, vol. 212, p. 112044, 11 2020.
- [6] M. Lualdi, A. Cavalleri, A. Bianco, M. Biasin, C. Cavatorta, M. Clerici, P. Galli, G. Pareschi, and E. Pignoli, “Ultraviolet C lamps for disinfection of surfaces potentially contaminated with SARS-CoV-2 in critical hospital settings: examples of their use and some practical advice,” *BMC Infectious Diseases*, vol. 21, no. 1, pp. 1–13, 12 2021. [Online]. Available: <https://bmcinfectdis.biomedcentral.com/articles/10.1186/s12879-021-06310-5>
- [7] B. Ma, P. M. Gundy, C. P. Gerba, M. D. Sobsey, and K. G. Linden, “UV Inactivation of SARS-CoV-2 across the UVC Spectrum: KrCl Excimer, Mercury-Vapor, and Light-Emitting-Diode (LED) Sources,” *Applied and Environmental Microbiology*, vol. 87, no. 22, 10 2021. [Online]. Available: <https://journals.asm.org/doi/full/10.1128/AEM.01532-21>

- [8] F. Saadatpour and F. Mohammadipanah, "Physicochemical susceptibility of SARS-CoV-2 to disinfection and physical approach of prophylaxis," *Health Science Reports*, vol. 3, no. 4, 12 2020. [Online]. Available: [/pmc/articles/PMC7709914/](https://pmc/articles/PMC7709914/)[https://www.ncbi.nlm.nih.gov/pmc/articles/PMC7709914/](https://www.ncbi.nlm.nih.gov/pmc/articles/PMC7709914/?report=abstracthttps://www.ncbi.nlm.nih.gov/pmc/articles/PMC7709914/)
- [9] F. Moshfegh, F. Khosraviani, N. Moghaddasi, S. F. S. J. Limoodi, and E. Boluki, "Antiviral optical techniques as a possible novel approach to COVID-19 treatment," *Journal of Innovative Optical Health Sciences*, vol. 14, no. 3, 5 2021. [Online]. Available: [www.worldscientific.com](http://www.worldscientific.com)
- [10] M. A. Khadre and A. E. Yousef, "Susceptibility of Human Rotavirus to Ozone, High Pressure, and Pulsed Electric Field," *Journal of Food Protection*, vol. 65, no. 9, pp. 1441–1446, 9 2002. [Online]. Available: <https://meridian.allenpress.com/jfp/article/65/9/1441/167394/Susceptibility-of-Human-Rotavirus-to-Ozone-High>
- [11] "Note # 75: Pohl, H.A., Karan Kaler, and Kent Pollock, "The Continuous Positive and Negative Dielectrophoresis of Microorganisms," June, 1978 | Oklahoma State University." [Online]. Available: [https://archivesspace.library.okstate.edu/repositories/3/archival\\_objects/24459](https://archivesspace.library.okstate.edu/repositories/3/archival_objects/24459)
- [12] A. S. Bahaj and A. G. Bailey, "Dielectrophoresis of microscopic particles," *Journal of Physics D: Applied Physics*, vol. 12, no. 10, p. L109, 10 1979. [Online]. Available: <https://iopscience.iop.org/article/10.1088/0022-3727/12/10/001https://iopscience.iop.org/article/10.1088/0022-3727/12/10/001/meta>
- [13] M. P. Hughes, H. Morgan, and F. J. Rixon, "Measuring the dielectric properties of herpes simplex virus type 1 virions with dielectrophoresis," *Biochimica et biophysica acta*, vol. 1571, no. 1, pp. 1–8, 5 2002. [Online]. Available: <https://pubmed.ncbi.nlm.nih.gov/12031284/>
- [14] H. R. Gelderblom, "Structure and Classification of Viruses," *Medical Microbiology*, 1996. [Online]. Available: <https://www.ncbi.nlm.nih.gov/books/NBK8174/>
- [15] H. Morgan and N. G. Green, "Dielectrophoretic manipulation of rod-shaped viral particles," *Journal of Electrostatics*, vol. 42, no. 3, pp. 279–293, 12 1997.
- [16] M. P. Hughes, H. Morgan, F. J. Rixon, J. P. Burt, and R. Pethig, "Manipulation of herpes simplex virus type 1 by dielectrophoresis," *Biochimica et Biophysica Acta (BBA) - General Subjects*, vol. 1425, no. 1, pp. 119–126, 9 1998.
- [17] D. Akin, H. Li, and R. Bashir, "Real-Time Virus Trapping and Fluorescent Imaging in Microfluidic Devices," *Nano Letters*, vol. 4, no. 2, pp. 257–259, 2 2004.
- [18] "grom2006."
- [19] I. Ermolina, J. Milner, and H. Morgan, "Dielectrophoretic investigation of plant virus particles: Cow Pea Mosaic Virus and Tobacco Mosaic Virus," *Electrophoresis*, vol. 27, no. 20, pp. 3939–3948, 10 2006.

- 
- [20] M. Nakano, Z. Ding, and J. Suehiro, "Dielectrophoresis and dielectrophoretic impedance detection of adenovirus and rotavirus," *Japanese Journal of Applied Physics*, vol. 55, no. 1, 1 2016.
  - [21] J. Ding, R. M. Lawrence, P. V. Jones, B. G. Hogue, and M. A. Hayes, "Concentration of Sindbis virus with optimized gradient insulator-based dielectrophoresis," *The Analyst*, vol. 141, no. 6, pp. 1997–2008, 3 2016. [Online]. Available: <https://pubmed.ncbi.nlm.nih.gov/26878279/>
  - [22] A. C. De Peña, N. H. M. Redzuan, M. K. Abajorga, N. Hill, J. A. Thomas, and B. H. Lapizco-Encinas, "Analysis of bacteriophages with insulator-based dielectrophoresis," *Micromachines*, vol. 10, no. 7, 7 2019.
  - [23] H. Morgan, M. P. Hughes, and N. G. Green, "Separation of submicron bioparticles by dielectrophoresis," *Biophysical Journal*, vol. 77, no. 1, pp. 516–525, 1999.
  - [24] F. R. Madiyar, L. U. Syed, C. T. Culbertson, and J. Li, "Manipulation of bacteriophages with dielectrophoresis on carbon nanofiber nanoelectrode arrays," *Electrophoresis*, vol. 34, no. 7, pp. 1123–1130, 4 2013.
  - [25] L. Javidpour, A. Božič, A. Naji, and R. Podgornik, "Electrostatic interactions between the SARS-CoV-2 virus and a charged electret fibre," *Soft Matter*, vol. 17, no. 16, pp. 4296–4303, 4 2021.
  - [26] W. W. F. Leung and Q. Sun, "Electrostatic charged nanofiber filter for filtering airborne novel coronavirus (COVID-19) and nano-aerosols," *Separation and Purification Technology*, vol. 250, p. 116886, 11 2020. [Online]. Available: <https://pubmed.ncbi.nlm.nih.gov/330116886/>
  - [27] M. A. Ahmad, F. Mustafa, L. M. Ali, J. V. Karakkat, and T. A. Rizvi, "Label-free capacitance-based identification of viruses," *Scientific Reports*, vol. 5, 5 2015.
  - [28] J. Kentsch, M. Dürr, T. Schnelle, G. Gradl, T. Müller, M. Jäger, A. Normann, and M. Stelzle, "Microdevices for separation, accumulation, and analysis of biological micro-And nanoparticles," *IEE Proceedings Nanobiotechnology*, vol. 150, no. 2, pp. 82–89, 11 2003.
  - [29] T. Masuda, H. Maruyama, A. Honda, and F. Arai, "Virus Enrichment for Single Virus Infection by Using 3D Insulator Based Dielectrophoresis," *PLOS ONE*, vol. 9, no. 6, p. e94083, 6 2014. [Online]. Available: <https://journals.plos.org/plosone/article?id=10.1371/journal.pone.0094083>
  - [30] B. H. Lapizco-Encinas, R. V. Davalos, B. A. Simmons, E. B. Cummings, and Y. Fintschenko, "An insulator-based (electrodeless) dielectrophoretic concentrator for microbes in water," *Journal of microbiological methods*, vol. 62, no. 3, pp. 317–326, 2005. [Online]. Available: <https://pubmed.ncbi.nlm.nih.gov/15941604/>
  - [31] R. C. Gallo-Villanueva, V. H. Perez-Gonzalez, B. Cardenas-Benitez, B. Jind, S. O. Martinez-Chapa, and B. H. Lapizco-Encinas, "Joule heating effects in optimized insulator-based dielectrophoretic devices: An interplay between post geometry and temperature rise," *Electrophoresis*, vol. 40, no. 10, pp. 1408–1416, 5 2019.

- [32] K. Park, D. Akin, and R. Bashir, "Electrical capture and lysis of vaccinia virus particles using silicon nano-scale probe array," *Biomedical Microdevices*, vol. 9, no. 6, pp. 877–883, 12 2007.
- [33] M. W. Johnson, G. W. Wagner, and J. B. Bancroft, "A Titrimetric and Electrophoretic Study of Cowpea Chlorotic Mottle Virus and its Protein," Tech. Rep., 1973.
- [34] *Electroporation and Electrofusion in Cell Biology*. Springer US, 1989.
- [35] G. Mernier, N. Piacentini, T. Braschler, N. Demierre, and P. Renaud, "Continuous-flow electrical lysis device with integrated control by dielectrophoretic cell sorting," *Lab on a Chip*, vol. 10, no. 16, pp. 2077–2082, 7 2010. [Online]. Available: <https://pubs.rsc.org/en/content/articlehtml/2010/lc/c000977f><https://pubs.rsc.org/en/content/articlelanding/2010/lc/c000977f>
- [36] S.-W. Lee and Y.-C. Tai, "A micro cell lysis device," Tech. Rep.
- [37] K. H. Schoenbach, R. P. Joshi, R. H. Stark, F. C. Dobbs, and S. J. Beebe, "Bacterial Decontamination of Liquids with Pulsed Electric Fields," Tech. Rep. 5, 2000.
- [38] C. De La Rosa, P. A. Tilley, J. D. Fox, and K. V. Kaler, "Microfluidic device for dielectrophoresis manipulation and electrodisruption of respiratory pathogen *Bordetella pertussis*," *IEEE transactions on bio-medical engineering*, vol. 55, no. 10, pp. 2426–2432, 10 2008. [Online]. Available: <https://pubmed.ncbi.nlm.nih.gov/18838368/>
- [39] K. H. Schoenbach, A. Abou-Ghazala, T. Vithoulkas, R. W. Alden, R. Tumer, and S. Beebe, "THE EFFECT OF PULSED ELECTRICAL FIELDS ON BIOLOGICAL CELLS," Tech. Rep.
- [40] J. R. Beveridge, K. Wall, S. J. MacGregor, J. G. Anderson, and N. J. Rowan, "Pulsed electric field inactivation of spoilage microorganisms in alcoholic beverages," *Proceedings of the IEEE*, vol. 92, no. 7, pp. 1138–1143, 2004.
- [41] S. J. Beebe, P. M. Fox, L. J. Rec, K. Somers, R. H. Stark, and K. H. Schoenbach, "Nanosecond pulsed electric field (nsPEF) effects on cells and tissues: Apoptosis induction and tumor growth inhibition," *IEEE Transactions on Plasma Science*, vol. 30, no. 1 II, pp. 286–292, 2 2002.
- [42] T. Kotnik, F. Bobanovic, and D. Miklavcic, "Sensitivity of transmembrane voltage induced by applied electric fields-a theoretical analysis," Tech. Rep., 1997.
- [43] T. Kotnik, L. M. Mir, K. Flisar, M. Puc, and D. Miklavcic, "Cell membrane electropermeabilization by symmetrical bipolar rectangular pulses q Part I. Increased efficiency of permeabilization," Tech. Rep., 2001. [Online]. Available: [www.elsevier.com/locate/bioelectchem](http://www.elsevier.com/locate/bioelectchem)
- [44] C. Church, J. Zhu, G. Huang, T.-R. Tzeng, and X. Xuan, "Integrated electrical concentration and lysis of cells in a microfluidic chip," 2010.
- [45] P. Vulto, G. Dame, U. Maier, S. Makohliso, S. Podszun, P. Zahn, and G. A. Urban, "A microfluidic approach for high efficiency extraction of low molecular

- weight RNA,” *Lab on a Chip*, vol. 10, no. 5, pp. 610–616, 3 2010. [Online]. Available: <https://pubs.rsc.org/en/content/articlehtml/2010/lc/b913481f><https://pubs.rsc.org/en/content/articlelanding/2010/lc/b913481f>
- [46] N. Ikeda, N. Tanaka, Y. Yanagida, and T. Hatsuzawa, “On-chip single-cell lysis for extracting intracellular material,” *Japanese Journal of Applied Physics, Part 1: Regular Papers and Short Notes and Review Papers*, vol. 46, no. 9 B, pp. 6410–6414, 9 2007. [Online]. Available: <https://iopscience.iop.org/article/10.1143/JJAP.46.6410><https://iopscience.iop.org/article/10.1143/JJAP.46.6410/meta>
- [47] “POVSholanov.”
- [48] T. Kotnik, D. Miklavcic, T. Slivnik<sup>~</sup>, and S. Slivnik<sup>~</sup>, “Time course of transmembrane voltage induced by time-varying electric fields-a method for theoretical analysis and its application,” Tech. Rep., 1998.
- [49] P. Marszalek, D. S. Liu, and T. Y. Tsong, “Schwan equation and transmembrane potential induced by alternating electric field,” *Biophysical Journal*, vol. 58, no. 4, pp. 1053–1058, 1990.
- [50] C. Grosse and R. Barchini, “The influence of diffusion on the dielectric properties of suspensions of conductive spherical particles in an electrolyte,” *Journal of Physics D: Applied Physics*, vol. 25, no. 3, p. 508, 3 1992. [Online]. Available: <https://iopscience.iop.org/article/10.1088/0022-3727/25/3/026><https://iopscience.iop.org/article/10.1088/0022-3727/25/3/026/meta>
- [51] D. Osorio-González, V. J. Muñoz-Orozco, C. P. González, M. Fuentes-Acosta, J. Mulia-Rodríguez, and L. A. Mandujano-Rosas, “Receptor Binding Domain (RBD) Structural Susceptibility in the SARS-CoV-2 Virus Spike Protein Exposed to a Pulsed Electric Field,” *Journal of Nuclear Physics, Material Sciences, Radiation and Applications*, vol. 8, no. 2, pp. 177–182, 2 2021.
- [52] B. Ghatak, S. Banerjee, S. B. Ali, R. Bandyopadhyay, N. Das, D. Mandal, and B. Tudu, “Design of a self-powered triboelectric face mask,” *Nano Energy*, vol. 79, 1 2021.
- [53] F. R. Madiyar, S. L. Haller, O. Farooq, S. Rothenburg, C. Culbertson, and J. Li, “AC dielectrophoretic manipulation and electroporation of vaccinia virus using carbon nano-electrode arrays,” *Electrophoresis*, vol. 38, no. 11, pp. 1515–1525, 6 2017.
- [54] N. Wood, “Trapping of nanoparticles with dielectrophoretic nano-probes.” Ph.D. dissertation, University of Louisville, 2012. [Online]. Available: <http://ir.library.louisville.edu/etd/1588>
- [55] H. Lu, M. A. Schmidt, and K. F. Jensen, “A microfluidic electroporation device for cell lysis,” *Lab on a Chip*, vol. 5, no. 1, pp. 23–29, 2005.
- [56] C. A. Chen, C. H. Chen, A. M. Ghaemmaghami, and S. K. Fan, “Separation of dendritic and T cells using electrowetting and dielectrophoresis,” in *2012 7th IEEE International Conference on Nano/Micro Engineered and Molecular Systems, NEMS 2012*, 2012, pp. 183–186.

- [57] K. Y. Lu, A. M. Wo, Y. J. Lo, K. C. Chen, C. M. Lin, and C. R. Yang, "Three dimensional electrode array for cell lysis via electroporation," *Biosensors and Bioelectronics*, vol. 22, no. 4 SPEC. ISS., pp. 568–574, 10 2006.
- [58] D. Huang, D. Zhao, J. Li, Y. Wu, W. Zhou, W. Wang, Z. Liang, and Z. Li, "High cell viability microfluidic electroporation in a curved channel," *Sensors and Actuators B: Chemical*, vol. 250, pp. 703–711, 10 2017.
- [59] S. B. Asokan, L. Jawerth, R. L. Carroll, R. E. Cheney, S. Washburn, and R. Superfine, "Two-dimensional manipulation and orientation of actin-myosin systems with dielectrophoresis," *Nano Letters*, vol. 3, no. 4, pp. 431–437, 4 2003. [Online]. Available: <https://pubs.acs.org/doi/abs/10.1021/nl0259434>
- [60] L. S. Jang, P. H. Huang, and K. C. Lan, "Single-cell trapping utilizing negative dielectrophoretic quadrupole and microwell electrodes," *Biosensors and Bioelectronics*, vol. 24, no. 12, pp. 3637–3644, 8 2009.
- [61] N. Mittal, A. Rosenthal, and J. Voldman, "nDEP microwells for single-cell patterning in physiological media," *Lab on a Chip*, vol. 7, no. 9, pp. 1146–1153, 8 2007. [Online]. Available: <https://pubs.rsc.org/en/content/articlehtml/2007/lc/b706342c><https://pubs.rsc.org/en/content/articlelanding/2007/lc/b706342c>
- [62] R. S. Thomas, H. Morgan, and N. G. Green, "Negative DEP traps for single cell immobilisation," *Lab on a Chip*, vol. 9, no. 11, pp. 1534–1540, 2009.
- [63] R. Krishnan, B. D. Sullivan, R. L. Mifflin, S. C. Esener, and M. J. Heller, "Alternating current electrokinetic separation and detection of DNA nanoparticles in high-conductance solutions," *ELECTROPHORESIS*, vol. 29, no. 9, pp. 1765–1774, 5 2008. [Online]. Available: <https://onlinelibrary.wiley.com/doi/full/10.1002/elps.200800037><https://onlinelibrary.wiley.com/doi/abs/10.1002/elps.200800037><https://analyticalsciencejournals.onlinelibrary.wiley.com/doi/10.1002/elps.200800037>
- [64] T. P. Hunt, H. Lee, and R. M. Westervelt, "Addressable micropost array for the dielectrophoretic manipulation of particles in fluid," *Applied Physics Letters*, vol. 85, no. 26, p. 6421, 12 2004. [Online]. Available: <https://aip.scitation.org/doi/abs/10.1063/1.1840109>
- [65] P. Tathireddy, Y. H. Choi, and M. Skliar, "Particle AC electrokinetics in planar interdigitated microelectrode geometry," *Journal of Electrostatics*, vol. 66, no. 11-12, pp. 609–619, 11 2008.
- [66] J. Auerswald and H. F. Knapp, "Quantitative assessment of dielectrophoresis as a micro fluidic retention and separation technique for beads and human blood erythrocytes," *Microelectronic Engineering*, vol. 67-68, pp. 879–886, 6 2003.
- [67] D. J. Bakewell and H. Morgan, "Dielectrophoresis of DNA: Time- And frequency-dependent collections on microelectrodes," *IEEE Transactions on Nanobioscience*, vol. 5, no. 1, pp. 1–8, 3 2006.
- [68] B. I. Morshed, M. Shams, and T. Mussivand, "Investigation of low-voltage pulse parameters on electroporation and electrical lysis using a microfluidic device with interdigitated

- electrodes,” *IEEE Transactions on Biomedical Engineering*, vol. 61, no. 3, pp. 871–882, 3 2014.
- [69] S. W. Lee and Y. C. Tai, “A micro cell lysis device,” *Sensors and Actuators A: Physical*, vol. 73, no. 1-2, pp. 74–79, 3 1999.
- [70] M. Popa and Serrano-Aroca, “Antiviral Characterization of Advanced Materials: Use of Bacteriophage Phi 6 as Surrogate of Enveloped Viruses Such as SARS-CoV-2,” *International Journal of Molecular Sciences* 2022, Vol. 23, Page 5335, vol. 23, no. 10, p. 5335, 5 2022. [Online]. Available: <https://www.mdpi.com/1422-0067/23/10/5335/html><https://www.mdpi.com/1422-0067/23/10/5335>
- [71] J. Barros, M. P. Ferraz, and F. J. Monteiro, “Bacteriophage Phi 6 as Surrogate and Human-Harmless Viruses to Study Anti-SARS-CoV-2 Approaches,” 2021. [Online]. Available: <https://repositorio-aberto.up.pt/bitstream/10216/138648/2/521330.pdf>
- [72] A. Fedorenko, M. Grinberg, T. Orevi, and N. Kashtan, “Survival of the enveloped bacteriophage Phi6 (a surrogate for SARS-CoV-2) in evaporated saliva microdroplets deposited on glass surfaces,” *Scientific Reports* 2020 10:1, vol. 10, no. 1, pp. 1–10, 12 2020. [Online]. Available: <https://www.nature.com/articles/s41598-020-79625-z>
- [73] C. D. Lytle, A. P. Budacz, E. Keville, S. A. Miller, and K. N. Prodouz, “DIFFERENTIAL INACTIVATION OF SURROGATE VIRUSES WITH MERCYANINE 540,” *Photochemistry and Photobiology*, vol. 54, no. 3, pp. 489–493, 9 1991. [Online]. Available: <https://onlinelibrary.wiley.com/doi/full/10.1111/j.1751-1097.1991.tb02047.x><https://onlinelibrary.wiley.com/doi/abs/10.1111/j.1751-1097.1991.tb02047.x><https://onlinelibrary.wiley.com/doi/10.1111/j.1751-1097.1991.tb02047.x>
- [74] S. B. Jeong, J. H. Shin, S. W. Kim, S. C. Seo, and J. H. Jung, “Design and Performance Evaluation of an Electrostatic Precipitator for Viral Aerosol Control Using a Surrogate for SARS-CoV-2,” *SSRN Electronic Journal*, 8 2022. [Online]. Available: <https://papers.ssrn.com/abstract=4166515>
- [75] P. Vatter, K. Hoenes, and M. Hessling, “Photoinactivation of the Coronavirus Surrogate phi6 by Visible Light,” *Photochemistry and Photobiology*, vol. 97, no. 1, pp. 122–125, 1 2021.
- [76] R. Bangiyev, M. Chudaev, D. W. Schaffner, and E. Goldman, “Higher Concentrations of Bacterial Enveloped Virus Phi6 Can Protect the Virus from Environmental Decay,” *Applied and environmental microbiology*, vol. 87, no. 21, p. e0137121, 10 2021. [Online]. Available: <https://pubmed.ncbi.nlm.nih.gov/34406830/>
- [77] A. M. Kropinski, A. Mazzocco, T. E. Waddell, E. Lingohr, and R. P. Johnson, “Enumeration of Bacteriophages by Double Agar Overlay Plaque Assay BT - Bacteriophages: Methods and Protocols, Volume 1: Isolation, Characterization, and Interactions,” *Methods in molecular biology (Clifton, N.J.)*, vol. 501, pp. 69–76, 2009. [Online]. Available: <http://www.ncbi.nlm.nih.gov/pubmed/19066811>[http://link.springer.com/10.1007/978-1-60327-164-6\\_7](http://link.springer.com/10.1007/978-1-60327-164-6_7)[https://doi.org/10.1007/978-1-60327-164-6\\_7](https://doi.org/10.1007/978-1-60327-164-6_7)

- [78] Y. P. Lu, J. W. Huang, I. N. Lee, R. C. Weng, M. Y. Lin, J. T. Yang, and C. T. Lin, "A Portable System to Monitor Saliva Conductivity for Dehydration Diagnosis and Kidney Healthcare," *Scientific Reports* 2019 9:1, vol. 9, no. 1, pp. 1–9, 10 2019. [Online]. Available: <https://www.nature.com/articles/s41598-019-51463-8>

- [79] Wu, Zong Min, et al. "Discolored bondpads caused by aluminium hydroxide formation." *Process Control and Diagnostics*. Vol. 4182. SPIE, 2000.
- [80] Younan, Hua, Chee Eddy, and Shailesh Redkar. "Investigation and elimination of discolored bondpads on microchip." *ICONIP'02. Proceedings of the 9th International Conference on Neural Information Processing. Computational Intelligence for the E-Age* (IEEE Cat. No. 02EX575). IEEE, 2002.
- [81] Zhang, J. F., et al. "Current–voltage characteristics and breakdown of different structural planar microelectrodes in atmospheric air." *AIP Advances* 11.6 (2021): 065301.
- [82] Townsend, John Sealy. *Electricity in gases*. Рипол Классик, 1915
- [83] Ono, Takahito, Dong Youn Sim, and Masayoshi Esashi. "Micro-discharge and electric breakdown in a micro-gap." *Journal of Micromechanics and Microengineering* 10.3 (2000): 445.
- [84] Lee, Dong Woo, and Young-Ho Cho. "A continuous electrical cell lysis device using a low dc voltage for a cell transport and rupture." *Sensors and Actuators B: Chemical* 124.1 (2007): 84-89
- [85] Fox, M. B., et al. "Electroporation of cells in microfluidic devices: a review." *Analytical and bioanalytical chemistry* 385.3 (2006): 474-485.
- [86] Veiga, Venicio F., et al. "Exposure of human leukemic cells to direct electric current." *Cell Biochemistry and Biophysics* 42.1 (2005): 61-74.
- [87] Zhou, Yao, Yi Wang, and Qiao Lin. "A microfluidic device for continuous-flow magnetically controlled capture and isolation of microparticles." *Journal of Microelectromechanical Systems* 19.4 (2010): 743-751.

---

# Glossary

## List of Acronyms

<b>LOC</b>	Lab On Chip
<b>mTAS</b>	micro-Total Analysis Systems
<b>PEF</b>	Pulsed Electric fields
<b>SARS CoV-2</b>	Severe Acute Respiratory Syndrome Corona Virus -2
<b>DEP</b>	Dielectrophoresis
<b>pDEP</b>	positive Dielectrophoresis
<b>nDEP</b>	negative Dielectrophoresis
<b>CM</b>	Clausius Mossotti
<b>TMV</b>	Tobacco Mosaic Virus
<b>HSV</b>	Herpes Simplex Virus
<b>DNA</b>	Deoxyribonucleic Acid
<b>CPMV</b>	Cowpea Mosaic Virus
<b>SEM</b>	Scanning Electron Microscope
<b>RBD</b>	Receptor Binding Domain
<b>PECVD</b>	Plasma Enhanced Chemical Vapour Deposition
<b>TEOS</b>	Tetraethyl Orthosilicate
<b>BSL-1</b>	bio safety level - 1
<b>BSL-3</b>	bio safety level - 3
<b>DLA</b>	double layer agar
<b>pfu</b>	plaque forming units

